Title
STRUCTURE ANALYSIS AND PHOTOCHEMISTRY OF ADSORBATES ON PLATINUM AND PALLADIUM SURFACES

Author
Grassian, V.H.

Publication Date
1987-05-01

LBL-23388

Lawrence Berkeley Laboratory
UNIVERSITY OF CALIFORNIA

Materials & Chemical Sciences Division

STRUCTURE ANALYSIS AND PHOTOCHEMISTRY OF ADSORBATES ON PLATINUM AND PALLADIUM SURFACES

V.H. Grassian
(Ph.D. Thesis)

May 1987

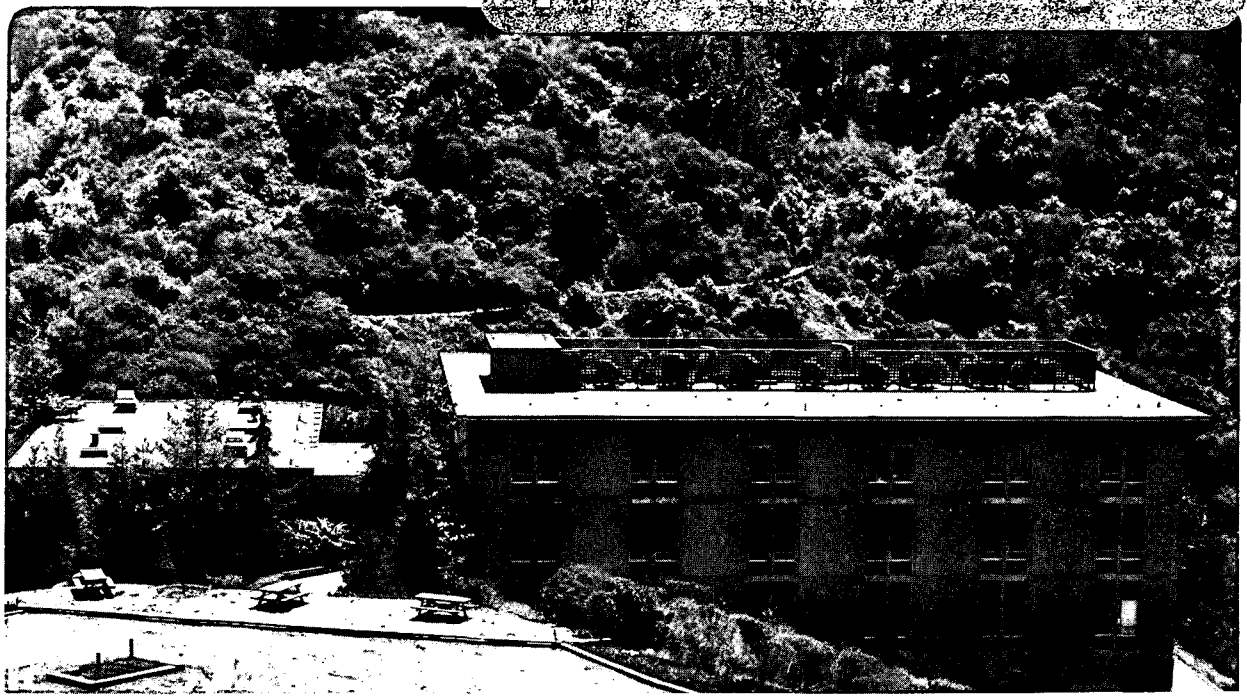

Prepared for the U.S. Department of Energy under Contract DE-AC03-76SF00098

DISCLAIMER

STRUCTURE ANALYSIS AND PHOTOCHEMISTRY OF ADSORBATES ON PLATINUM AND PALLADIUM SURFACES

Vicki Helene Grassian

(Ph.D. Thesis)

Materials and Molecular Research Division

Lawrence Berkeley Laboratory

and

Department of Chemistry

University of California

Berkeley, California 94720

April 1986

This work is supported by the Director, Office of Energy Research, Office of Basic Energy Sciences, Chemical Science Division of the U.S. Department of Energy under Contract No. DE-AC0376SF00098.

STRUCTURE ANALYSIS AND PHOTOCHEMISTRY OF ADSORBATES ON Pt AND Pd SURFACES

Vicki Helene Grassian

ABSTRACT

The adsorption of hydrocarbons on Pt(111) and Pd(111) surfaces under ultra-high vacuum conditions has been investigated. The vibrational spectra of both aromatics and 1,2-di-substituted ethenes adsorbed on these two surfaces were recorded by the technique of electron energy loss spectroscopy. The vibrational spectra of these molecules were used to determine adsorption structures. In addition, the photochemical reactivity of the di-substituted ethenes was followed by electron energy loss spectroscopy.

The vibrational spectra of benzene and toluene when adsorbed on Pd(111) indicates at 180K these molecules weakly bond to the surface. The adsorption of benzene and toluene on Pt(111) is much stronger as indicated by large frequency shifts from gas phase values. Pyridine adsorption on both Pt(111) and Pd(111) was studied as a function of temperature. At room temperature pyridine decomposes on the surface to form an α-pyridyl fragment (NC_5H_4) on Pt(111), whereas the molecule remains intact on Pd(111). The electron energy loss spectra of pyridine adsorbed on these surfaces is compared to the IR spectra of two osmium cluster compounds: $Os_3(CO)_{11}(NC_5H_5)$, a pyridine complex, and $HOs_3(CO)_{10}(NC_5H_4)$, a pyridyl complex. The stronger interaction of these molecules to the platinum surface is a consequence of the stronger

bonding of the 5d orbitals as compared to the 4d orbitals.

The UV photochemistry of 2-butene and 1,2-dichloroethene when adsorbed on Pt and Pd surfaces was also studied. Broadband photolysis of multilayer quantities of trans 2-butene and cis and trans 1,2-dichloroethene results in isomerization. This is similar to the photochemistry of these molecules in the liquid phase, as would be expected. Of a more interesting nature, UV photochemistry of monolayer quantities of both cis and trans 1,2-dichloroethene is markedly different. Dehalogenation was observed after UV broadband photolysis of chemisorbed 1,2-dichloroethene for both isomers. These differences between the physisorbed and chemisorbed states is attributed to different molecular structures and therefore excitation chromophores for these two ad-layers. These studies have demonstrated that photochemistry can occur in the vicinity of a metal surface. It can then be concluded, from these experiments, that chemical reactivity is competitive with any energy decay mechanisms to the metal surface.

TABLE OF CONTENTS

LIST OF TABLES

LIST OF FIGURES

Chapter I

INTRODUCTION

In the last 10-15 years the increase in our understanding of interfacial processes, and in particular interfacial chemistry, has been substantial. The chemistry which occurs at an interface is of extreme importance in biological as well as physical systems. However, the study of interfacial chemistry has always been extremely difficult, and a real challenge to the experimentalist. There are many reasons for these difficulties, one primary factor is that bulk measurements essentially obscure measurements from the interface. The ratio of molecules at an interface relative to the number in the bulk is approximately 1×10^{-8}!! To experimentally probe the wide variety of phenomena which occur at an interface, whether the solid-liquid, liquid-gas or solid-gas interface, techniques must be employed which are particularly sensitive to the properties of the interface and the molecules which make up the interface.

Some examples of important interfacial phenomena are described below. Lubrication is an important process which occurs between the solid and liquid phase, yet not much is known about wetting on a microscopic level. Electrochemical oxidation-reduction reactions which occur at an electrode surface constitutes another example of a solid-liquid process which is of current interest to many researchers. Liquid-gas interfacial phenomena include such fundamental behavior as vaporization and surface tension. The study of the solid-gas interface is the subject of this thesis, more specifically, adsorption of

hydrocarbons on clean, well defined single crystal transition metal surfaces.

Adsorption of gases on solid surfaces has been under investigation for the past fifty years. However, only within the last fifteen years has a detailed molecular description of the adsorbate-substrate bond begun to emerge. This clearly is due in part to the development of ultra-high vacuum equipment and techniques and the subsequent development of spectroscopic techniques which are surface sensitive. The ultra-high vacuum environment is needed in these studies to provide a clean surface. The spectrocopic techniques developed to study the solid-gas interface usually involve electrons as a probe. This is due to the inherent surface sensitivity of electrons in contrast to light. The penetration depth of an electron beam impinging on a solid surface is only 2-15Å (this distance being dependent on the energy of the electron beam), whereas, the penetration depth of light is on the order of a few hundred angstroms (this distance being dependent on wavelength). The different spectroscopic techniques which have been developed are many. The interested reader is referred to reference 1 for a complete overview of these techniques. The techniques used in these studies will be described later in more detail.

One of the most important goals of ultra-high vacuum surface studies is to understand on a microscopic level heterogenous catalysis. Although no practical catalyst works in an ultra-high vacuum environment, the idealized conditions obtainable under ultra-high vacuum permit fundamental understandings of these well defined systems. In the model systems under study, i.e., single crystal surfaces and one or two component gases, hopefully the catalyzed reaction mechanism can be

deduced, and of course, subsequently the knowledge derived from the model system study can be applied to "real world" catalysis. The importance of delineating the active sites and the detailed reaction mechanism of a catalyzed reaction is clear, heterogenous catalysis is of great importance and economic significance.

The first step in unraveling the mechanistic steps which ensue during the course of a catalyzed reaction is determining the structure of the adsorbed molecule before reaction. The adsorption structure is a key factor in understanding the subsequent chemical reactivity. Just as the gas phase and solution phase chemists use Nuclear Magnetic Resonance and Infrared Spectroscopy to determine molecular structure, the surface scientist also utilizes spectroscopic probes to determine adsorption structure. The most powerful tool to date in determining the structure of adsorbates on metal surfaces is electron energy loss spectroscopy.[2] Using electron energy loss spectroscopy the vibrational spectra of multilayer, monolayer and sub-monolayer quantities can be recorded. The techniques used in these studies include Auger electron spectroscopy, low energy electron diffraction, thermal desorption spectroscopy and electron energy loss spectroscopy. The studies presented in this thesis is described in two sections. In the first section the adsorption of aromatics on the (111) face of platinum and palladium surfaces is discussed. In the second section results and discussion of photochemical studies of adsorbates on Pt(111) and Pd(111) are presented.

These two metals, palladium and platinum, offer a comparison on the effects of a second row transition metal versus a third row transition metal. Besides the fact that these two elements are in the same

periodic column, these metals, together, form a similar pair. Both metals have the face-centered cubic crystal structure, interatomic distances are almost identical, 2.746Å for platinum and 2.751Å for palladium,[3] and the work functions of these metals are within 2% of each other, 5.7 eV-Pt(111) and 5.6 eV-Pd(111).[4] The only macroscopic quantity which shows significant differences between these two metals, and the effect of second versus third transition metal row, is the heat of atomization.[5] This thermodynamic quantity has been experimentally measured to be 135 kcal/mole for platinum and 91 kcal/mole for palladium. The larger value of $\Delta H_{atomization}$ for platinum is attributable to the greater orbital extent of the 5d orbitals, as compared to the 4d orbitals, which results in better overlap and therefore stronger bonding between the platinum atoms. As will be shown in subsequent chapters these ideas can be extended to surface phenomena and surface bonding.

The (111) crystallographic orientation, used in these studies, is of hexagonal symmetry, and is shown in figure 1. The other two low Miller index planes, the (100) and (110), are also shown for comparison. The adsorption sites which are available on the (111) surface are top, bridge and three-fold sites. The surface atoms differ from the interior atoms in that the bonding capacities of the surface atoms are not fulfilled. The surface atoms are then extremely reactive, the extent of this reactivity is dependent on both d-orbital filling and periodic row.

The adsorption of aromatics on the Pt(111) and Pd(111) surfaces is described in chapter 3; this includes benzene, toluene and pyridine. Aromatic molecules are an important product in the catalyzed reforming

Figure 1. The three low Miller index planes (111), (100) and (110) for a face-centered cubic structure are shown. Platinum and palladium metal both form face-centered cubic structures.

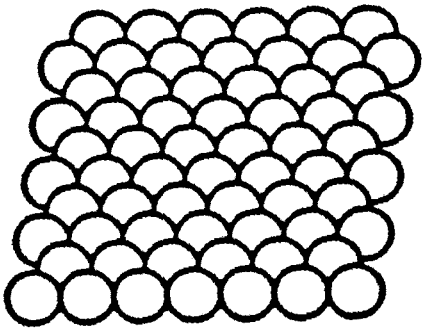

fcc (111)

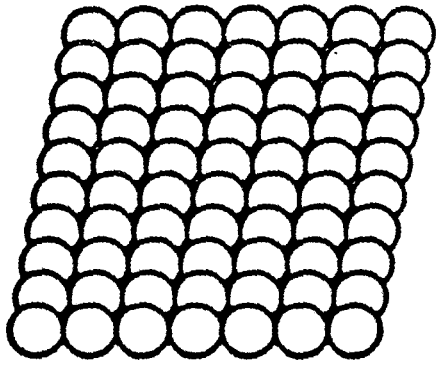

fcc (100)

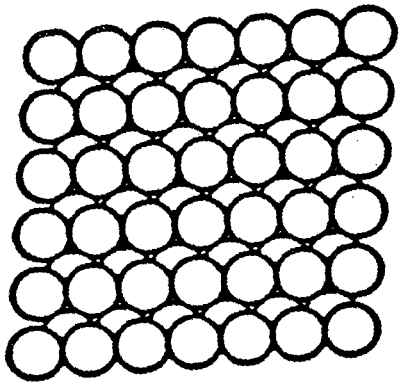

fcc (110)

XBL 802-8036

reaction of alkanes used in the petroleum industry. The increase in the concentration of aromatics relative to saturated hydrocarbons improves the octane number and therefore the overall efficiency in fuel combustion. The adsorption of these hydrocarbons on catalytically important metals can aid in the understanding of some of these catalyzed reactions. The adsorption of these molecules on these two surfaces is very different as is evident from the very different electron energy loss spectra. The adsorption of pyridine is particularly interesting, in that the nitrogen lone-pair as well as the π and π^* orbitals are involved in bonding. The possible decomposition of pyridine, upon adsorption, to form an alpha-pyridyl surface species has been explored. The infrared spectrum of two model complexes $Os_3(CO)_{11}(NC_5H_5)$, a pyridine complex, and $HOs_3(CO)_{10}(NC_5H_4)$, a pyridyl complex, were recorded and served as a guide in determining what surface structures were being formed.

The second part of this thesis, photochemical studies of adsorbates, explores the possibilities and potential of photocatalyzed reactions. Photocatalysis is becoming an important area of research in electrochemistry.[6] Light initiated oxidation-reduction reactions on semiconductor electrodes is potentially promising in the development of solar energy converters. The prospects for photocatalyzed reactions on transition metal surfaces has yet to be explored.

Photo-induced desorption has been the most common process investigated thus far, and it is gaining increased popularity among researchers. Both ultra-violet and infrared light sources have been shown to cause molecules to desorb from metal surfaces.[7] Typically, intense pulsed laser light sources is used to cause desorption. The

photochemical studies discussed in this thesis differs from the photodesorption type studies just described above in several aspects. Much lower level light intensities are used; a medium pressure Hg lamp was used as an ultra-violet radiation source for electronic excitation. Most importantly photoreaction was determined by vibrational spectroscopy and not mass spectrometry. This eliminates any background problems which can occur in any desorption study, whether photo or thermal in nature.

In particular we have studied the electronic excitation of substituted ethenes adsorbed on platinum and palladium surfaces. Isomerization and dehalogenation are some of the photoreactions which are observed. Photolysis products for these reactions were dependent on several factors. These factors include the wavelength of light, and whether the molecule is physisorbed or chemisorbed to the surface.

Finally, this initial study on photochemistry of adsorbates, as well as the photodesorption studies, points to a potentially new area of surface science. The possibilities and potential of combining these two areas of chemistry, photochemistry and surface science, looks promising.

Chapter II

EXPERIMENTAL

These experiments were performed in a single-stage ultra-high vacuum (UHV) chamber. Typically, after an eighteen hour bake-out at 200°C, the base pressure of the chamber was 2×10^{-10} torr. Five 40 liter/sec ion pumps (Varian) were used to give a combined pumping speed of 200 liter/sec. An auxillary titanium sublimation pump (Varian) was also used, especially after bake-out when the pressure of the chamber was higher then normal. A Varian nude ion-gauge measured the pressure in the chamber as well as pressure-time exposures for gases being introduced in the chamber. Pressure readings were not corrected for differing ion-gauge sensitivities. The spectroscopic techniques employed in this study are described below.

Auger electron spectroscopy is routinely used in ultra-high vacuum studies to determine surface composition. The Auger spectrometer (Varian) consists of an electron gun, power supply, sweep generator, lock-in amplifier for signal modulation, and a retarding field energy analyzer for signal detection. The electron beam impinges on the surface with a beam energy of approximately 2000eV. The electron beam is directed at grazing angle to the surface for maximum surface sensitivity. The Auger process is a two electron ionization process; first an incident electron knocks out an inner shell electron of an atom creating an inner hole vacancy, a second electron then drops down to the vacant hole. The energy released from this atomic transition can occur in one of two ways either an x-ray or an outer shell electron is emitted

from the atom. The kinetic energy of the emitted electron, known as an Auger electron, is characteristic of the element, thus making the technique suitable for composition analysis. Auger electron spectroscopy is sensitive down to approximately 1% of a monolayer.

Besides elemental composition the characterization of a single crystal surface must include the surface crystallographic orientation. Low energy electron diffraction readily determines surface structure. Low energy electrons on the order of 50 eV are diffracted from the surface and are accelerated onto a phosphorescent screen. The arrangement of the surface atoms can then be deduced from the diffraction pattern. Low energy electron diffraction is sensitive to both the substrate as well as organic overlayers. Figure two shows a picture of a low energy electron diffraction pattern of a clean Pd(111) surface. The hexagonal symmetry of this surface can readily be seen.

The ultra-high vacuum chamber is also equipped with a quadropole mass spectrometer (Vacuum Generator). The mass spectrometer was used for several functions. Background gases in the chamber were monitored. The major gas components in the ultra-high vacuum chamber were H_2, CO, H_2O, CO_2 and Ar, in approximate order of decreasing concentration. The purity of the gases being introduced in the chamber for adsorption studies were also checked by mass spectrometry. And finally the mass spectrometer was used to measure individual masses in thermal desorption spectroscopy (TDS) experiments. A tantalum cup with a 2mm pinhole was placed over the head of the spectrometer to minimize any background effects in these TDS experiments. The crystal was placed within a centimeter of the mass spectrometer during these experiments.

Thermal desorption spectroscopy is a technique which detects

Figure 2. Low energy electron diffraction pattern of a clean Pd(111) surface. The hexagonal symmetry of this surface face can be easily seen.

LEED Pattern 70eV

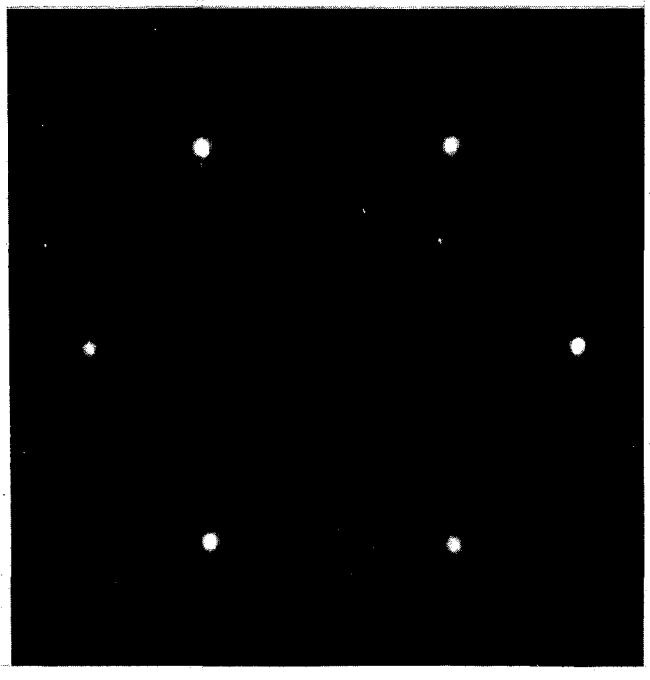

reaction products and provides a rough estimate of the binding energies of adsorbates. Reaction products are detected by monitoring individual masses. If chemical reaction has taken place and the product is stable with respect to decomposition on the surface, product identification can be made fairly easily by its mass spectral fragmentation pattern. The temperature at which the product molecule desorbs can be either desorption-limited or reaction-limited. A desorption-limited process is one in which product is formed below the temperature at which the molecule characteristically desorbs from the surface. Reaction-limited desorption occurs when the product is formed at a temperature above its characteristic desorption temperature, and therefore its desorption is limited by its formation.

Determining activation energies and other kinetic parameters from temperature programmed desorption data, of adsorbates is a bit more difficult and requires several approximations concerning the desorption process. The theory has been worked out in detail by Redhead[8] and only the final result will be presented here. The expression for a first-order desorption process at constant temperature can be written as:

$$dn/dt = n\nu e^{-Ea/RT} \qquad (1)$$

For both a linear heating rate ($T = T_o + \beta t$) and $10^{13} > (\nu/\beta) > 10^{8}$, E_a is given as:

$$Ea = RT_{max}\ln\nu(T_{max}/\beta) - 3.64RT_{max} \qquad (2)$$

where n = surface coverage

β = heating rate in deg/sec

T_{max} = desorption rate temperature maximum

R = gas constant

ν = frequency factor

Other assumptions which have been made include the assumption that the desorption rate dn/dt is much faster then the pumping speed and that the activation energy is independent of coverage. Another common practice is to assume a frequency factor, commonly the value of 10^{13} sec^{-1} is used. This value is based on typical frequency factors for gas-phase unimolecular reactions. Finally the heat of desorption can be determined if it is assumed that the desorption process is a non-activated process. The heat of adsorption, which is equal and opposite in sign to $\Delta H_{desorption}$, is then known. As one can see there are many assumptions and care must be taken when considering ΔH_{ads} derived from temperature programmed desorption data.

The chemical identity of an adsorbate can be characterized by its vibrational spectrum. The technique of electron energy loss spectroscopy (EELS) has proven to be a powerful technique in determining structural information of adsorbates.[2] This technique is extremely surface sensitive and can detect monolayer and sub-monolayer quantities. The resolution however is poor when compared to optical spectroscopies. There are several reasons for the difficulties in producing a monoenergetic beam of low energy electrons. The two most important considerations are the repulsive space charge effects in the electron beam itself and the second is the non-uniform electric fields throughout the spectrometer. These factors have kept the resolution of these spectrometers between 30 - 100 cm^{-1}, as defined by the full width

half maxima of the the elastically scattered electron beam. There is a cost in signal for higher resolution and the lower limit of 30 cm^{-1}, can only be applied to strong scatterers. Infrared reflection absorption spectroscopy is also commonly used to obtain vibrational spectra of adsorbates.[9] The resolution is approximately a factor of ten better then electron energy loss spectroscopy, the sensitivity however is reduced by a factor of twenty for this method relative to EELS. This has then limited the application of this technique to molecules with large extinction coefficients, particularly carbon monoxide.

An extensive derivation of the theory of electron energy loss spectroscopy can be found in reference 2. The details will not be discussed here but some of the more important factors will be. The electrons interact with the adsorbate in one of two ways, either through a long or short range interaction. The descripton of the long range interaction is one in which the electrons and the dipole derivative (dynamic dipole) of the adsorbate are considered. This leads to similar selection rules derived for traditional infrared spectroscopy with an additional constraint, in that only vibrational modes with dipole derivatives which are perpendicular to the surface will be excited. This consideration is due to the free electrons in the metal which will screen motions that are parallel to the surface. This is shown more clearly in figure 3. The intensity of the loss peak from this scattering mechanism can be written as:[2]

$$I_{inelastic} = I_{elastic} \frac{4\pi(1-2\theta_e)^{1/2} n_s}{a_o E_i \cos\theta_i \varepsilon^2} \left|\langle 0|\mu_z|\nu\rangle\right|^2 \; Fs(\theta_c) \qquad (3)$$

Figure 3. Vibrational motions parallel to the surface are screened by the conducting electrons in the metal. The total dipole derivative is zero for motions parallel to the surface when the image dipole is considered. Vibrational motions perpendicular to the surface are enhanced by the conducting surface. For vibrational motions which are perpendicular to the surface the net dipole is $2(d\mu/dr)$ when the image dipole is considered.

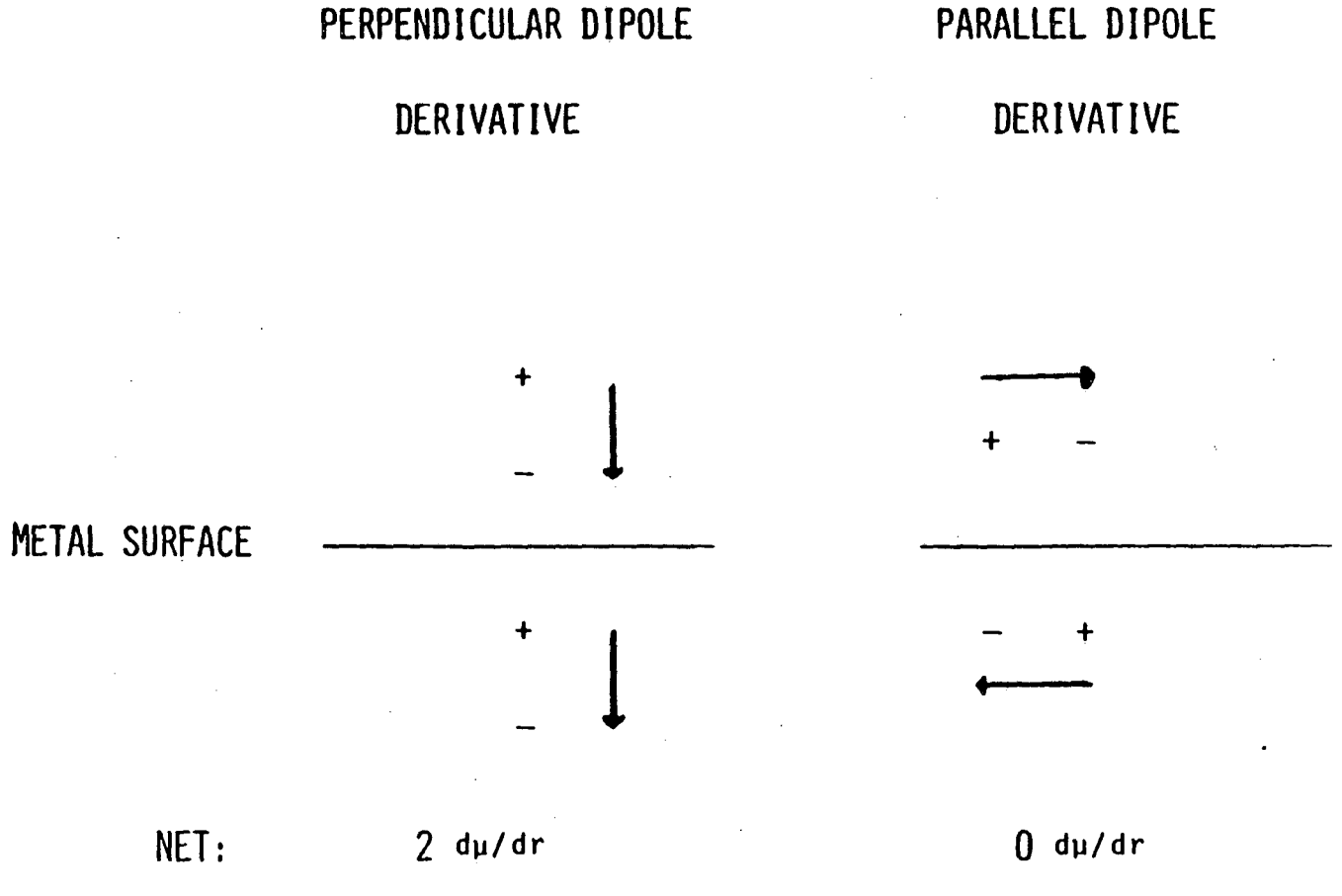
PERPENDICULAR DIPOLE
DERIVATIVE
PARALLEL DIPOLE
DERIVATIVE
METAL SURFACE
NET:
2 dμ/dr
0 dμ/dr

where $I_{inelastic}$ = Intensity of the loss peak

$I_{elastic}$ = Intensity of the elastically scattered beam

E_i = Energy of the incident beam

θ_i = Angle of incidence, defined as the angle between the specular beam and the surface normal.

θ_e = $h\omega/2E_i$, characteristic deflection angle

ϵ_β = Average dielectric constant of the metal and the adsorbate

$F_s(\theta)_c$ = A function of the acceptance angle of the spectrometer

$|\langle 0|\mu_z|v\rangle|^2$ = Expectation value of the perpendicular component of the dipole moment

a_o = Bohr radius

n_s = number of scatterers

The dipole scattering mechanism has an angular profile which peaks at the specular angle. Structural information can be deduced from dipole scattered loss peaks, from both the frequencies of the vibrational modes and the intensity of the loss peaks in the specular direction.

A second scattering mechanism by which the incident electrons can interact with the adsorbate is through a shorter range interaction known as impact scattering. The intensity of the loss peaks for this type of scattering mechanism can be written as:[2]

$$I_{inelastic} = I_{elastic} \frac{E}{4 h \omega_s} \frac{m}{M_r} \frac{1}{M^2_{opt}} \qquad (4)$$

where E = Energy with of the beam

h = Plancks constant

ω_s = frequency of the excited mode

m = mass of an electron

M_r = reduced mass

M_{opt} = optical magnification between exit aperature of the monochromator and its image on the sample

The angular distribution of the scattered electrons is much broader then that is observed for dipole scattered electrons, since in the impact scattering regime the scattered electrons are distributed rather uniformly over the entire solid angle. The loss peaks from impact scattered electrons cannot be used to derive orientational information since the intensity of the peaks is not proportional to $(d\mu/dz)$ as is the case for dipole scattering. The nature of a loss peak can be discerned, i.e. whether attributable to dipole or impact scattering, from the angular distribution of the intensity of the loss peaks about the specular direction. This can be experimentally determined in one of two ways: either the sample can be rotated about the crystal axis or the analyzer can be rotated away from the specular angle. In these experiments the crystal orientation is changed and the analyzer position is fixed. Usually the most intense loss peaks observed at the specular angle are attributed to the dipole scattering mechanism and therefore vibrational modes which have dipole changes perpendicular to the surface. The less intense peaks can be due to either impact or dipole scattered electrons, to discern between the two the intensity of the peak should be measured at a few degrees (10°) off the specular

direction. If there is a decrease in intensity of a particular loss peak off the specular direction it can be attributed to a vibration with a dipole derivative perpendicular to the surface.

Another short range scattering mechanism is resonance scattering. Here the electron is trapped by the molecule forming a negative ion resonance. This type of mechanism is found widely in gas phase electron spectroscopy, and only a few cases have been observed for molecules adsorbed on surfaces.[2]

The EEL spectrometer used in these experiments is an electrostatic lens device which has been described in detail elsewhere and is shown in figure 4.[10] The spectrometer consists of two 120° cylindrical sectors, the monochromator an the analyzer. The electrons are produced by a tungsten filament and are focused by three electrostatic lenses onto the entrance slit of the monochromator. The electrons pass through the monochromator and are accelerated onto the crystal with lenses B1 and B2. The electrons scatter from the crystal either elastically or inelastically, losing energy via excitation of the vibrational modes of the adsorbed molecule. Thus the following energy expression is obtained:

$$E_{final} = E_{initial} - h\nu \qquad (5)$$

The electrons are energy analyzed by sweeping the voltages of the analyzer sector, and the zero is set by the peak of the elastically scattered electrons. The electrons are detected by an electron multiplier (channeltron) which is biased at 2500 volts. The collected electrons are then amplified, discriminated and counted by a ratemeter

Figure 4. The electron energy loss spectrometer used in these experiments consists of two 120^0 cylindrical sectors, the monochromator and the analyzer.

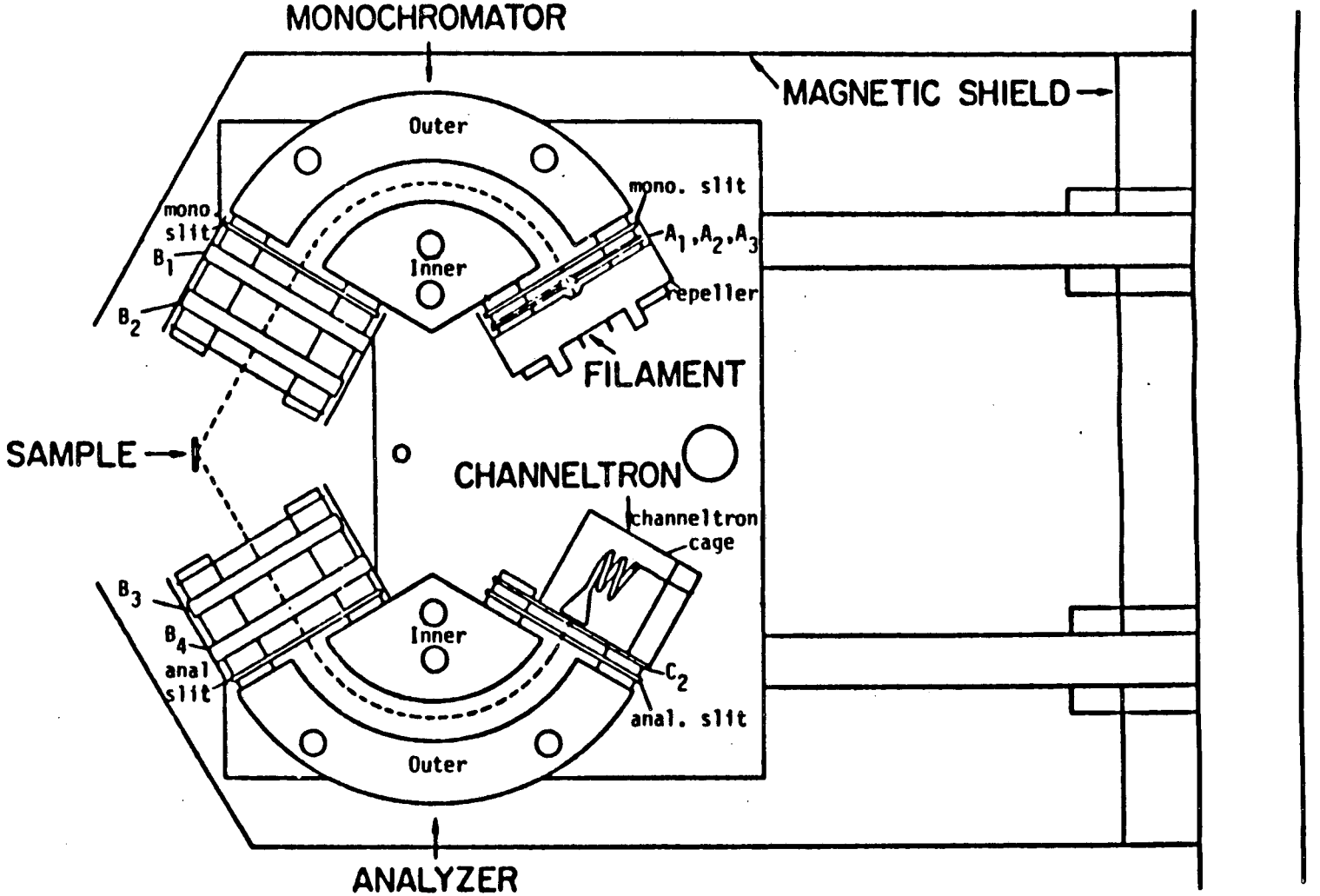

ELECTRON ENERGY LOSS SPECTROMETER

(Ortec).

The power supply for the EEL spectrometer was designed and built at Lawrence Berkeley Laboratories and has been described in detail elsewhere.[11] The tuning proceedure to obtain a spectrum can be a tedious task especially when the correct sample position is unknown, i.e. whether the electron beam is hitting the crystal and no other part of the sample manipulator. Usually one tunes the potentials and repositions the crystal and retunes the potentials etc. while trying to maximize the counts of the elastically scattered electron beam. When the exact position of the sample is unknown the voltages across the monochromator and the analyzer sectors are made large (0.700 Volts). This increases the pass energy, the pass energy can be expressed as:[2]

$$E = \frac{1/2\ V}{\ln(r_0/r_i)} \qquad (6)$$

where V = the potential across the inner and outer sectors

r_0 = radius of the outer sector

r_i = radius of the inner sector

After the sample position is found and the counts are high for the elastic peak (on the order of $10^4 - 10^5$ counts/sec) the sample is then dosed with CO and an EEL spectrum is taken so loss peaks at the correct frequency are observed. The pass energy is then lowered to increase the resolution. Once the sample position is known the tuning procedure is much easier, usually tuning involves changing the potentials before the

crystal B1 and B2 (as well as ΔB1 and ΔB2) and right after the crystal B3 and B4 (ΔB3 and ΔB4) as well as the crystal bias. The EEL spectra were either recorded on an x-y chart recorder or were collected by an LSI 11-23 computer. The EELS programs for data collection and display were written by Joe Katz from Lawrence Berkeley Labs, and modified by Kirk L. Shannahan.

The vibrational analysis of an EEL spectrum can range from being exceedingly simple to uninterpretable. The low resolution of the EEL spectra limits isotope experiments to the use of deuterium, as compared to a wider range of isotope experiments which are typically used in an infrared analysis, such as O^{18}, C^{13}, and N^{15}. If the molecule has retained its molecular integrity upon adsorption on a metal surface the analysis of the EEL spectrum can be made by direct comparison to the infrared spectrum of the molecule in the gas or liquid phase. If however the adsorbed molecule has substantially rehybridized, rearranged or dissociated on the surface the IR spectrum of the molecule in the gas or liquid phase is no longer applicable and the analysis is much more difficult.

An example of this type of molecular rearrangement upon adsorption on the surface occurs when ethylene adsorbs on Pt(111) at 300K. The molecular formula of the surface species has been determine to be C_2H_3.[12,13] After several years of debate the adsorption structure was determined to be ethylidyne on the surface ($\equiv C\text{-}CH_3$).[13] The last and most conclusive piece of evidence for the formation of ethylidyne on the surface was the excellent agreement between the EEL spectrum of ethylidyne with the infrared spectrum of $Co_3(CO)_9(CCH_3)$, a tri-cobalt ethylidyne cluster complex.[14] This finally laid to rest the question of

surface structure for ethylene adsorbed on Pt(111) at room temperature.

This example illustrates the need for structural models in determining hydrocarbon adsorption structures. Prototype model complexes will preferably be hydrocarbon fragments bonded to metal clusters. But in the absence of the synthesis of metal complexes appropriate gas and liquid phase structures can be used. In this thesis the vibrational analysis of EEL spectra will utilize the IR spectra of model compounds including both molecular metal complexes and pertinent hydrocarbon compounds.

Sample Preparation and Procedures

Single crystals of either platinum or palladium metal were spark cut and oriented along the (111) direction using Laue X-ray back diffraction. The platinum crystal, 1 cm in diameter, was polished according to the following procedures. The sample was mechanically polished with four grades of alumina papers, the finest particle size was 10 microns, this was followed by 1 micron diamond paste and finally 0.05 micron alumina in water. The procedure for the palladium crystal differed only in the final step in that polishing with 0.25 micron diamond paste followed the 1 micron diamond paste polishing. The palladium crystal was approximately twice the diameter of the platinum crystal. The crystal surfaces were checked under the microscope to ensure absence of pits and scratches, once again checked by Laue back diffraction to be sure the correct orientation was achieved, before the sample was introduced into the vacuum chamber.

The crystal was spot-welded to two platinum wires 15 mil in diameter which mounted the crystal to a copper block. The crystal was cooled in a similar manner as described previously with minor

modifications.[15] Liquid nitrogen was passed through two copper cold fingers connected by copper braids 5" long and 0.0032" in diameter to the copper block on which the sample was mounted. The crystal temperature, as monitored by a chromel-alumel thermocouple spot-welded to the bottom of the crystal, reached a minimum temperature of 110K. During the course of the experiments done in these studies the cooling system was modified several times. The method described above is the one which worked best and was used for most of the studies in this thesis. There are however several experiments conducted at T = 180K and these will be noted when applicable throughout the text. The sample was heated resistively through the same copper braids to override the cooling of the crystal. The copper block which mounted the crystal was mechanically attached to a stainless steel manipulator offset 2" from the center of the chamber so the sample could be rotated to any part of chamber desired. A tilt mechanism permitted the crystal to be rotated on the crystal axis for off-specular measurements.

The cleaning treatments differed somewhat for the two metals. For the platinum crystal surface carbon was removed by heating the sample to 1000K in the presence of oxygen at a pressure of 1×10^{-6} torr. After the crystal was free of carbon impurities (as shown by Auger spectra). Sulfur impurities that remained after this treatment can then be removed by heating the crystal to 800K in oxygen again at a pressure of 1×10^{-6} torr. Oxygen that remained on the surface after these cleaning treatments was removed by briefly heating the crystal to 1200K. Calcium was removed from the crystal surface by sputtering the surface with argon ions at an Ar pressure of 1×10^{-5} torr and an incident beam energy of 600eV with the sample temperature at 300K. These procedures

were repeated until the surface was determined to be clean by Auger electron spectroscopy. The palladium crystal was cleaned by repeated oxygen and heat treatments. To remove large amounts (> 5% of a monolayer) of sulfur from the surface, the sample was heated to 780K and sputtered with argon ions at a beam energy of 1000eV and an argon pressure of 1×10^{-5} torr. Then the crystal was annealed by raising its temperature to 1200K momentarily. To remove small amounts of sulfur and carbon from the surface the sample was heated to 575K in a 5×10^{-6} torr atmosphere of oxygen. Any residual oxygen on the surface was removed by briefly heating the sample to 1100K.

The liquid and gas samples used in these experiments are listed in Table 1. Gases were introduced into the chamber after several freeze-pump thaw cycles. Gas exposures were done using a variable leak valve, with a needle valve doser. The leak valve was turned until the desired pressure was reached, as determined by the ion gauge reading. The pressure was then held at this value typically for 50-200 seconds. Exposures are noted in units of Langmuirs with 1 Langmuir = 1×10^{-6} torr-sec.

Synthesis of Tri-Osmium Cluster

The tri-osmium cluster compounds were synthesized in a procedure slightly modified from that previously described by Yin et. al..[16,17] Standard vacuum and Schlenk line techniques were used in preparation of these compounds: reactions were carried out under an atmosphere of nitrogen. Using 300 mg of $Os_3(CO)_{12}$ (Strem Chemicals) dissolved in 100 mls of methylene chloride, excess of reagent grade pyridine (or perdeuterated pyridine), 1 ml, was transferred into the reaction flask. A solution of trimethlamine oxide $(CH_3)_3NO$ (35 mg of $(CH_3)_3NO$

TABLE 1

LIST OF CHEMICALS

Compound	Source
NC_5H_5	Mallinckrodt, Inc.
NC_5D_5	Merck, Sharp and Dohme
$Os_3(CO)_{12}$	Strem Chemicals
C_6H_6	Mallinkrodt, Inc.
C_6D_6	Aldrich Chemical Co.
$C_6H_5CH_3$	Mallinckrodt, Inc.
$C_6D_5CH_3$	Merck, Sharp and Dohme
$C_6H_5CD_3$	Merck, Sharp and Dohme
$C_6D_5CD_3$	Aldrich Chemical Co.
trans 2-butene	Matheson
cis 2-butene	Matheson
trans 1,2-dichloroethene	Aldrich Chemical Co.
cis 1,2-dichloroethene	Aldrich Chemical Co.
d^2-cis and trans 1,2-dichloroethene	MSD Isotopes

dissolved in 35 mls of methylene chloride) was added dropwise to the osmium reaction mixture. The progress of the reaction was monitored by infrared spectroscopy in the 1700 - 2100 cm^{-1} region where carbonyl adsorption occurs. Trimethylamine oxide was added until the 2070 cm^{-1} band corresponding to the reactant, $Os_3(CO)_{12}$ disappeared. The solvent was pumped off, the product $Os_3(CO)_{11}(NC_5H_5)$ was redissolved in methylene chloride and pentane and the recrystallized. The solvent was decanted and evaporated off under vacuum.

The product $Os_3(CO)_{11}(NC_5H_5)$ (100 mg) was used in the preparation of the pyridyl complex, $HOs_3(CO)_{10}(NC_5H_4)$. $Os_3(CO)_{11}(NC_5H_5)$ was dissolved in 50 mls of n-octane containing a few drops of pyridine, and the mixture was refluxed for one hour. The pyridyl complex was isolated by chromatography using a silica column and pentane elutant. After the compound was collected, the solvent was evaporated. The structures of the pyridine and pyridyl complexes were determined by Yin et. al. using NMR spectroscopy as well as IR spectroscopy in the 1700 - 2100 cm^{-1} spectral region.

The infrared spectra of both these compounds were recorded over the spectral range 400 - 3200 cm^{-1} using a Perkin Elmer 283 infrared spectrometer with a spectral resolution of 2-3 cm^{-1} and a frequency accuracy of 1-2 cm^{-1}. Anhydrous KBr was used in the preparation of the KBr discs.

Photolysis Experiments

A General Electric medium pressure mercury arc lamp (AH4), with its envelope removed, was used as the broadband photolysis source. An 1" quartz lens, with a 7 cm focal length, focused the light into the vacuum chamber and onto the crystal through an 1" sapphire window (Varian). A

CsI filter was placed in fromt of the Hg lamp when light below 237 nm was unwanted.

Chapter III

ADSORPTION OF AROMATICS ON THE (111) FACE OF PLATINUM AND PALLADIUM

1. INTRODUCTION

The bonding of aromatic molecules on many different single crystal metals and different crystallographic planes has been a subject of considerable interest. Benzene has been the most studied aromatic molecule so far and by several different surface science techniques including photoelectron spectroscopy, low energy electron diffraction, thermal desorption spectroscopy (TDS) and electron energy loss spectroscopy (EELS). The adsorption geometry of benzene on the low Miller index surface planes of many transition metals Pt[18], Ni,[19] Pd,[20] Rh,[21] Ir,[22] Ru[23] is thought to be very similar. The proposed structure is one in which the ring plane of benzene is oriented parallel to the surface plane. The π and π^* orbitals of benzene are considered to interact with the metal orbitals in forming the chemisorption bond. While this model is generally agreed upon for benzene adsorption, there is debate however on the exact adsorption site and the symmetry of the benzene surface complex. This model does not account for the large discrepancies from one metal surface to another (up to 200 cm^{-1}) in frequencies of the loss peaks for benzene adsorbed on the different metals. In this thesis we compare the adsorption of benzene on the (111) face of platinum and palladium metal. In the case of benzene adsorbed on Pt(111) there is a large perturbation of the vibrational modes of benzene indicating chemisorption and a strong interaction of the molecule with the platinum surface. Adsorption of benzene on the Pd(111) surface is quite different. Although there are frequency shifts

observed for benzene adsorbed on palladium relative to liquid phase benzene they are much less then what was observed on platinum. In contrast to previous interpretations, this difference has been re-interpretated as benzene having two very different adsorption structures on these two metal surfaces.

Toluene and pyridine adsorption was also studied on these surfaces, in the case of heteroaromatics there is the possibility of a similar interaction between the π and π^* orbitals of the adsorbate and the metal atoms. However, there is now the possibility of an interaction between the metal and the nonbonding lone pair of electrons localized on the heteroatom which can bond to the surface in a conventional sigma donor type interaction.

The importance of both of these interactions for heteroaromatics adsorbed on metal surfaces has been observed with pyridine on Ag(111)[24] and Ni(100).[25] Both vibrational and electronic electron energy loss spectroscopy of pyridine adsorbed on Ag(111) have shown the conversion of a π bonded to nitrogen bonded pyridine as the pyridine coverage is increased. For coverages below 0.50 monolayers pyridine adsorbs with the ring plane parallel to the surface plane in a geometry similar to that of benzene on the Ag(111) surface. For coverages above 0.5 monolayers there is a "phase transformation" to a nitrogen bonded species. Recently a study by DiNardo et al.[25] again using electron energy loss spectroscopy of pyridine adsorbed on Ni(100) showed the existence of two nitrogen bonded species. The surface chemistries of pyridine, deuterium labeled pyridines,[26] and methyl substituted pyridines[27] have been studied on the Ni(100) and Ni(111) surfaces.

We present first a vibrational study of pyridine adsorbed on

Pt(111) as a function of temperature. The complimentary technique of thermal desorption spectroscopy was also employed. The infrared spectra of two prototype cluster compounds $Os_3(CO)_{11}(NC_5H_5)$ and $HOs_3(CO)_{10}NC_5H_4$ (and their perdeuterated analogues) were also recorded for comparison. Triosmium and tricobalt cluster compounds have been extremely useful as prototype structural models in identifying adsorbed species on metal surfaces.[28,29,30]

In the second part of this section the study of benzene and perdeuterobenzene adsorbed on Pd(111) is discussed. The electron energy loss spectra of toluene and isotopically substituted toluenes, d^3-$C_6H_5CD_3$, d^5-$C_6D_5CH_3$, and d^8-$C_6D_5CD_3$, as well as pyridine and perdeuteropyridine were also recorded. In summary, we compare the adsorption of these molecules on palladium relative to that on platinum where there is a greater metal-adsorbate interaction.

2. RESULTS AND DISCUSSION

A. PYRIDINE ADSORBED ON Pt(111) AT 120 AND 300K: COMPARISON TO BENZENE AND TOLUENE ADSORPTION

Infrared Spectra of $Os_3(CO)_{11}(NC_5H_5)$ and $HOs_3(CO)_{10}NC_5H_4$

We present the infrared spectra recorded for $Os_3(CO)_{11}(NC_5H_5)$ (1a) and $HOs_3(CO)_{10}(NC_5H_4)$ (1b) (Fig. 5) first so we may use these results when discussing the electron energy loss spectrum recorded for pyridine adsorbed on Pt(111). Figure 6a shows the infrared spectra in the spectral range from 400 to 1650 cm^{-1} for the two osmium cluster compounds. The infrared spectra for the perdeuterated analogues are shown in Figure 6b. In both the pyridine and the pyridyl tri-osmium complexes the pyridine moiety is bonded to one of the metal atoms in the cluster through the nitrogen. In the pyridyl complex the pyridine moiety is additionally bonded to the metal cluster through the α carbon.

In Table 2 we list the low frequency absorption bands (400-610 cm^{-1}) for the pyridine and pyridyl cluster compounds along with the corresponding frequencies for $Os_3(CO)_{12}$.[31] The comparison of the low frequency bands observed in the IR spectra (Fig. 6) of the two prototype model compounds (1a and 1b), match reasonably well to the observed absorption bands in the IR spectra of $Os_3(CO)_{12}$. This indicates that these absorptions are dominated by the bending and stretching modes of the metal framework, the metal carbon stretching motion and the metal carbonyl bending motions. The spectral region from 600-1650 cm^{-1} is of more interest in this study, the absorption bands which occur at these frequencies are due to the vibrations of the pyridine and pyridyl fragments of the cluster. The assignment for the bands in this region are made by comparison to the vibrational spectrum and the assignment

Figure 5. The two cluster compounds $Os_3(CO)_{11}(NC_5H_5)$ (1a) and $HOs_3(CO)_{10}(NC_5H_4)$ (1b) were used as prototype model compounds in this study.

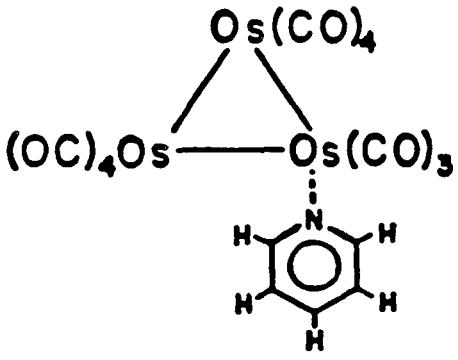

(1a)

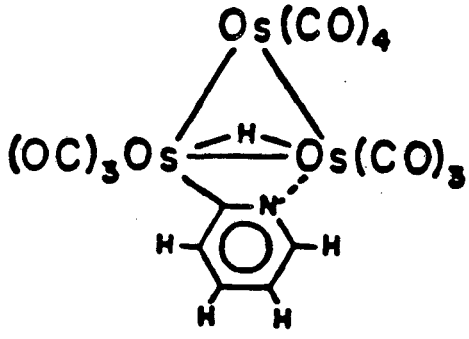

(1b)

Figure 6. The infrared spectrum of $HOs_3(CO)_{10}(NC_5H_4)$ and $Os_3(CO)_{11}(NC_5H_5)$ (and the perdeuterated compounds) in the 400 - 1600 cm^{-1} spectral region, a. perhydro compounds b. perdeutero compounds.

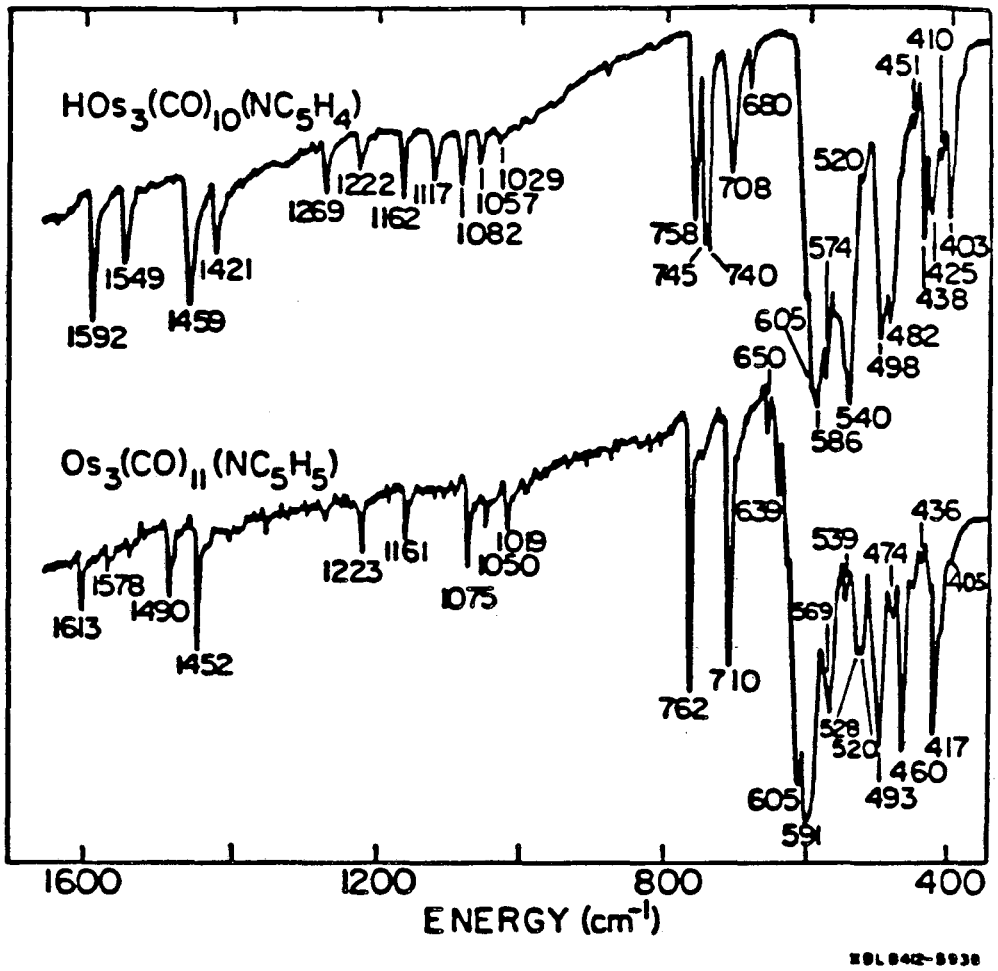
HOs3(CO)10(NC5H4)
1592
1549
1459
1421
1269
1222
1162
1117
1082
1057
1029
758
745
740
708
680
605
586
574
540
520
498
482
451
438
425
410
403
Os3(CO)11(NC5H5)
1613
1578
1490
1452
1223
1161
1075
1050
1019
762
710
650
639
605
591
569
539
528
520
493
474
460
436
417
405
1600
1200
800
400
ENERGY (cm-1)

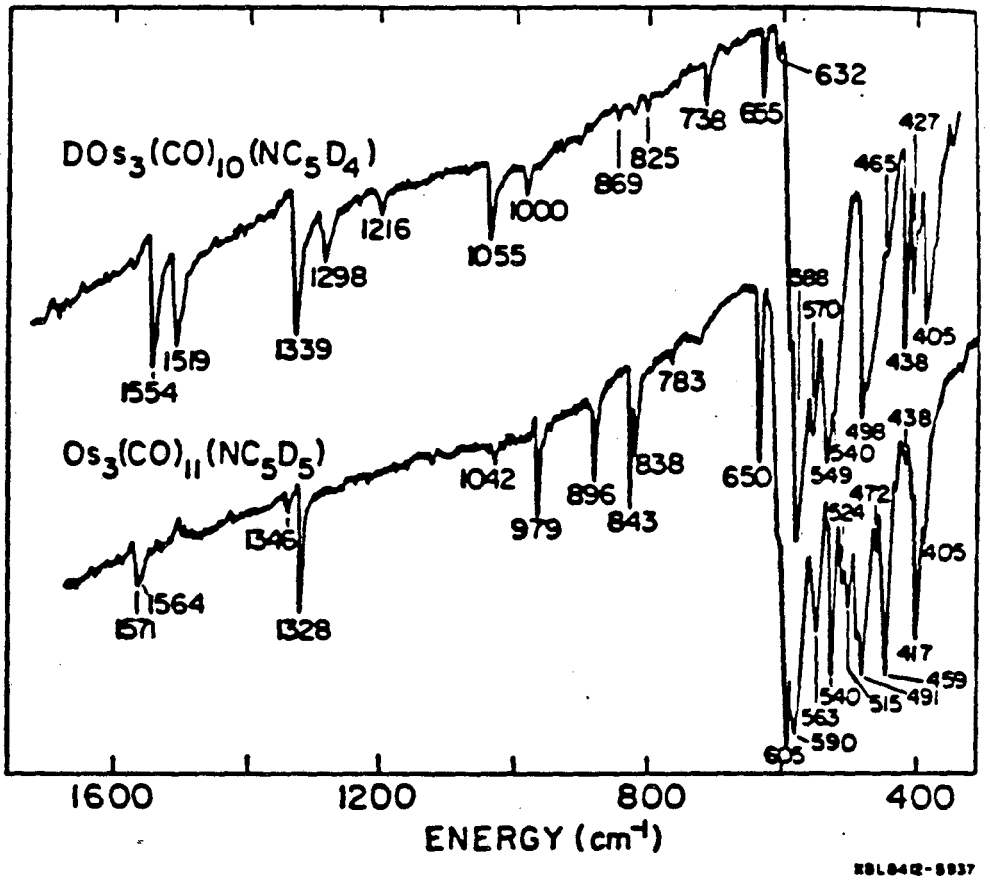
DOs3(CO)10(NC5D4)
Os3(CO)11(NC5D5)
1554
1519
1339
1298
1216
1055
1000
869
825
738
655
632
427
465
405
438
1571
1564
1346
1328
1042
979
896
843
783
838
650
588
570
549
540
498
438
524
472
405
417
459
491
515
540
563
590
605
1600
1200
800
400
ENERGY (cm-1)

Table 2

Corresponding Frequencies of the Low Frequency Modes (400-610 cm^{-1}) for Tri-Osmium Complexes

$Os_3(CO)_{12}$[a]	$Os_3(CO)_{11}(NC_5H_5)$	$HOs_3(CO)_{10}(NC_5H_4)$
400 W[b]	405	403
410 S	417	410
429 M	436	425,438
448 W		451
462 S	460	
474 W	474	482
496 S	493	498
516 W	520	520
534 W	528,539	540
562 M	569	574
583 S	591	586
606 S	605	605

[a] Reference: S.F.A. Kettle and P.L. Strangelin, Inorganic Chemistry, Vol. 18, 2749 (1979)

[b] W=weak, M=medium, S=strong

made for liquid pyridine (Table 3)[32] The frequencies of the absorption bands for these cluster compounds compare well with the vibrational frequencies for uncomplexed pyridine. The correspondence of the spectral features between pyridine and complexed pyridine (or pyridyl) permits the use of liquid phase vibrational assignments for guidance as we interpret the spectral observations. The average frequency shift from liquid pyridine frequencies is calculated to be 13 cm^{-1} for the pyridine complex (1a). As would be expected the frequencies of the vibrations of the pyridyl fragment do not correlate as well to liquid pyridine frequencies with an average frequency shift of 27 cm^{-1}. However, qualitatively these infrared spectra confirm that the fingerprint regions for pyridine and pyridyl are reasonably similar if looked at with sufficiently low resolution, as is the case of a vibrational spectrum recorded using the technique of electron energy loss spectroscopy.

Room Temperature Adsorption of pyridine on Pt(111)

The electron energy loss spectrum recorded in the specular direction of pyridine adsorbed at room temperature onto platinum (the 111 surface) is shown in Figure 7a. Loss peaks listed in order of approximate decreasing intensity are observed at 1450, 1150, 740, 3080, 1570, 1230, and 1010 cm^{-1}. Perdeuteropyridine, similarly studied (Fig. 7b), displays loss peaks in the specular direction, in order of decreasing intensity, at 1330, 685, 2275, 1540, 860, 1230, and 1010 cm^{-1}. Table 4 lists these frequencies with their liquid phase counterparts, again we feel that their correspondence to liquid phase pyridine permit the use of liquid phase vibrational assignments as a

Table 3

Vibrational Assignment of $Os_3(CO)_{11}(NC_5H_5)$ and $HOs_3(CO)_{10}(NC_5H_4)$

(600 - 1650 cm^{-1})

Symmetry, Mode No.		Description	$NC_5H_5(NC_5D_5)^C$		$Os_3(CO)_{11}(NC_5H_5)$ h^5	(d^5)	$HOs_3(CO)_{10}(NC_5H_4)$ h^4	(d^4)
A_1	4 (8a)[B]	C-C, C-N Stretch	1583	(1554)	1613	(1571)	1592	(1554)
	5 (19a)	C-C, C-N Stretch	1483	(1340)	1490	(1346)	1459	(1339)
	6 (9a)	C-H in-plane bend	1218	(882)	1223	(896)	1222	(869)
	7 (18a)	C-H in-plane bend	1072	(823)	1075	(838)	1082	(869)
	8 (12)	asymmetric ring breathing	1032	(1014)	1050	(1042)	1057	(1055)
	9 (1)	ring breathing	991	(963)	1019	(979)	1029	(1000)
	10 (6a)	in-plane ring distortion	601	(579)	639	A	680	A
B_2	23 (5)	o.o.p. ring distortion	1007	(828)	1019	(838)	1029	(869)
	24 (10b)	o.o.p. ring distortion	936	(765)		(783)		(738)
	25 (4)	C-H o.o.p. bend	744	(631)	762	(650)	758	(680)
	26 (11)	C-H in-phase o.o.p. bend	700	(526)	710	(540)	745,740	(549)
	27 (16b)	ring o.o.p. distortion	403	(367)		A		A
B_1	13 (8b)	C-C, C-N stretch	1581	(1546)	1578	(1564)	1549	(1519)
	14 (19b)	C-C, C-N stretch	1442	(1303)	1452	(1328)	1421	(1298)
	15 (14)	C-C ring stretch	1362	(1046)				
	16 (3)	C-C in-plane bend	1227	(1226)			1269	(1216)
	17 (15)	C-H in-plane bend	1143	(856)	1161	(843)	1162,1117	(825)
	18 (18b)	C-H in-plane bend	1079	(835)	1075	(838)	1082	(869)
	19 (6b)	in-plane ring distortion	652	(625)	650	A	708	632

A. Hidden under more intense absorption bands from low frequency vibrations not due to the pyridine moiety.
B. Wilson Mode Numbers for Benzene
C. Colson, S.D., J. Phys. Chem. 88, 6067 (1984).

Figure 7. Electron energy loss spectrum of pyridine adsorbed on Pt(111) at room temperature and saturation coverage, a. NC_5H_5 b. NC_5D_5.

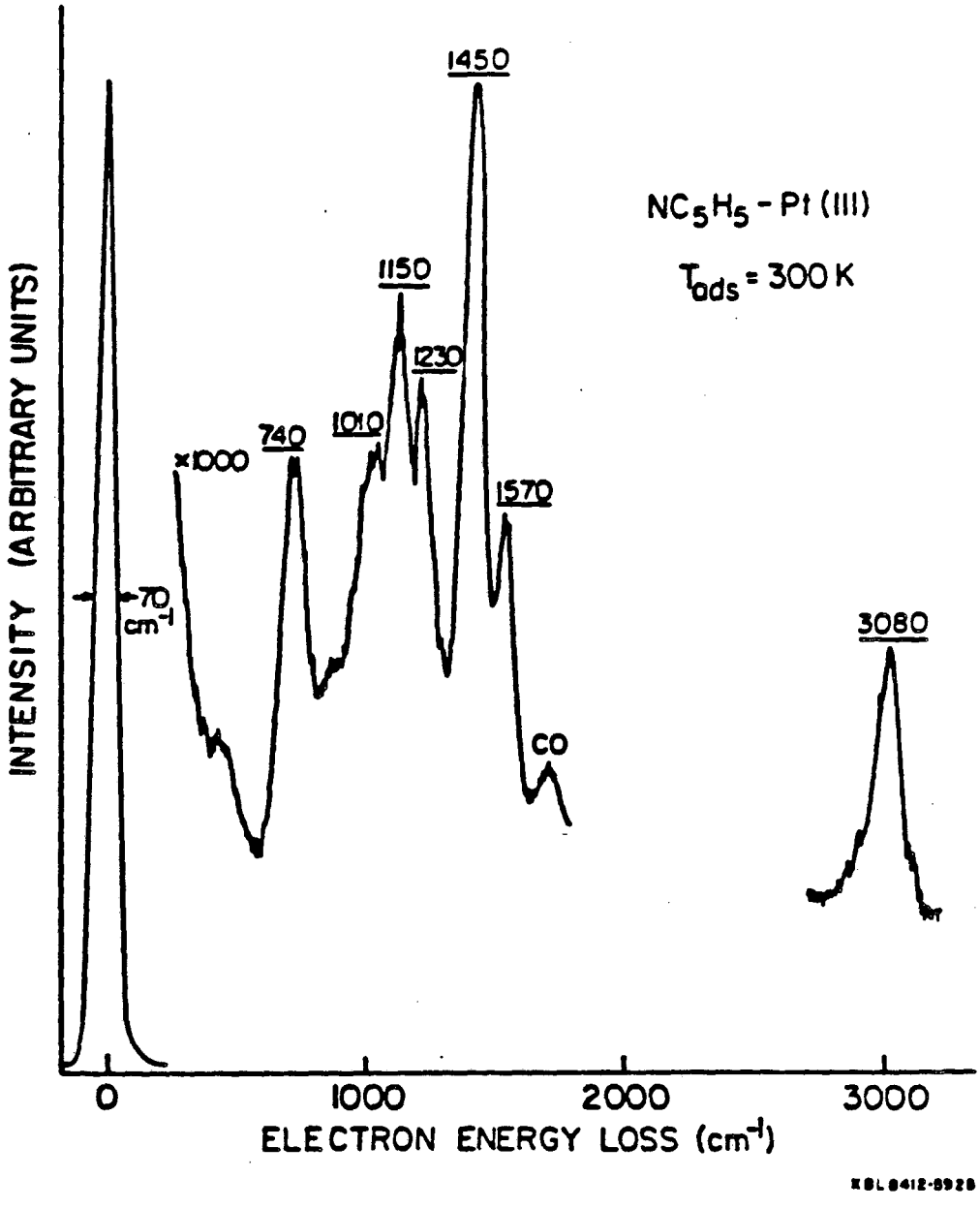
1450
1150
1230
1010
740
×1000
1570
3080
CO
70 cm⁻¹
NC5H5 - Pt (111)
Tads = 300 K
INTENSITY (ARBITRARY UNITS)
0
1000
2000
3000
ELECTRON ENERGY LOSS (cm⁻¹)
XBL 8412-8928

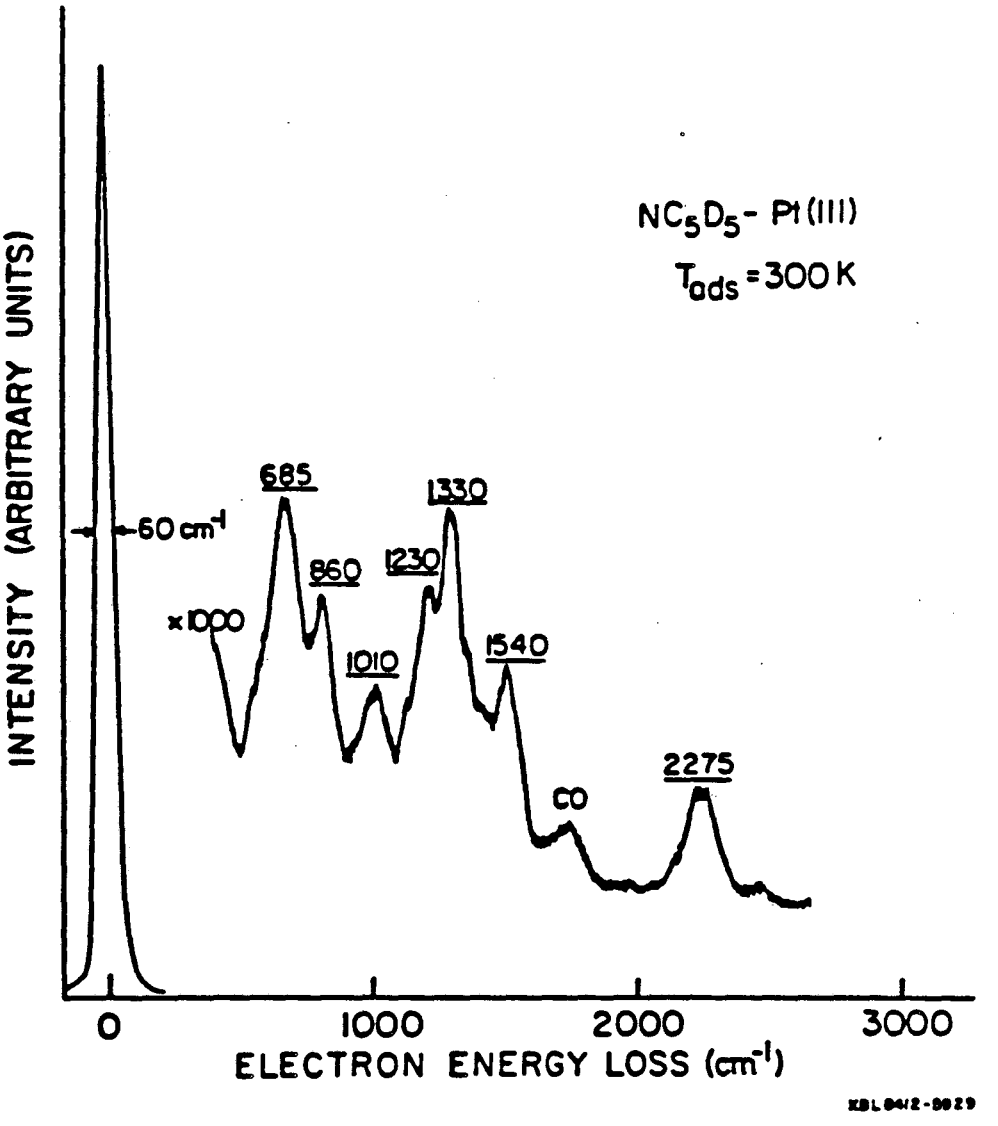
NC5D5 - Pt(111)
Tads = 300 K
INTENSITY (ARBITRARY UNITS)
60 cm-1
x1000
685
860
1010
1230
1330
1540
CO
2275
0
1000
2000
3000
ELECTRON ENERGY LOSS (cm-1)

Table 4

Vibrational Frequencies and Assignment for the Electron Energy Loss Spectra of Pyridine and d^5 Pyridine Adsorbed on on Pt(111)

Symmetry, Mode No.		Description	$NC_5H_5(NC_5D_5)$[A]		Pyridine-Pt(111) T=300K		Pyridine-Pt(111) T=120K	
					h^5	(d^5)	h^5	(d^5)
A_1	1 (2)[B]	C-H stretch	3094	(2302)	3080	(2275)	3070	(2270)
	2 (13)	C-H stretch	3072	(2276)	3080	(2275)	3070	(2270)
	3 (20A)	C-H stretch	3030	(2268)	3080	(2275)	3070	(2270)
	4 (8a)	C-C, C-N stretch	1583	(1554)	1570	(1540)	1610	(1570)
	5 (19a)	C-C, C-N stretch	1483	(1340)	1450	(1330)	1470	(1330)
	6 (9a)	C-H in-plane bend	1218	(882)	1150	(860)	1230	(830)
	7 (18a)	C-H in-plane bend	1072	(823)				
	8 (12)	asymmetric ring breathing	1032	(1014)	1010	(1010)	1050	(1010)
	9 (1)	ring breathing	991	(963)	1010	(1010)	1050	(1010)
	10 (6a)	in-plane ring distortion	601	(579)				
B_2	23 (5)	o.o.p. ring distortion	1007	(828)				
	24 (10b)	o.o.p. ring distortion	936	(765)				
	25 (4)	C-H o.o.p. bend	744	(631)				
	26 (11)	C-H in-phase o.o.p. bend	700	(526)			840	(580)
	27 (16b)	ring o.o.p. distortion	403	(367)				
B_1	11 (20b)	C-H stretch	3087	(2289)	3080	(2275)	3070	(2270)
	12 (7b)	C-H stretch	3042	(2256)	3080	(2275)	3070	(2270)
	13 (8b)	C-C, C-N stretch	1581	(1546)	1570	(1540)	1610	(1570)
	14 (19b)	C-C, C-N stretch	1442	(1303)	1450	(1330)	1470	(1330)
	15 (14)	C-C ring stretch	1362	(1046)				
	16 (3)	C-C in-plane bend	1227	(1226)	1230	(1230)	1230	(1250)
	17 (15)	C-H in-plane bend	1143	(856)	1150	(860)		
	18 (18b)	C-H in-plane bend	1079	(835)			1050	(830)
	19 (6b)	in-plane ring distortion	652	(625)	740	(685)	660	c
							νPT-N	(290)

A. Pyridine Frequencies and Assignments Taken From: Wiberg, K.B., Walters, V.A., Wong, K.N. and Colson, S.D., J. Phys. Chem. 88, 6067 (1984).

B. Wilson Mode #'s for Benzene

C. Loss Peak Not Observed at This Frequency, Most Probably Hidden Under More Intense Loss Peak at 580 cm^{-1}.

guide.

One of the most significant aspects to the spectrum in Figure 7 is the prominence of the loss at 3080 cm^{-1}. The frequency and the deuterium shift to 2275 cm^{-1} definitively identify the characteristic aromatic C-H stretching motion. Since C-H stretching modes are intrinsically in-plane vibrations, their intensity in the specular direction indicates that pyridine is not adsorbed with its skeletal plane parallel to the metal surface. This conclusion is strengthened by the high intensities observed in the spectral region 1000-1600 cm^{-1} where C-C stretching and C-H in plane bending modes occur. It is also consistent with the striking difference from the corresponding spectra of benzene[18] and toluene[33] on platinum (111) surfaces. These substances, when adsorbed, have EEL spectra with extremely weak loss features both in the C-H aromatic stretching region and in the, 1000-1600 cm^{-1} range.

The electron energy loss spectrum of two specifically labeled pyridines $4d^1$ pyridine and $2,6d^2$ pyridine adsorbed on Pt(111) at 300K have also been measured. In Figure 8 we show the EELS spectrum in the spectral region from 2000 to 3200 cm^{-1} for these two specifically labeled compounds along with the EELS spectrum for normal and perdeuterated pyridine in the same region for reference. There is a large difference in the intensities of the loss peaks associated with the C-D and C-H stretching motion between the two compounds $4d^1$ pyridine and $2,6d^2$ pyridine. The intensity of the loss peak at 2275 cm^{-1} (the C-D stretching mode) is very weak in the specular direction for $2,6d^2$ pyridine. The intensity of this loss peak increases when the sample is tilted 10° off the specular angle. Clearly this loss peak is non-

Figure 8. The carbon-hydrogen and carbon-deuterium stretching frequency region for specifically labeled pyridines, 4-d^1 pyridine and 2,6-d^2 pyridine are shown, in addition the perhydro and perdeuterated pyridine spectra are also shown for comparison.

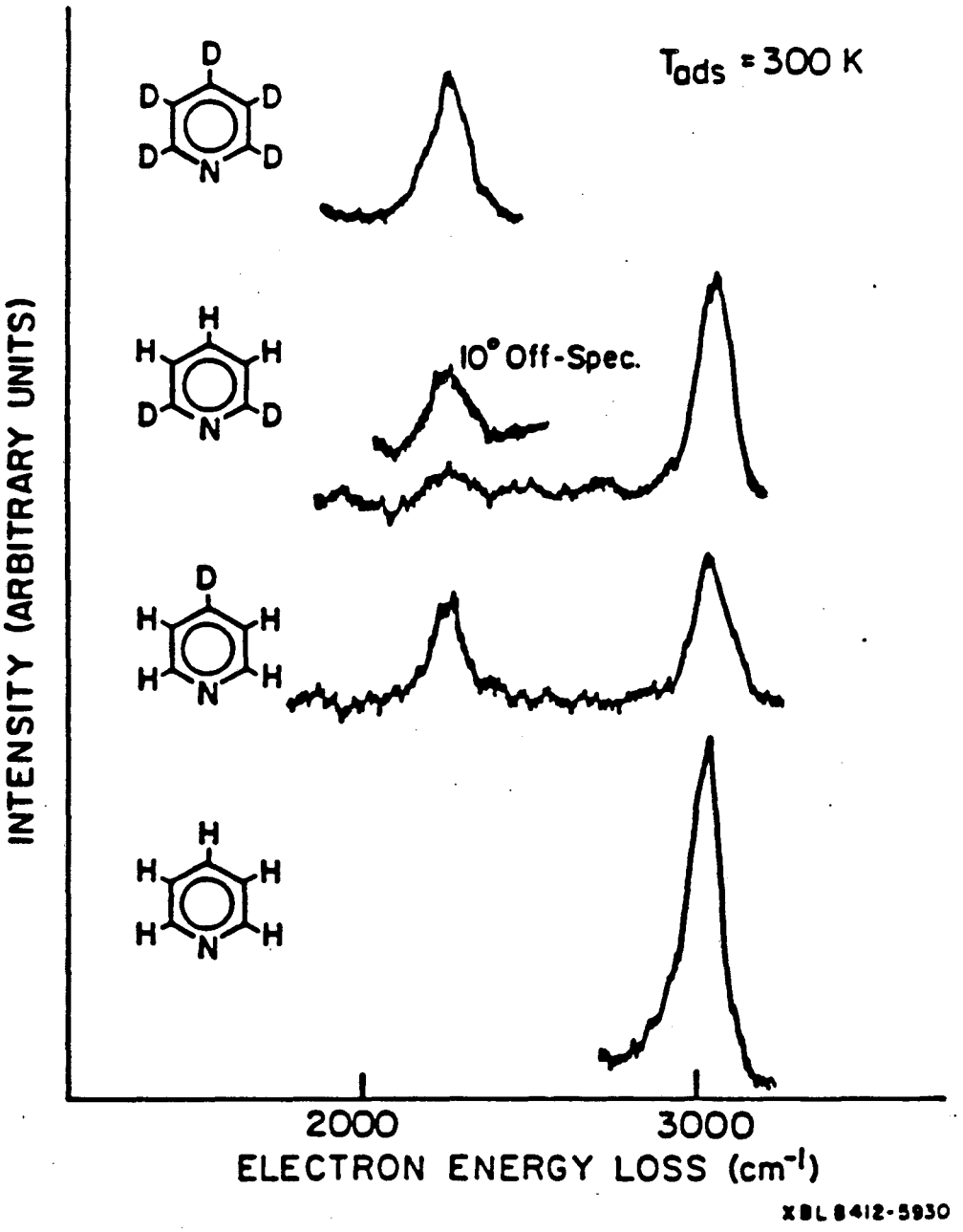
T_{ads} = 300 K
10° Off-Spec.
INTENSITY (ARBITRARY UNITS)
2000
3000
ELECTRON ENERGY LOSS (cm^{-1})
XBL 8412-5930

dipolar in nature. This is in contrast to $4d^1$ pyridine where there is a significant dipole contribution to the intensity of the loss peak. The results from these specifically labeled compounds will be useful in determining the orientation and adsorption geometry of the pyridine ring.

The thermal desorption spectrum of pyridine adsorbed on Pt(111) at room temperature is shown in Figure 9. This figure shows the trace of the parent ion which corresponds to an AMU of 79. There is one molecular desorption peak in the thermal desorption curve, this peak has a temperature desorption rate maximum at approximately 473K. As the coverage is increased the intensity of the peak also increases until saturation coverage is reached.

The decomposition of pyridine as monitored by the thermal desorption hydrogen curves for pyridine, d^5 pyridine, $4d^1$ pyridine, $2,6d^2$ pyridine, and $3,5d^2$ pyridine has been discussed previously.[26] For normal pyridine (NC_5H_5) there are three hydrogen peaks in the thermal desorption spectrum. The desorption rate temperature maxima for these peaks occur at approximately 335K, 515K, and 620K. Through the use of the specifically labeled pyridines it was determined that the low temperature hydrogen (deuterium) peak was due to carbon-hydrogen bond cleavage at the α-carbon only. The regiospecific bond breaking of the α carbon-hydrogen bond led the authors to suggest the formation of an α-pyridyl intermediate, although no spectroscopic evidence was available at that time. The intensity ratio of the hydrogen desorption peaks was 0.5:2:2 for the 335K, 515K, and 620K peaks, respectively. The deviation from unity by the low temperature peak was attributed to the observed of immediate hydrogen desorption upon pyridine adsorption. Our results on

Figure 9. Thermal desorption spectrum for pyridine adsorbed on Pt(111) at room temperature (monitoring the parent ion AMU=79) for molecular desorption. The heating rate was 25-30 degrees/sec in these thermal desorption experiments.

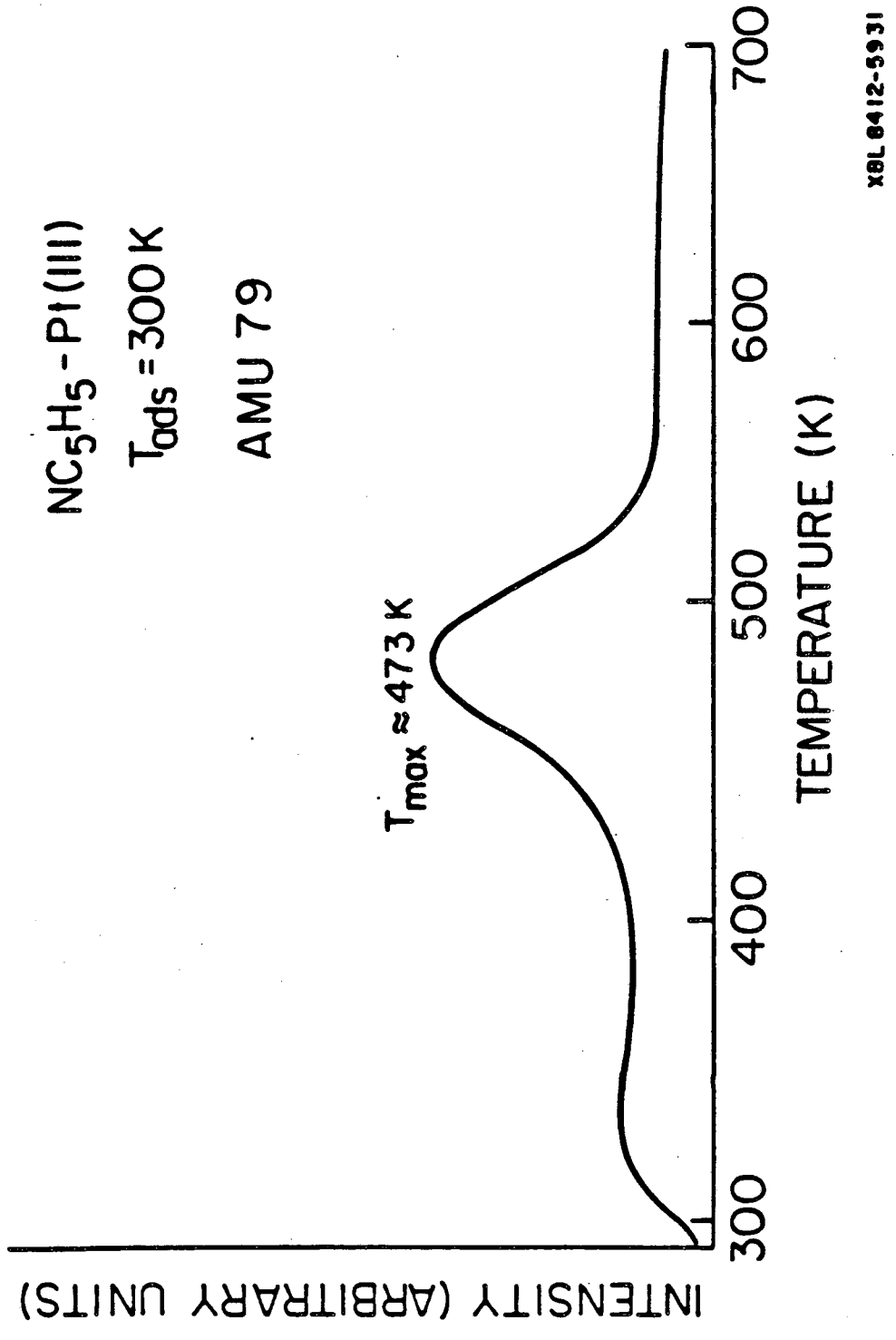
NC_5H_5-Pt(111)
T_{ads} = 300 K
AMU 79
$T_{max} \approx 473$ K
INTENSITY (ARBITRARY UNITS)
300
400
500
600
700
TEMPERATURE (K)
XBL 8412-5931

the decomposition of pyridine on Pt(111) is in qualitative agreement with these earlier results. Figure 12 shows H_2 desorption from low temperature pyridine adsorption, which will be discussed further in the next section. H_2 evolution for room temperature pyridine adsorption is similar except for the intensity of the first desorption maxima which is approximately one-half in the room temperature spectrum.

The amount of irreversibly bound pyridine can be calculated using the peak-to-peak height ratios of the carbon 272 eV Auger electron peak relative to the platinum 237 eV Auger electron peak. An Auger spectrum was taken after the crystal first was exposed to pyridine to reach saturation coverage which was then compared to the Auger spectrum taken after the thermal desorption experiment. The amount of carbon on the surface was calculated using equation (7).[34]

$$\frac{I(272)}{I(237)} \times 0.64 = \Theta_{carbon} \qquad (7)$$

The amount of pyridine which irreversibly adsorbs was calculated to be approximately 60% ± 5% for pyridine adsorbed at room temperature.

Low Temperature Adsorption of Pyridine on Pt(111)

The electron energy loss spectrum recorded for pyridine adsorbed on Pt(111) at 120K and saturation coverage is shown in Figure 10. This spectrum is substantially different than the spectrum for pyridine adsorbed at room temperature (see Fig. 7). Loss peaks are observed in order of approximate decreasing intensity at: 840, 1050, 3070, 1610, 1470, 660 and 1230 cm^{-1}. And for perdeuteropyrdine adsorbed on this platinum surface at 120K loss peaks are observed at 830, 580, 2270,

Figure 10. Electron energy loss spectrum of pyridine adsorbed on Pt(111) at 120K and a coverage of one monolayer, a. NC_5H_5 b. NC_5D_5.

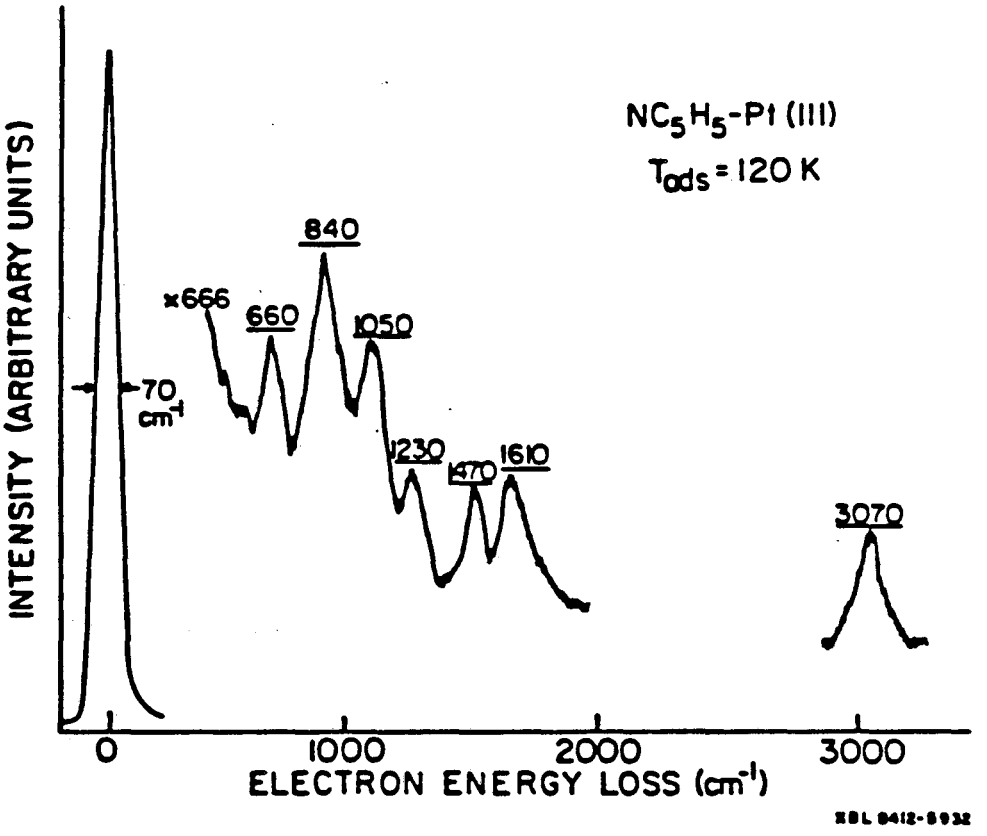
NC5H5-Pt (111)
Tads = 120 K
INTENSITY (ARBITRARY UNITS)
70 cm-1
x666
660
840
1050
1230
1470
1610
3070
0
1000
2000
3000
ELECTRON ENERGY LOSS (cm-1)
XBL 8412-8932

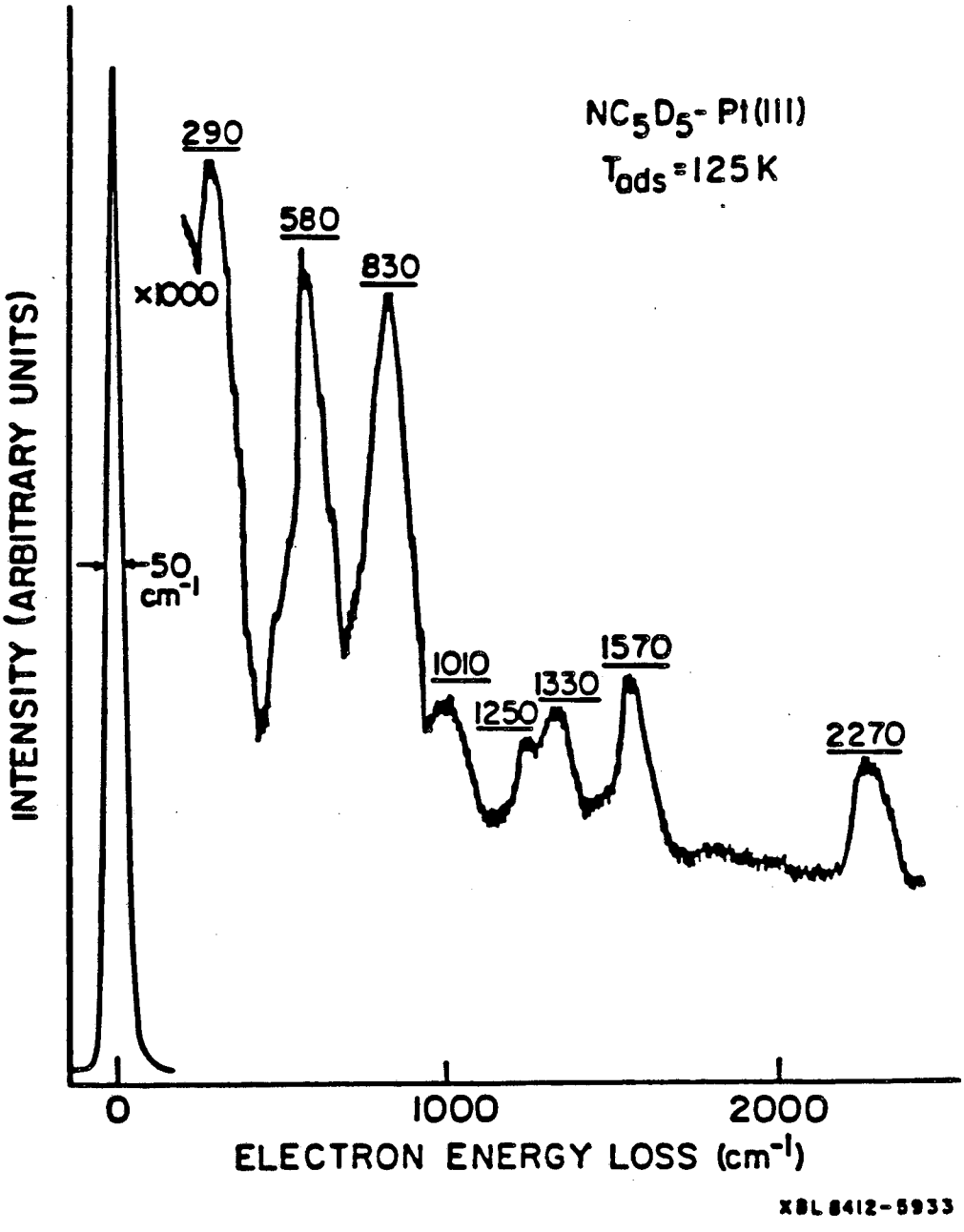
NC5D5- Pt(111)
Tads = 125 K
290
580
830
1010
1250
1330
1570
2270
×1000
50 cm-1
INTENSITY (ARBITRARY UNITS)
0
1000
2000
ELECTRON ENERGY LOSS (cm-1)
XBL 8412-5933

1570, 290, 1330, 1010 and 1250 cm^{-1}. For monolayer or submonolayer quantities of pyridine adsorbed on the Pt(111) surface at 120K we again find most of the modes observed in the specular direction can be characterized as primarily in-plane modes, as was seen in the room temperature spectrum. However, the relative intensities of the loss peaks differ greatly between spectra for room temperature and low temperature adsorption of pyridine. In addition to intensity differences between the EELS spectrum for pyridine adsorption at 120K and 300K we find no loss peak at 740 cm^{-1} in the low temperature EELS spectrum of normal pyridine. There are two new loss peaks observed in the low temperature spectrum at 660 cm^{-1} and 840 cm^{-1}. In Table 4 the vibrational frequencies for pyridine adsorbed on Pt(111) at 120K are compared to the vibrational frequencies for uncomplexed liquid or gas phase values of pyridine.

Figure 11 shows the thermal desorption spectrum of pyridine adsorbed at 120K, again monitoring the parent ion (AMU=79) as a function of coverage. At low coverages there are two molecular desorption peaks. As the coverage increases the intensity of the low temperature peak increases with coverage and the temperature of the rate maxima shifts to lower temperature. At low coverages (0.1 monolayers) T_{max} = 347K, the maxima shift to a T_{max} of 260K at saturation coverage. The high temperature peak with a T_{max} = 483K at Θ=0.11 shifts down to T_{max} = 450K at Θ=4.0. As the coverage increases a third desorption peak develops with a temperature desorption rate maximum at 190K. As the coverage is increased further, this is the only peak which increases in intensity.

The amount of pyridine which irreversibly adsorbs decreases when

Figure 11. Thermal desorption spectrum for reversible molecular desorption of pyridine adsorbed on Pt(111) at 120K as a function of coverage.

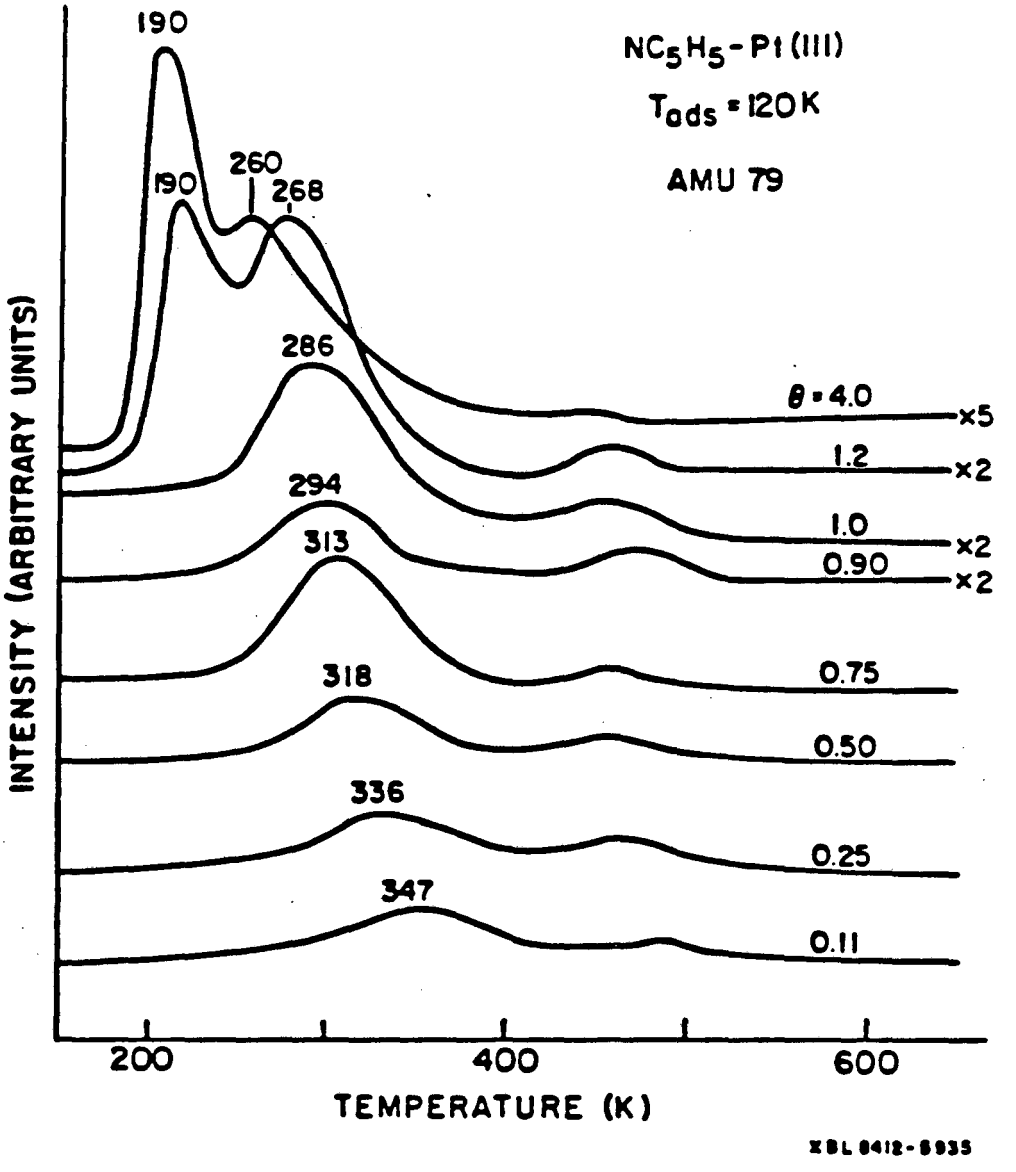
190
190
260
268
286
294
313
318
336
347
NC5H5-Pt(111)
Tads = 120K
AMU 79
θ = 4.0
x5
1.2
x2
1.0
x2
0.90
x2
0.75
0.50
0.25
0.11
INTENSITY (ARBITRARY UNITS)
200
400
600
TEMPERATURE (K)
XBL 8412-8935

pyridine is adsorbed at low temperatures. The amount of decomposition is calculated using equation 6 to be 25%. This is less then half the amount of irreversible desorption when pyridine is adsorbed at room temperature. The thermal desorption hydrogen curve, for saturation coverage, is shown in Figure 12. Three peaks are observed in the spectrum with temperature maxima of 335K, 515K, and 620K.

Toluene and Benzene - Pt(111)

The EEL spectra for benzene (T=140-300K) and toluene adsorbed on Pt(111) (T= 200-300K) have been reported previously.[18,33] In addition to the work already done we have recorded the electron energy loss spectrum of specifically labeled toluenes d^3 and d^5 adsorbed on Pt(111) at 300K. Figure 13 shows the C-H and C-D region for d^0, d^3, d^5, and d^8 labeled toluene. The electron energy loss spectra of perhydro toluene and benzene on Pt(111) are very similar. In Table 5 we list the frequencies of the loss peaks for benzene and toluene, both perhydro and perdeutero, chemisorbed on the platinum (111) surface face.

DISCUSSION

Pyridine Room Temperature Adsorption

The C_{2V} molecular symmetry of normal pyridine and d^5 pyridine breaks up the 27 fundamental modes of vibration into the irreducible representation as follows: $10a_1$, $3a_2$, $9b_1$, and $5b_2$ modes. The A_2 modes are Raman active only and the A_1, B_1, and B_2 modes are both infrared and Raman active. The A_2 and B_2 modes are out-of-plane modes and the 19 A_1 and B_1 modes are in-plane modes. The key question in this study is which modes will be active for pyridine adsorbed on the Pt(111)

Figure 12. Thermal desorption spectrum monitoring hydrogen evolution, AMU=2. Three hydrogen peaks are observed with temperature maxima at 335K, 515K and 620K.

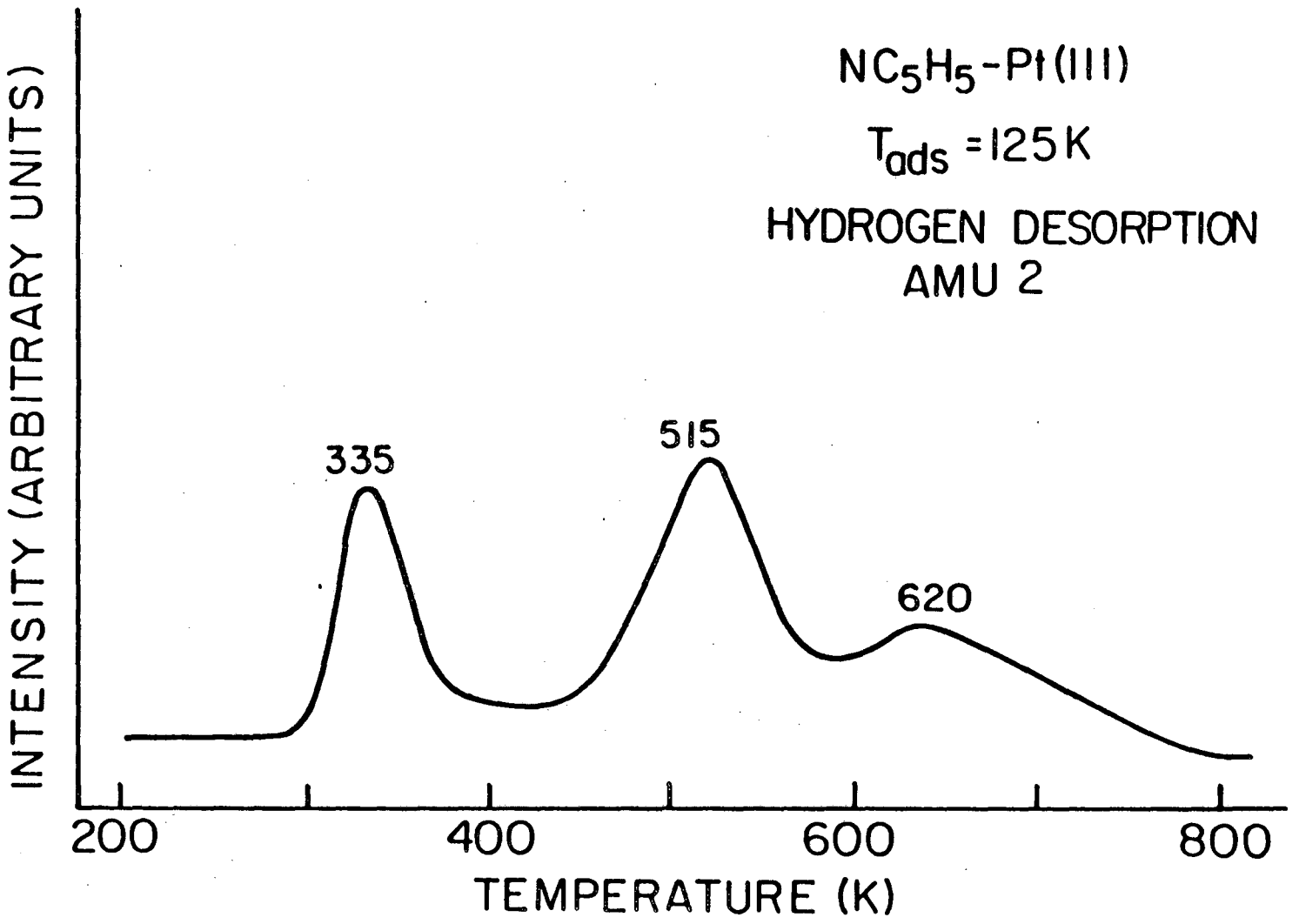

XBL 8412-5936

Figure 13. Electron energy loss spectra for d^0, d^3, d^5, d^8 toluene adsorbed on Pt(111) in the 2000 - 3000 cm^{-1} spectral region, at T=300K.

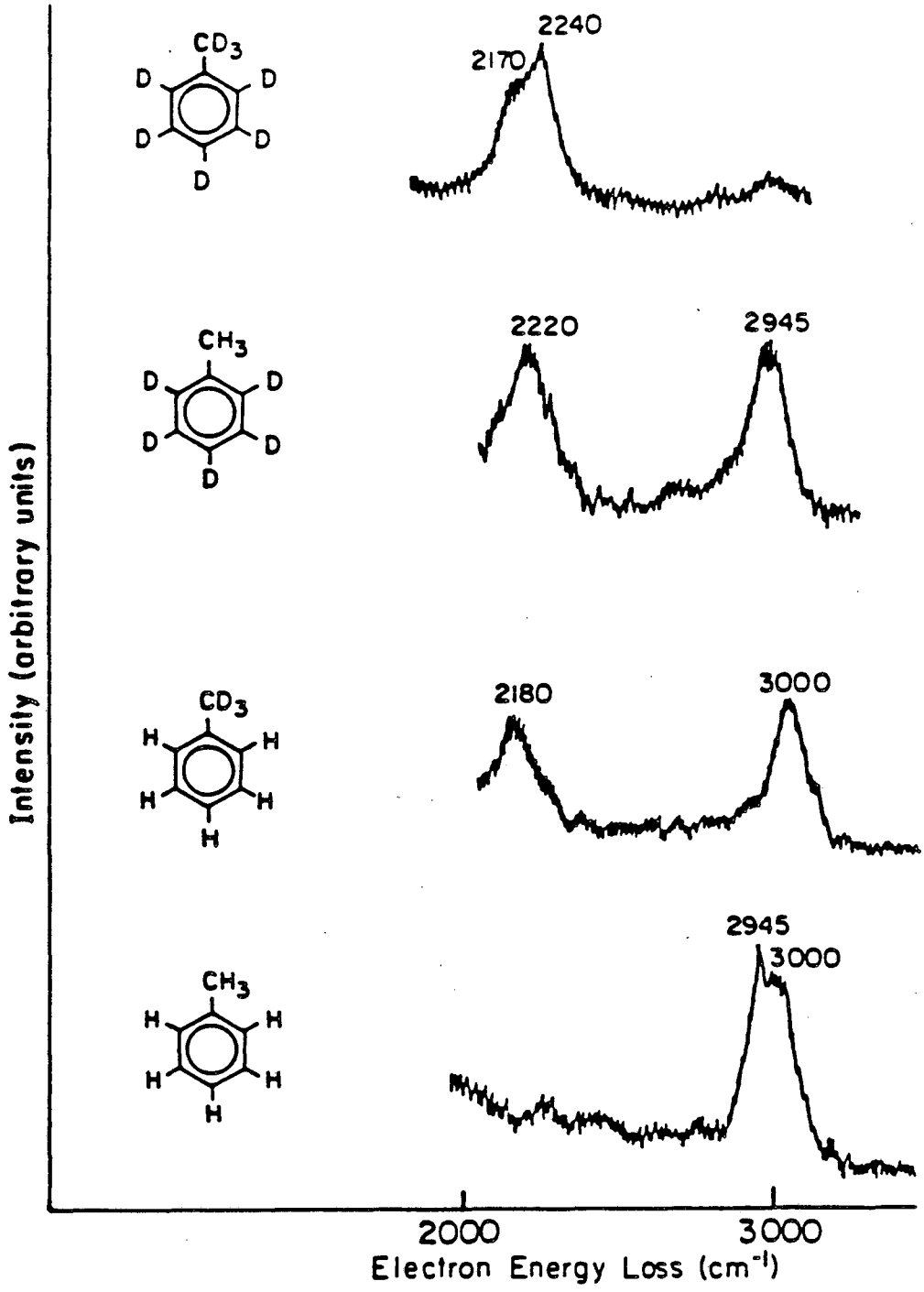
CD3
D
D
D
D
D
2240
2170
CH3
D
D
D
D
D
2220
2945
CD3
H
H
H
H
H
2180
3000
CH3
H
H
H
H
H
2945
3000
Intensity (arbitrary units)
2000
3000
Electron Energy Loss (cm-1)

XBL 863-7564

TABLE 5

VIBRATIONAL FREQUENCIES FOR BENZENE (d^0 and d^6) and TOLUENE (d^0 and d^8) ADSORBED ON Pt(111)

BENZENE-Pt(111)		TOLUENE-Pt(111)	
C_6H_6[a]	C_6D_6[a]	$C_6H_5CH_3$[b]	$C_6D_5CD_3$[b]
360(m)	350(m)	355(m)	340(m)
570(m)	n.o.	550(m)	n.o.
830(s)	610(s)	830(s)	615(s)
920(s,sh)	700(s,sh)	910(s,sh)	700(s,sh)
		1015(m)	1010(m)
1130(w)	800(w,sh)	1155(w)	805(m)
1420(m)	1350(m)	1435(m)	1350(m)
		2945(m)	2170(m)
3000(mw)	2240(mw)	3000(m)	2240(m)

a. Frequencies taken from reference 18.
b. Frequencies from this laboratory, in agreement with reference 33.

surface. To answer it, we take advantage of the fact that the infrared spectra recorded for the two cluster compounds $Os_3(CO)_{11}(NC_5H_5)$ and $Os_3(CO)_{11}(NC_5H_5)$ were similar enough in the 600-1650 cm^{-1} region for the use of liquid pyridine absorption frequencies in the interpretation of orientation of the molecule on the surface regardless of whether it is pyridine or pyridyl on the surface. The EELS active modes will be dependent on the adsorption site and the orientation of the molecule on the surface. The surface normal dipole selection rule states that only modes which are totally symmetric with respect to all symmetry elements (A_1 modes) will be dipole active and therefore be strongly dependent on scattering angle. The intensity of those loss peaks will be at a maximum in the specular direction in the EELS spectrum if there is a significant dipole scattering contribution to the cross section of the loss peak. The symmetry of the pyridine-platinum complex can retain the C_{2V} symmetry of molecular pyridine or it can be reduced to C_S symmetry. If the pyridine molecule was nitrogen bonded to the surface and tilted at some angle away from the surface or lying in a flat configuration π-bonded parallel to the surface the only symmetry element would be the mirror plane perpendicular to the molecular plane that bisects the nitrogen atom and the C-H unit in the 4 position. If there was partial decomposition of the pyridine molecule to form a pyridyl fragment, (NC_5H_4), the point group symmetry of the pyridyl fragment would again be C_S but now the molecular plane would be the mirror plane. In this case both the A_1 and B_1 irreducible representations of the C_{2V} point group would be lowered to the A' irreducible representation of the point group C_S and the vibrations of this representation would be "EELS allowed".

In Table 4 we show the frequencies for the normal modes of vibration of uncomplexed pyridine and compare these frequencies to the frequencies observed in the electron energy loss spectrum for pyridine adsorbed at 300K on the Pt(111) surface. Due to the poor resolution of EELS the frequencies of some of the modes have been used more than once in assigning the spectrum of adsorbed pyridine. Also some of the vibrations which are inherently weak transitions (i.e. weak absorption bands in the infrared spectrum of liquid phase pyridine) are not observed. There is some uncertainty in the assignment of the loss peak at 740 cm^{-1} in the pyridine EELS spectrum. This loss peak might be assigned to either of the strong absorptions at 700 cm^{-1} (ν_{26}) or 744 cm^{-1} (ν_{25}) for pyridine in the liquid phase which are assigned to out-of-plane motions of a pyridine. However, the corresponding loss peak in the NC_5D_5 spectrum (Fig. 7b) at 685 cm^{-1} displays a deuterium shift by a factor of only 1.08, much smaller than those displayed for liquid pyridine, 1.18 for ν_{25} amd 1.33 for ν_{26}. Hence, the 740 cm^{-1} loss peak is assigned to the B_1 ν_{19} mode which implies that this mode shifts up in frequency by 13%. In the pyridyl molecular complex the ν_{19} mode is assigned to the band at 708 cm^{-1} and is therefore also shifted to higher frequency, here by 9%. It is unclear why this low frequency in-plane ring deformation would be more perturbed than other in-plane ring modes in the pyridyl structure. A detailed force-field coordinate analysis would perhaps answer this question.

As noted previously there are intense in-plane modes in the electron energy loss spectrum for pyridine adsorbed at 300K on the Pt(111) surface. As shown in Table 4 the modes observed in this spectrum are modes of A_1 and B_1 type symmetry, i.e. in-plane modes.

These in-plane modes have high intensity at the specular angle, so they are the one with significant dipole derivatives perpendicular to the platinum surface.

The results for the specifically labeled pyridines support the proposal of the presence of a pyridyl fragment on the surface at room temperature. If only a dipolar contribution to the intensities of the loss peaks for the C-D stretching modes and the C-H stretching modes is considered in the specular direction, the expected intensity ratio for the C-H stretching mode relative to the C-D stretching mode depends upon the component of $\frac{d\mu}{dr}$ perpendicular to the metallic surface and the fact that $\text{Intensity}_{(C-H)} \simeq 2\text{Intensity}_{(C-D)}$. For a "stand-up" geometry with the N-Pt bond perpendicular to the metallic surface, this ratio $\frac{I_{C-H}}{I_{C-D}}$ is predicted to be 4 for both the 2,6-dideutero and 4-monodeutero pyridines. For a geometry with one of the N-C bonds parallel to the metallic surface, the ratio $\frac{I_{C-H}}{I_{C-D}}$ is predicted to be infinity for the 2,6-dideuteropyridine (one of the deuterium atoms being lost to form an α C-Pt bond) and it would be 2 for the 4-monodeutero pyridine. The spectra in Figure 2 show for the 2,6-dideutero pyridine a very small C-D feature (at specular reflection) with a ratio $\frac{I_{C-H}}{I_{C-D}} = 10$. For the 4-monodeutero pyridine the experimental ratio is about 1.5. Thus the spectra distinctly favor the parallel N-C bond geometry with the loss of an α hydrogen to permit platinum bonding to both the nitrogen and one of the α carbon atoms.

In the case of room temperature adsorption of pyridine on Pt(111) the predominant reaction scheme proposed based on the evidence presented is:

$$NC_5H_5(g) + Pt(111) \xrightarrow{T = 300K} NC_5H_4 - Pt(111) + H\text{-}Pt(111)$$

$$2H - Pt(111) \xrightarrow[(T > 300K)]{\Delta} H_2(g)$$

$$2NC_5H_4 - Pt(111) \xrightarrow[(T > 425K)]{\Delta} NC_5H_5(g) + 3/2\ H_2(g) + Pt(111) - N,5C$$

An α-pyridyl species is formed upon pyridine adsorption on the Pt(111) surface. Atomic hydrogen on the surface desorbs as H_2 with a T_{max} = 335K. The pyridyl structure was determined by electron energy loss spectroscopy to be stable up to a temperature of 425K. When the temperature is increased above 425K, disproportionation must occur, as revealed by the desorption of molecular pyridine (see Figure 9). Some pyridyl fragments undergo further decomposition. The available hydrogen from this process can then recombine with a remaining pyridyl fragment which then desorbs as molecular pyridine (AMU = 79). Although hydrogen evolution peaks at a somewhat higher temperature (T_{max} = 515K (see Figure 12)) then the pyridine desorption peak (T = 473K), the two processes, decomposition and desorption, begin at about the same temperature, near 425K.

Low Temperature Adsorption

The assignment for low temperature monolayer or submonolayer pyridine covered surface is also given in Table 4. The loss peak observed at 660 cm^{-1} is assigned to the ν_{19} ring deformation mode, close to the liquid phase value, 652 cm^{-1}, but distinctly different from 740 cm^{-1} in the room temperature spectrum. The loss peak at 840 cm^{-1} (which shifts to 580 cm^{-1} for d^5 pyridine) is assigned to the ν_{26} mode which corresponds to an in-phase out-of-plane bending motion. The increase of

the C-H out-of-plane bending mode relative to the frequency of the free molecule is also observed for benzene adsorbed on Pt(111)[22] (see discussion on benzene adsorption). The plane of the pyridine molecules is tilted from the surface plane as is suggested by the relative intensities of the in-plane modes. Although the pyridine ring is tilted away from the surface plane there is still an appreciable interaction with the surface metal d orbitals and the π and π^* orbitals of pyridine, and perhaps a rehybridization of the molecule. This can be seen by the increase in frequency of the C-H out-of-plane bend from 700 cm^{-1} for liquid pyridine to 840 cm^{-1} for pyridine adsorbed on Pt(111) at 120K. At saturation coverage, a value of 52° has been calculated for the angle between the pyridine ring and the Pt surface plane from Near Edge X-Ray Absorption Fine Structure data.[35] This is consistent with the electron energy loss spectroscopy results presented here. The bonding of pyridine to the surface at low temperatures appears to be through both the lone pair of electrons which are localized on the nitrogen atom and the delocalized molecular π orbitals on the ring. The lowest energy configuration is then a combination of these two different modes of bonding. The bonding configuratons, as derived from EELS and NEXAFS, of pyridine adsorbed at both low and room tempertures are depicted in Fig. 14.

The thermal desorption spectrum for pyridine adsorbed on Pt(111) at a temperature of 120K shows three molecular desorption peaks. The low temperature (190K) peak which begins to appear only at coverages greater than a monolayer is attributed to the desorption of multilayer pyridine. Using Redheads equation for first-order reaction kinetics,[8] and assuming a pre-expotential factor of 10^{13} sec^{-1}, for a temperature

Figure 14. The adsorption of pyridine is dependent on temperature. The proposed adsorption structures for pyridine adsorbed at 120 and 300K on Pt(111) are shown. The angle between the ring plane of pyridine and the surface plane has been calculated to be 52 and 85 degrees for the low and room temperature structures from NEXAFS data (see reference 35).

PYRIDINE ADSORPTION GEOMETRY ON THE Pt(111) SURFACE

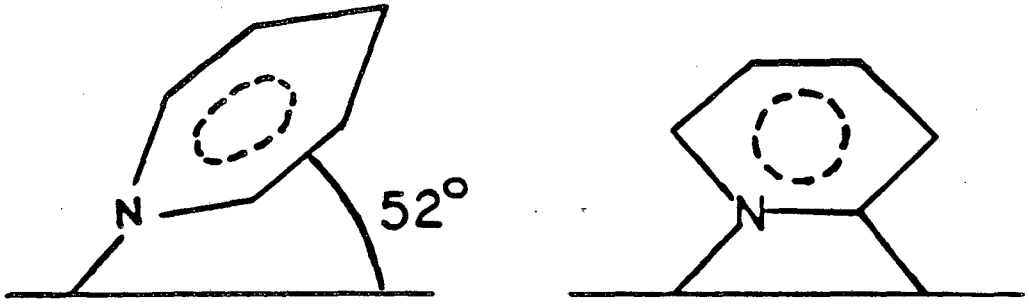

Pt Pt

T = 120K T = 300K

maximum of 190K the desorption energy was calculated to be 10.8 kcal/mole. The second molecular pyridine desorption peak has a temperature maximum which is coverage dependent (low coverages T_{max} = 347K; saturation coverage T_{max} = 260K), such behavior could be caused by a second order desorption process which follows second order reaction kinetics or a first order desorption process with an energy of activation that is coverage dependent. A first-order process with a coverage dependent energy of activation is the more probable cause of the variaton of the temperature maximum as a function of coverage, due to the low mobility of the pyridine molecule at these temperatures. Again using a pre-exponential factor of 10^{13} sec^{-1} the energy of activation at low coverages is calculated to be 21.8 kcal/mole while at saturation coverage the energy of activation drops to 15.0 kcal/mole. The high temperature molecular desorption peak with a desorption rate maximum centered at T=483K at Θ=0.11L which shifts to T=450K at Θ=4.0L is the only molecular desorption peak for pyridine adsorbed at room temperature. This peak discussed previously for room temperature results corresponds to the disproportionation of a NC_5H_4 fragment with a hydrogen atom which then desorbs as molecular pyridine.

For low temperature adsorption when the substrate is warmed the following reaction scheme is deduced:

$$NC_5H_5(g) + Pt(111) \xrightarrow{T = 120K} NC_5H_5 - Pt(111)$$

$$2NC_5H_5 - Pt(111) \xrightarrow{\Delta} NC_5H_5(g) + H\text{-}Pt(111) + NC_5H_4 - Pt(111)$$

$$2H - Pt(111) \xrightarrow{\Delta} H_2(g)$$

$$2NC_5H_4 - Pt(111) \xrightarrow{\Delta} NC_5H_5(g) + 3/2\ H_2(g) + Pt(111) - N,5C$$

Initally the pyridine adsorbs on the surface through the nitrogen atom, which presumably acts as a convential electron donor. Then as the sample is warmed some pyridine desorbs molecularly, with the temperature maximum of the desorption rate depending on the initial coverage. At saturation coverage approximately 50% of the pyridine desorbs from the surface at 260K. The remaining adsorbed pyridine molecules fragment to form the pyridyl-surface complex at ~T=300K. On further heating the behavior is identical to that observed for pyridine adsorbed at room temperature. The recombination of a hydrogen atom and a NC_5H_4 fragment then recombine and desorb to desorb as molecular pyridine at temperatures greater than 400K. The amount of pyridine desorbing in this high temperature peak and the amount of decomposition is less when pyridine is adsorbed at low temperature. This supports the earlier conclusion that disproportionation of the pyridyl complex occurs when the temperature is raised above 400K.

The infrared spectra for the two cluster compounds provide additional supportive evidence for the proposed structure of pyridine adsorbed on Pt(111) at 120K and 300K. The absorption bands of the pyridine and pyridyl complexes which shift the most in frequency are the ones that offer the best differentiation, but superimposed on that must be the certainty with which the assignment can be made. Based on these criteria ν_5 and ν_{14} at 1483 cm^{-1} and 1442 cm^{-1} for liquid pyridine, are the bands which are chosen first for the cluster-surface comparison. The difference in frequency of these two vibrational modes when comparing the pyridine complex to that of the pyridyl is +31 for both ν_5 and ν_{14}, i.e. $\Delta\nu = (\nu_{\text{pyridine cluster}} - \nu_{\text{pyridyl cluster}}) = +31\ cm^{-1}$ for each of these two modes. If this is now compared to the loss peaks in

the EEL spectra for pyridine adsorbed at 120K, where we contend there is an intact pyridine on the surface, to that of pyridine adsorbed at 300K, where we contend decomposition of pyridine to form a pyridyl fragment occurs, a similar increase of +20 cm^{-1} is observed in this region for the 120 K spectrum (ν_5 and ν_{14} are not resolved in the EEL spectrum). Following this comparison with modes ν_4 and ν_{13} observed at 1583 cm^{-1} and 1581 cm^{-1} for liquid pyridine respectively, the pyridine complex is +21 and +29 cm^{-1} higher in frequency relative to the pyridyl complex for these modes. Again a similar increase in frequency of these modes are observed for the 120K EEL spectrum of +40 cm^{-1} relative to the 300K spectrum.

The in-plane ring distortion mode ν_{19} at 652 cm^{-1} in pyridine shifts very little in the pyridine complex at 650 cm^{-1}. In the EELS spectrum for pyridine adsorbed at 120K this mode is assigned to the loss peak at 660 cm^{-1} which is similary unperturbed relative to liquid pyridine. In the pyridyl complex this mode shifts dramatically to 708 cm^{-1}, an increase of 56 cm^{-1} relative to the liquid pyridine value. As noted previously a similar behavior is observed for pyridine adsorbed at room temperature, the ν_{19} mode has been assigned to the loss peak at 740 cm^{-1}. Table 6 lists the shift in frequencies of these modes which offer the greatest distinction between pyridine and pyridyl. Lastly there is a large increase in the intensity of the adsorption in the perdeutero pyridine complex in the 800 cm^{-1} region shifted from the 1100 to 1200 cm^{-1} region in the perhydro pyridine cluster compound. A similar increase is observed in the 800 cm^{-1} region for low temperature perdeutero pyridine EEL spectrum.

Concluding, surface chemistry of pyridine on Pt(111) has been

Table 6

COMPARISON OF INFRARED SPECTRA OF $Os_3(CO)_{11}(NC_5H_5)$ AND $HOs_3(CO)_{10}(NC_5H_4)$ TO THE ELECTRON ENERGY LOSS SPECTRA OF PYRIDINE ADSORBED ON Pt(111) at 120 and 300 KELVIN

MODE	INFRARED $[Os_3(NC_5H_5) - HOs_3(NC_5H_4)]$[a]	EELS [120 - 300 K]
ν_5 (1483)	+31	+20[b]
ν_{14} (1442)	+31	
ν_4 (1583)	+21	+40
ν_{13} (1581)	+29	
ν_{19} (652)	-58	-86

a. $Os_3(NC_5H_5) = Os_3(CO)_{11}(NC_5H_5)$ and $HOs_3(NC_5H_4) = HOs_3(CO)_{10}(NC_5H_4)$

b. Modes ν_5 and ν_{14}, as well as ν_4 and ν_{13}, are not resolved in the EEL spectra

studied as a function of temperature. We have shown in the case of room temperature adsorption that there is partial decomposition of the pyridine molecule with an α-hydrogen abstracted, thereby forming a pyridyl surface species. For low temperature adsorption, pyridine adsorbs molecularly with the ring plane tilted toward but not parallel to the surface plane. A new reaction channel is seen for low temperature adsorption from the thermal desorption data. As the temperature is increased from 120K to approximately 260K (this temperature is dependent on the initial pyridine coverage) 50% of the pyridine desorbs as molecular pyridine. The remaining pyridine molecules form a pyridyl surface complex at about room temperature. Figure 14 shows the proposed adsorption structure of pyridine on Pt(111) at 300K and 120K. The infrared spectra recorded for $Os_3(CO)_{11}(NC_5H_5)$ and $HOs_3(CO)_{10}(NC_5N_4)$ aided in the interpretation of the EELS data for the pyridine-platinum system.

Pyridine chemisorption at both low- and room- temperature on Pt(111) has been shown to involve the nitrogen lone pair in bonding to the surface. In the case of benzene and toluene adsorption the bonding to the surface must be dissimilar in that respect to pyridine. The electron energy loss spectrum recorded for benzene adsorbed on Pt(111) was first reported by Lehwald et. al..[18] The toluene EEL spectra is similar to the benzene spectra and as one would expect very different from the pyridine EEL spectrum on this surface.

Benzene and Toluene - Pt(111)

The spectrum for less than a monolayer quantity of benzene does not change in the 140-320K temperature range. Similarly, the electron energy loss spectrum does not change in the 200-300K range for toluene

adsorbed on this surface.[33] The frequencies of the loss peaks observed in the EELS spectrum for both benzene and toluene on this surface is listed in Table 5.

The largest discrepancy in the correlation between liquid and chemisorbed frequencies of benzene is in the C-H out-of-plane bending motion which occurs at 673 cm^{-1} for liquid benzene. The shift, when C_6H_6 is adsorbed on Pt(111), to 830 and 920 cm^{-1} (these two values have been interpreted in terms of two different adsorption sites), is 157 and 247 cm^{-1} higher, respectively. This enormous shift indicates a structural change of the benzene molecule from its planar D_{6h} structure, when adsorbed on this platinum surface. The large perturbation in the frequencies of the normal modes for benzene when adsorbed on platinum is indicative of a strong interaction of the molecule with the platinum surface.

We propose a new structure, based on the electron energy loss spectrum, for benzene adsorbed on the Pt(111) surface. For benzene chemisorbed on Pt(111) we propose that the six carbon-carbon bonds are no longer equivalent, as in the gas phase, but now consist of two double bonds and four single bonds. This is similar to the structure of benzene in its first excited triplet state. The structure proposed is shown in figure 15.

Carbon atoms 3 and 6 are covalently bonded to the platinum surface. There are two double bonds, between carbon atoms 1 and 2 as well as 4 and 5, and four carbon-carbon single bonds , i.e., 2 "short" and 4 "long" bonds. The bridge site shown offers the best geometrical fit for this structure, if we assume bond distances of 1.54Å and 1.34Å for a C-C single and double bond, respectively, and a Pt-Pt interatomic distance

of 2.76Å.

The structure proposed is also comparable to the structure of 1,4-cyclohexadiene. If we compare the infrared spectra of benzene and 1,4-cyclohexadiene in the liquid phase to the EELS spectrum of benzene on Pt(111) (Table 7) we see the 1,4 cyclohexadiene structure is clearly favored. Smaller shifts are observed for most of the modes when comparing to observed frequencies for benzene chemisorbed on Pt(111). For toluene adsorption on the Pt(111) surface an analagous comparison could be made to the IR spectra of 1,4 3-methyl cyclohexadiene and 1,4 1-methyl cyclohexadiene.

We must consider whether this structure is energetically feasible. The delocalization or resonance energy is shown to be 36 kcal/mole for gas phase benzene. We must account for this loss in energy when considering the above adsorption structure. This loss in resonance energy must be made up for in the two Pt-C bonds, i.e. the bond energy, D_{Pt-C}, of each must be greater than 33 kcal/mole, ((resonance energy + 1 double bond)/2) =((36+60)/2)kcal/mole)[36]. There is a limited amount of thermochemical data for metal-carbon bond dissociation energies on surfaces. However, ≈48 kcal/mole is a reasonable value for a metal-carbon bond energy in organometallic complexes.[37] In the case of pyridine adsorption at 300K the alpha C-H bond is cleaved, resulting in the formation of an alpha-pyridyl species. Here again we must consider whether the energetics are favorable for the formation of an alpha-pyridyl species. The C-H bond is approximately 100 kcal/mole, and the H-Pt bond from thermal desorption spectroscopy has been determined to be 57 kcal/mole.[38] This reaction is also entropically favored and proceeds readily at room

Figure 15. Adsorption structure of benzene on Pt(111) at room temperature. The loss of aromaticity is attributed to the formation of two strong Pt-C bonds.

BENZENE ADSORPTION GEOMETRY ON THE Pt(111) SURFACE

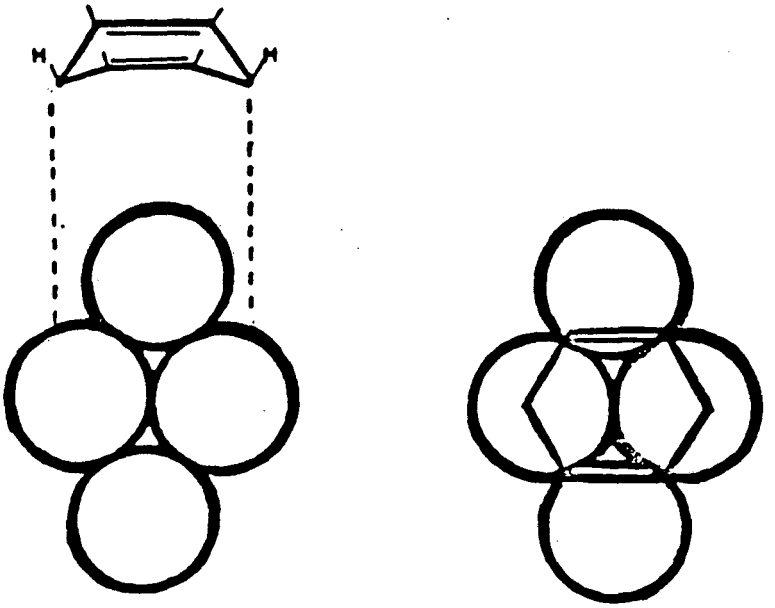

TABLE 7

Comparison of Vibrational Frequencies for Liquid Benzene.

Liquid 1,4-Cyclohexadiene and Benzene Chemisorbed on Pt(111)

$\Delta\nu$[a]	Benzene[b]	Benzene-Pt(111)[c]	1,4-Cyclo-hexadiene[d]	$\Delta\nu$[e]
+164	404	570(m)[f]	620(s)	-50
+157	673(vs)	830(vs)[g]	883(vs)	-53
+247	673(vs)	920(s)[g]	959(s)	-39
-20	1150(w)	1130(mw)	1178(w)	-38
+100	1320(w)	1420(m)	1430(m)	-10
-62	3062(m)	3000(mw)	2860(s)	+140
			3040(s)	-40

a. $\Delta\nu = (\nu_{C_6H_6\text{-Pt(111)}} - \nu_{C_6H_6})$

b. Frequencies taken from reference 42.

c. Frequencies taken from reference 18

d. Frequencies taken from The Coblentz Society, Molecule No.5627.

e. $\Delta\nu = (\nu_{C_6H_6\text{-Pt(111)}} - \nu_{C_6H_8})$

f. This has been previously assigned to a metal-carbon stretch, but there was some uncertainty in that assignment

g. These two peaks were assigned to the same mode for two different adsorption sites,(See Ref. 18).

temperature. Thus, the Pt-C bond energy would need to be at most 43 kcal/mole for this reaction to proceed.

The surface chemistry of hydrocarbons chemisorbed on palladium surfaces under ultra-high vacuum (UHV) conditions appears to be quite complex and very different from Pt surface chemistry. The hydrogenation of many different unsaturated hydrocarbons, when coadsorbed with hydrogen, has been demonstrated under UHV conditions to occur readily on the Pd(111) and Pd(100) surface faces[39](e.g. ethylene to ethane, acetonitrile to ethylamine and norbornadiene to norbornane). The extent of hydrogenation reactions on palladium, i.e. yields and variety of hydrocarbons which will hydrogenate, is special for the Ni, Pd, Pt series and for group VIII metals in general in this low pressure regime (See Ref. 39). Another extremely interesting reaction which has been observed on all three low Miller index planes of palladium (111,110,100) is the trimerization of acetylene to benzene.[40] The yield of this reaction is dependent upon the crystallographic plane, with the (111) surface having the greatest acetylene to benzene conversion. The hexagonal symmetry of the (111) face presumably orients the molecules favorably for this reaction to occur, causing an increase in the benzene yields. This reaction has been proposed to occur on the Ni(111) surface[41] based on electron energy loss data but does not occur on Pt(111), nor has the reaction been observed on any platinum surface thus far. These special reaction pathways for molecules adsorbed on Pd surfaces have prompted us into a vibrational study of molecules adsorbed on Pd(111) as discussed next.

2. RESULTS AND DISCUSSION

B. BENZENE, TOLUENE AND PYRIDINE ADSORBED ON Pd(111)

Benzene

The electron energy loss spectrum of benzene (C_6H_6) adsorbed on Pd(111) at 180K is shown in figure 16a. The spectrum recorded in the specular direction shows an intense loss peak at 695 cm^{-1} and a much weaker feature at 3050 cm^{-1}. The EEL spectrum of perdeuterobenzene (recorded in the specular direction) is shown in figure 16b. The two loss peaks corresponding to vibrations associated with C_6D_6, are observed at 505 cm^{-1}(vs) and 2280 cm^{-1}(vw). The deuterium shifts are 1.38 and 1.34, respectively, for these two peaks. The assignment of the bands is given in Table 8. The agreement between IR liquid phase frequecies,[42] and the frequencies for benzene chemisorbed on Pd(111) indicates no significant alterations in the bonding in the benzene molecule itself has occurred. This allows the use of the vibrational frequencies and assignment for liquid phase benzene as a guide in interpreting the spectral features. The EEL spectrum shown in figure 16 represents a saturation coverage, i.e., 1 monolayer. The EEL spectra for low (down to 0.1 Langmuirs) exposures are essentially identical to the ones shown in figure 16, with only a decrease in the intensity of the existing loss peaks.

Benzene chemisorption on Pd(111) at room temperature has been studied by Waddill and Kesmodel.[20] The electron energy loss spectrum exhibited peaks in the specular direction at 720(vs), 810(s), 1100(w), 1410(w) and 2990(m)cm^{-1}. These peaks shift upon deuteration to 525(vs), 640(sh), 830(m), 1355(vw), and 2230(mw) cm^{-1}. It is interesting to note

Figure 16. Electron energy loss spectrum recorded in the specular direction for benzene adsorberd on Pd(111) at T=180K and saturation coverage, a. C_6H_6 b. C_6D_6.

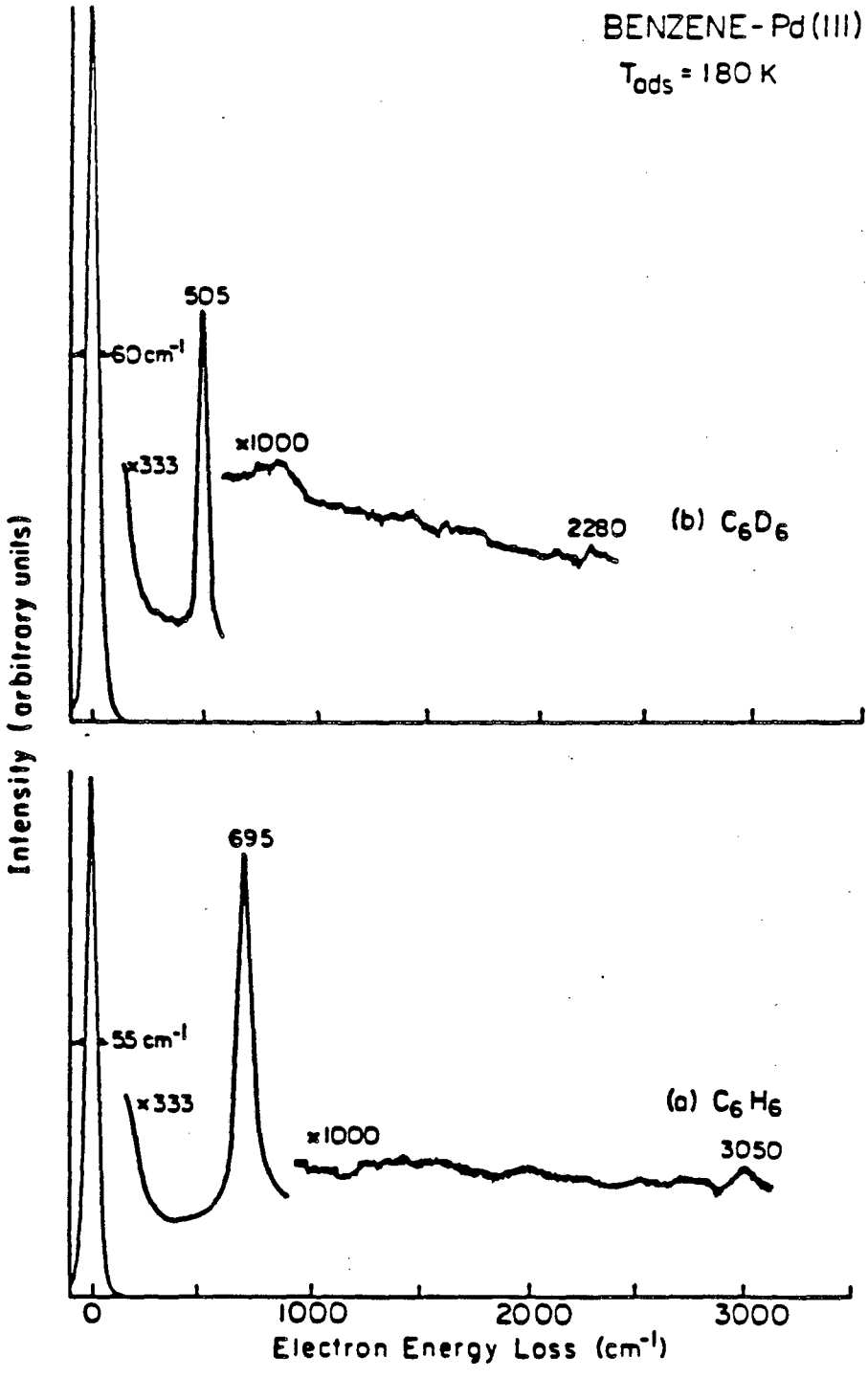
BENZENE-Pd(111)
T_{ads} = 180 K
505
60 cm^{-1}
×1000
×333
2280
(b) C_6D_6
695
55 cm^{-1}
×333
×1000
3050
(a) C_6H_6
Intensity (arbitrary units)
0
1000
2000
3000
Electron Energy Loss (cm^{-1})

XBL 863-7565

TABLE 8

VIBRATIONAL ASSIGNMENT OF BENZENE

ADSORBED ON Pd(111) at T=180K

Mode Description	Benzene (liquid)[a]			Benzene-Pd(111)		
	C_6H_6	C_6D_6	(ν_{H/ν_D})	C_6H_6	C_6D_6	(ν_{H/ν_D})
C-H out-of-plane bending motion, ν_{11}[b]	673	497	1.35	695(vs)	505	1.38
C-H stretching motion	3062	2293	1.34	3050(w)	2280	1.34

a. Frequencies for liquid benzene from reference 42.
b. Wilson mode #'s.

the increase in the number of observed modes in the spectrum at 300K as compared to the spectrum at 180K.

Toluene

The electron energy loss spectrum recorded in the specular direction for toluene ($C_6H_5CH_3$) adsorbed on Pd(111) at 180K is shown in figure 17a. The loss peaks observed in order of decreasing intensity are: 740, 470, 220, 1460, 2945, 3030, and 1060 cm^{-1}. These peaks shift to 565, 420, 210, 1390, 2220, 2300, and 1070 cm^{-1} for perdeuterotoluene, as shown in figure 17b. The frequencies of these vibrations and the vibrational assignment for toluene adsorbed on this surface are given in Table 9. The vibrational assignment of adsorbed toluene is made again by direct comparison to liquid phase assignments.[43] The two most intense loss peaks in the spectra correspond to out-of-plane motions. The relatively small shifts in the frequencies for the vibrational normal modes of toluene indicates that the molecule maintains its molecular integrity at 180K and is only slightly perturbed when adsorbed on this Pd surface. The deuterium labeled toluenes d^5-$C_6D_5CH_3$ and d^3-$C_6H_5CD_3$ were similarly studied and are shown in Fig. 18. The spectra of these molecules clearly distinguish the C-H(D) stretching motions for the methyl and aromatic hydrogens (deuteriums). The frequencies for the deuterium labeled toluenes are given in Table 9. As was observed with benzene no significant coverage dependence of the EEL spectra was observed with toluene.

The EEL spectrum for toluene adsorption at room temperature is quite different from the 180K spectrum and is shown in figure 19. Loss peaks are observed at 760, 3020, 1420, 945 and 525 cm^{-1} for perhydrotoluene.

Figure 17. Electron energy loss spectra for toluene adsorbed on Pd(111) at T=180K and saturation coverage, a. $C_6H_5CH_3$ b. $C_6D_5CD_3$.

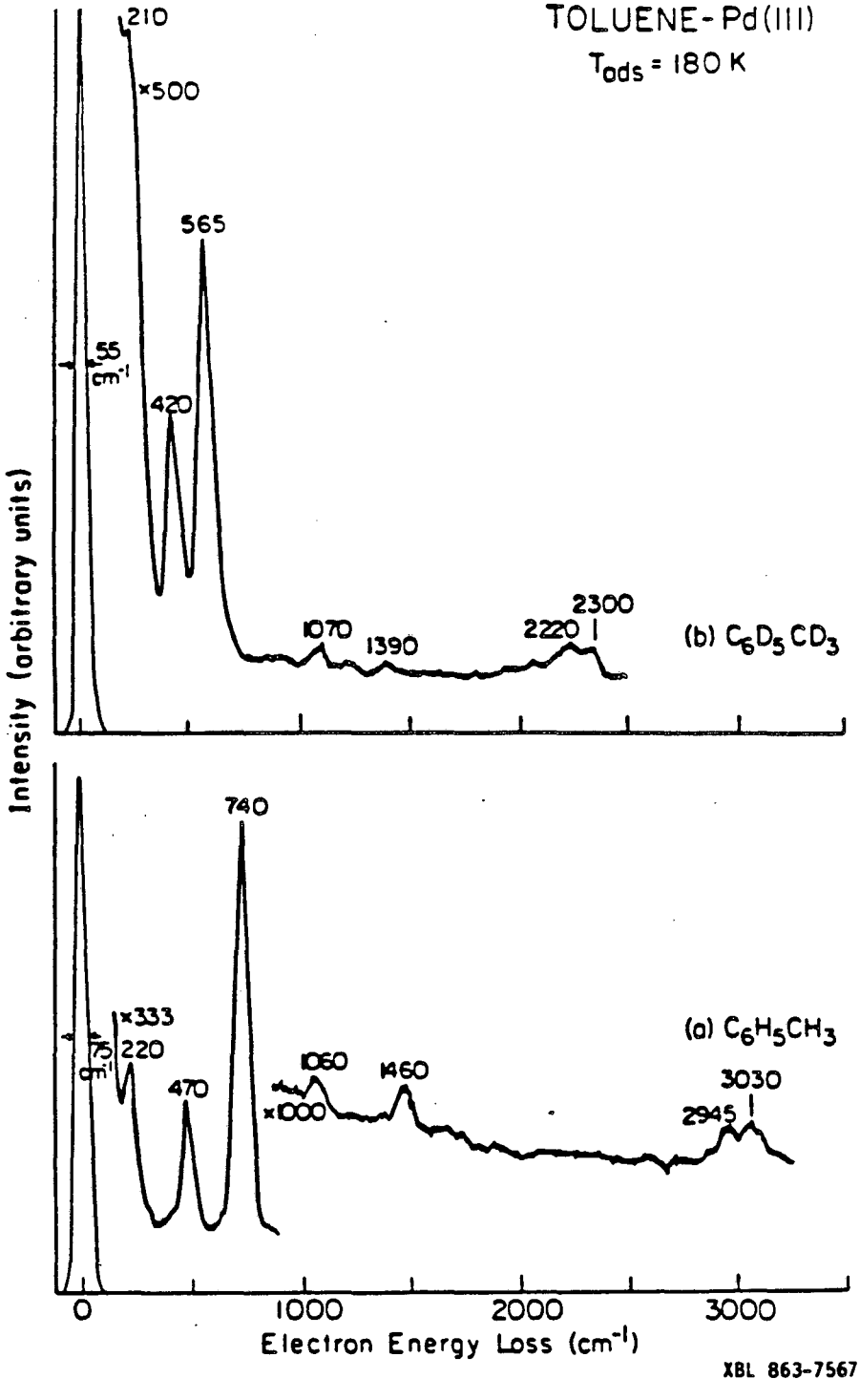
TOLUENE-Pd(111)
T_{ads} = 180 K
210
×500
565
55 cm⁻¹
420
1070
1390
2220
2300
(b) $C_6D_5CD_3$
740
×333
75 cm⁻¹
220
470
1060
×1000
1460
3030
2945
(a) $C_6H_5CH_3$
Intensity (arbitrary units)
0
1000
2000
3000
Electron Energy Loss (cm^{-1})
XBL 863-7567

Figure 18. Deuterium labeled toluenes adsorbed on Pd(111) at T=180K and saturation coverage, a. d^5-$C_6D_5CH_3$ b. d^3-$C_6H_5CD_3$.

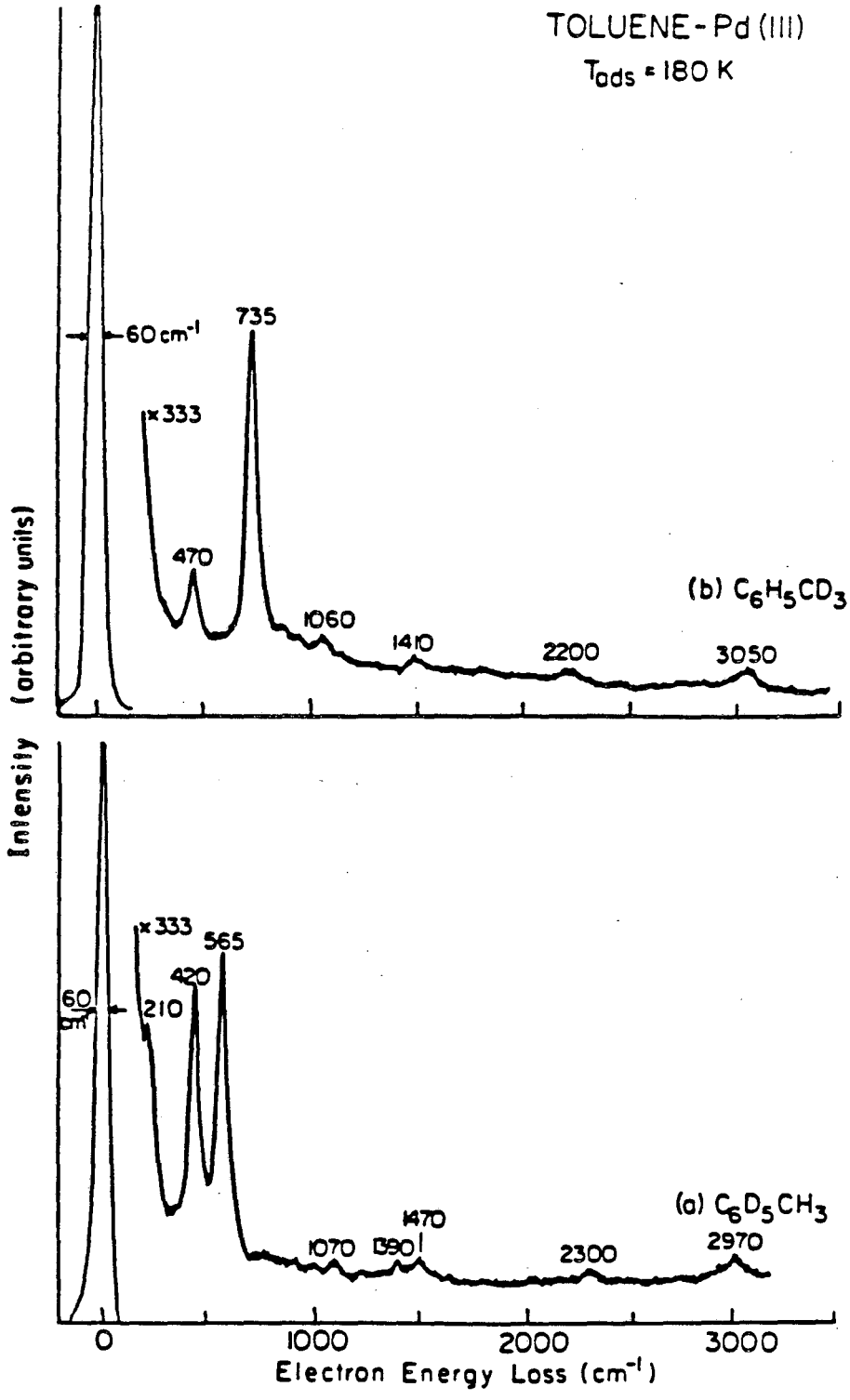
TOLUENE - Pd (111)
T_{ads} = 180 K
60 cm⁻¹
735
×333
470
1060
1410
2200
3050
(b) $C_6H_5CD_3$
Intensity (arbitrary units)
×333
565
420
60 cm⁻¹
210
1470
1070
1390
2300
2970
(a) $C_6D_5CH_3$
0
1000
2000
3000
Electron Energy Loss (cm⁻¹)

XBL 863-7566

TABLE 9

VIBRATIONAL FREQUENCIES AND ASSIGNMENT OF TOLUENES

(d^0, d^3, d^5, d^8) ADSORBED ON Pd(111) at T=180K

Mode Description	$C_6H_5CH_3$	$C_6H_5CD_3$	$C_6D_5CH_3$	$C_6D_5CD_3$	$(\nu_{H/\nu_D})^d$
Pd-C stretch	220	n.o.	210	210	1.01
o.o.p.[a] C-C bend	470	470	420	420	1.12
ν_{16b}[b]	(464)[c]				
o.o.p. C-H(D)	740	735	565	565	1.31
ν_{11}	(729)				
in-plane C-C bend	1060	1060	1070	1070	0.99
ν_{12}	(1004)				
in-plane C-C bend	1460	1410	1390 1470	1390	1.05
$\nu_{19b,19a}$	(1455)				
C-H(D) stretch	2945	2200	2970	2220	1.33
(methyl)	(2920) (2952) (2930)				
C-H(D) stretch	3030	3050	2300	2300	1.32
(aromatic)	(3056)				

a. o.o.p. = out-of-plane
b. Wilson Mode #'s.
c. Frequencies for liquid phase toluene from reference 43.
d. Ratio for perhydro and perdeutero toluenes.

Figure 19. Electron energy loss spectrum of perhydro toluene adsorbed on Pd(111) at room temperature.

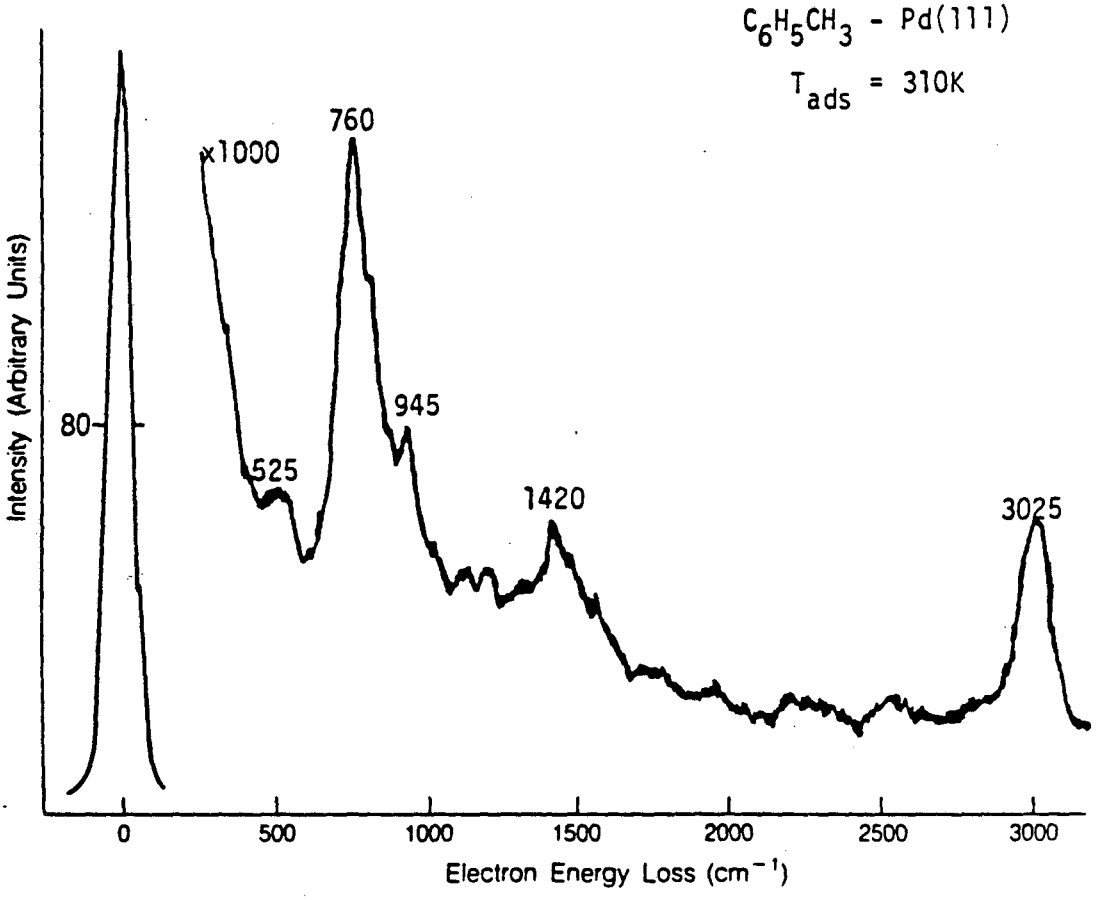
$C_6H_5CH_3$ - Pd(111)
T_{ads} = 310K
x1000
760
945
525
1420
3025
80
Intensity (Arbitrary Units)
0
500
1000
1500
2000
2500
3000
Electron Energy Loss (cm^{-1})

Pyridine

Pyridine (NC_5H_5) and perdeuteropyridine associatively adsorb on this surface at 170K and in a similar manner as benzene and toluene. The electron energy loss spectra, shown in figure 20a for perhydro pyridine and 20b for perdeutero, give loss peaks at 410(380), 725(545), 1060(1030), 1230(870), 1460(1340), 1600(1580), 3080(2270) cm^{-1}. The assignment for the vibrational spectra for pyridine adsorbed on Pd(111) is given in Table 10. The EEL spectra shown in figure 20 for pyridine chemisorbed on Pd(111) are very similar to the low coverage spectra of pyridine adsorbed on Ag(111). On Ag(111) the low coverage spectrum of pyridine (d^5-pyridine) loss peaks are observed at[24a] 200 w, 400(365) m, 610(560) w shoulder, 705(565) vs, 1040(1020) m, 1220(870) w, 1440(1305) w, 1570(1540) mw and 3040(2260) w cm^{-1}. The coverage dependence of the EEL spectrum for pyridine on Pd(111) was similar to that observed for toluenes and benzene on this surface, i.e. an increase in intensity of the loss peaks with coverage occured without frequency shifts or changes in relative intensity.

As was demonstrated for pyridine adsorbed on Pt(111) a temperature dependent adsorption structure is also observed for pyridine adsorbed on Pd(111). Figure 21 shows the electron energy loss spectrum recorded for pyridine adsorbed on Pd(111) at 310K. Loss peaks are observed in the specular direction at 430(w), 660(m), 740(s), 880(m), 1170(mw), 1340(w), 1460(m), 1570(vw), and 3080(s) cm^{-1}. Perdeuteropyridine adsorbed at room temperature was also studied. Loss peaks were observed at 400(vw), 555(s), 630(m), 745(w), 870(w), 1370(m), 1560(vw) and 2280(s) cm^{-1}. These frequencies along with the vibrational assignment are given in Table 10.

Figure 20. Low temperature electron energy loss spectrum of pyridine adsorbed at T=170K and saturation coverage, a. NC_5H_5 b NC_5D_5.

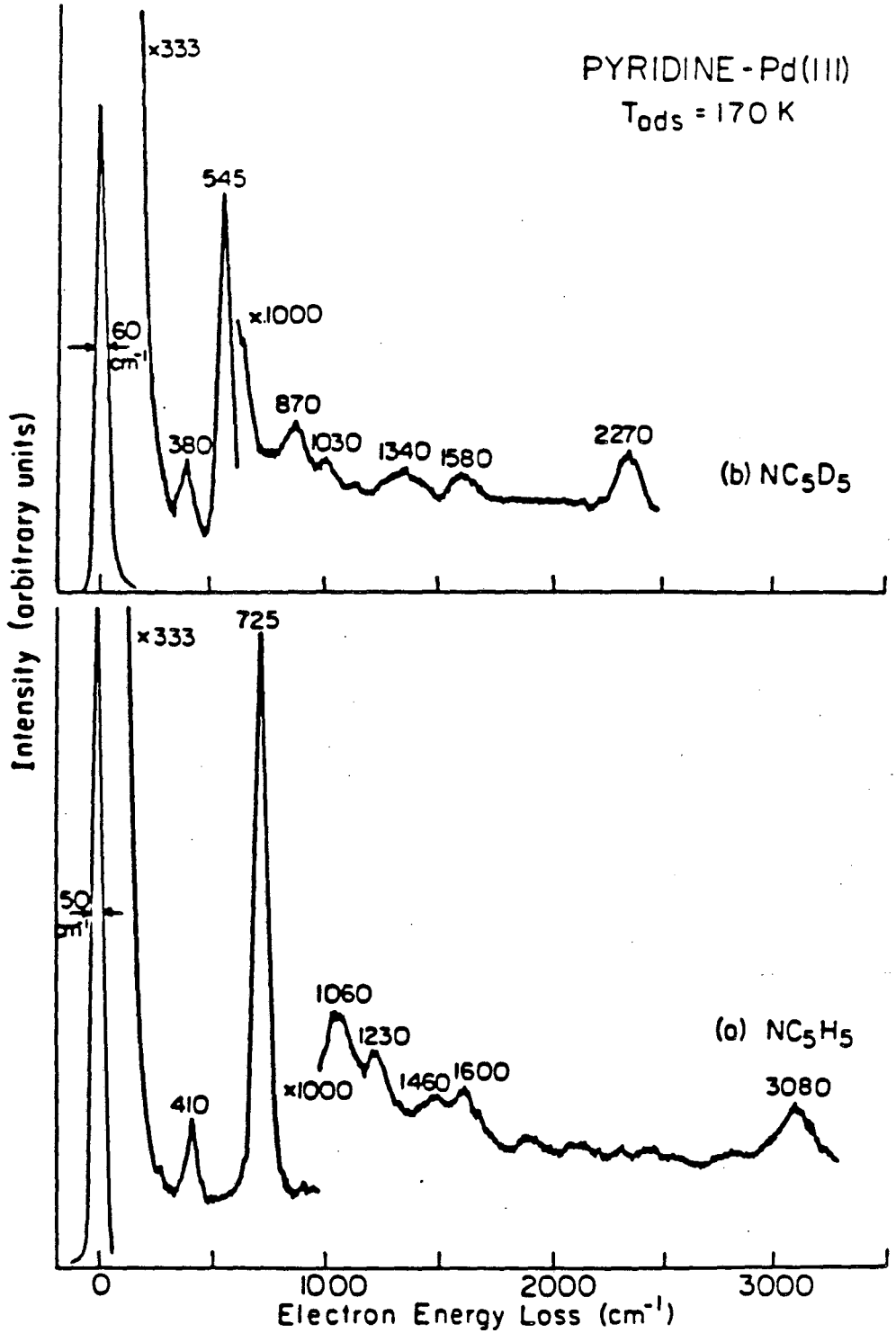
PYRIDINE - Pd(111)
T_{ads} = 170 K
×333
545
×1000
160 cm⁻¹
870
380
1030
1340
1580
2270
(b) NC_5D_5
Intensity (arbitrary units)
×333
725
50 cm⁻¹
1060
1230
(a) NC_5H_5
×1000
1460
1600
3080
410
0
1000
2000
3000
Electron Energy Loss (cm⁻¹)

XBL 863-7568

Figure 21. Electron energy loss spectrum of pyridine adsorbed at room temperature and saturation coverage on Pd(111), a. NC_5H_5 b. NC_5D_5.

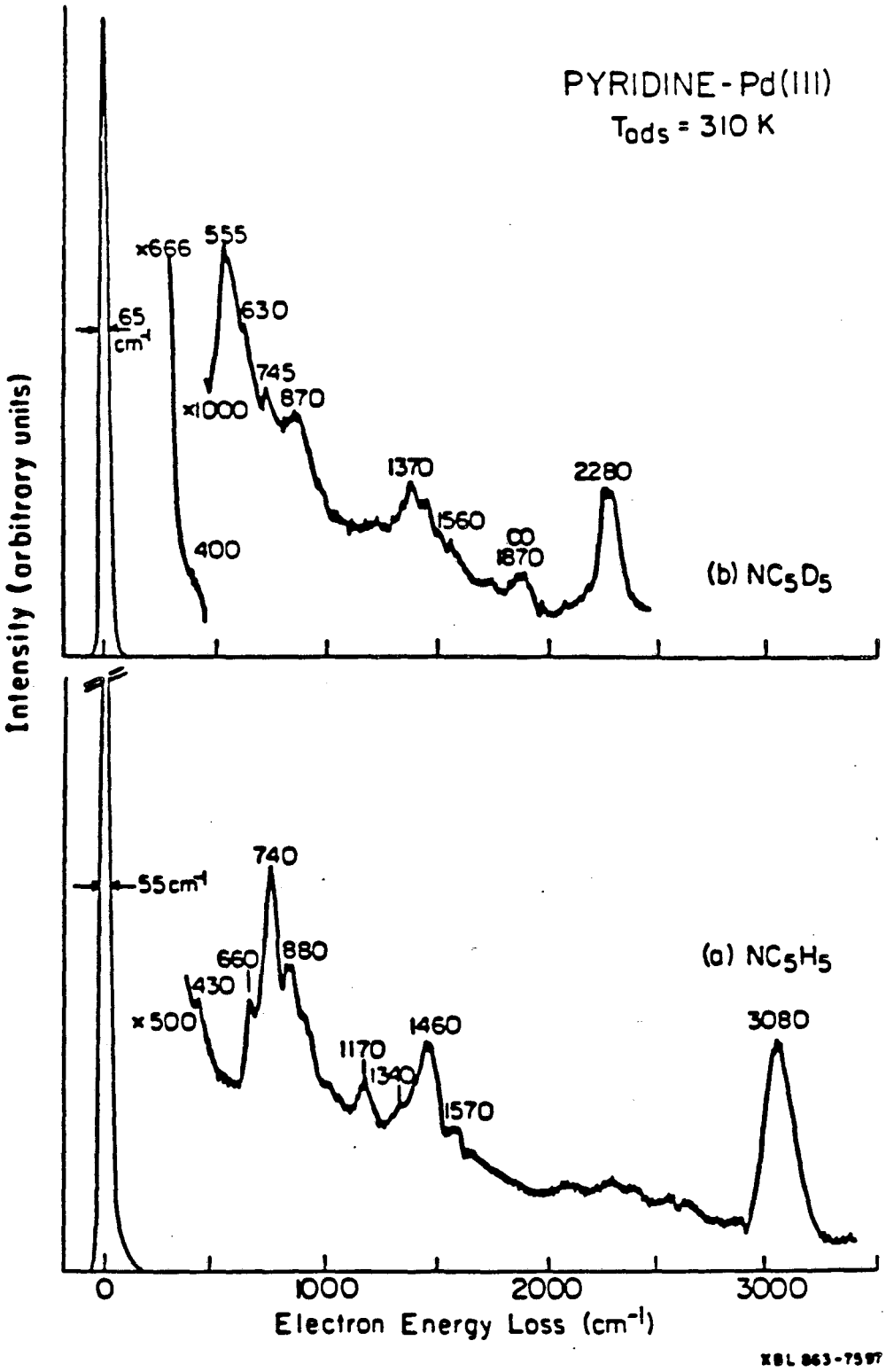
PYRIDINE - Pd(111)
T_{ads} = 310 K
Intensity (arbitrary units)
65 cm⁻¹
×666
555
630
745
870
×1000
400
1370
1560
00
1870
2280
(b) NC_5D_5
55 cm⁻¹
740
660
880
430
×500
1460
1170
1340
1570
3080
(a) NC_5H_5
0
1000
2000
3000
Electron Energy Loss (cm⁻¹)
XBL 863-7597

Table 10

Vibrational Frequencies and Assignment for the Electron Energy Loss Spectra of Pyridine and d^5 Pyridine Adsorbed on on Pd(111)

Symmetry, Mode No.		Description	NC_5H_5 (NC_5D_5)[A]		Pyridine-Pd(111) T=170K		Pyridine-Pd(111) T=310K	
					h^5	(d^5)	h^5	(d^5)
A_1	1 (2)[B]	C-H stretch	3094	(2302)	3080	(2270)	3070	(2280)
	2 (13)	C-H stretch	3072	(2276)	3080	(2270)	3070	(2280)
	3 (20A)	C-H stretch	3030	(2268)	3080	(2270)	3070	(2280)
	4 (8a)	C-C, C-N stretch	1583	(1554)	1600	(1580)	1570	(1560)
	5 (19a)	C-C, C-N stretch	1483	(1340)	1460	(1340)	1460	(1370)
	6 (9a)	C-H in-plane bend	1218	(882)	1230	(870)		
	7 (18a)	C-H in-plane bend	1072	(823)				
	8 (12)	asymmetric ring breathing	1032	(1014)	1060	(1030)		
	9 (1)	ring breathing	991	(963)				
	10 (6a)	in-plane ring distortion	601	(579)				
B_2	23 (5)	o.o.p. ring distortion	1007	(828)				
	24 (10b)	o.o.p. ring distortion	936	(765)			880	(745)
	25 (4)	C-H o.o.p. bend	744	(631)				
	26 (11)	C-H in-phase o.o.p. bend	700	(526)	725	(545)	740	(555)
	27 (16b)	ring o.o.p. distortion	403	(367)	410	(380)	430	(400)
B_1	11 (20b)	C-H stretch	3087	(2289)	3080	(2270)	3080	(2280)
	12 (7b)	C-H stretch	3042	(2256)	3080	(2270)	3080	(2280)
	13 (8b)	C-C, C-N stretch	1581	(1546)	1600	(1580)	1570	(1560)
	14 (19b)	C-C, C-N stretch	1442	(1303)	1460	(1340)	1460	(1370)
	15 (14)	C-C ring stretch	1362	(1046)			1340	
	16 (3)	C-C in-plane bend	1227	(1226)				
	17 (15)	C-H in-plane bend	1143	(856)			1170	(870)
	18 (18b)	C-H in-plane bend	1079	(835)				
	19 (6b)	in-plane ring distortion	652	(625)			660	(630)

A. Pyridine Frequencies and Assignments Taken From: Wiberg, K.B., Walters, V.A., Wong, K.N. and Colson, S.D., J. Phys. Chem. 88, 6067 (1984).

B. Wilson Mode #'s

DISCUSSION

In the electron energy loss spectra for saturation coverages of benzene, toluene and pyridine adsorbed on Pd(111) at 180K an intense loss peak is observed in the 700-750 cm^{-1} region. From the deuterium shift of 1.38, 1.31, 1.33 for benzene, toluene, and pyridine, respectively, and the close comparison to liquid phase values, this peak can be assigned to the C-H in phase out-of-plane bending motion for all three aromatics. The frequency for the aromatic C-H stretch stretching motion, as well as the deuterium shift of 1.33, compare well to liquid phase values for all three molecules. Other loss peaks observed in the EEL spectra for pyridine and toluene are also in good agreement to liquid phase values.[32,43] This close agreement between liquid phase and adsorbed frequencies indicates that potential functions for the vibrational motions of these molecules remain relatively unchanged upon adsorption on Pd(111) at this temperature.

There is a greater number of loss peaks observed in the EEL spectra for toluene and pyridine relative to the benzene spectrum. The additional modes observed in the EEL spectra for toluene and pyridine are $\nu_{16b}(b_2)$, $\nu_{12}(a_1)$, and $\nu_{19a,19b}(a_1,b_1)$, where the symmetry of these modes under the molecular C_{2v} point group are noted in parenthesis. The spectra for the perhydro species ($C_6H_5CH_3$ and NC_5H_5) show that the intensities of these modes relative to the intensity of ν_{11} are approximately the same for both of these molecules. The out-of-plane ring distortion, ν_{16b}, at 470 cm^{-1} for toluene and 410 cm^{-1} for pyridine are both of strong intensity whereas modes ν_{12} and $\nu_{19a,19b}$ are much weaker features in both the toluene and pyridine perhydro spectra. There are two modes observed for pyridine which are not observed in the

toluene spectra. These are $\nu_{9a}(a_1)$ at 1230(870) cm^{-1} and $\nu_{8a,8b}(a_1,b_1)$ at 1600(1580) cm^{-1}, both of these modes are of relatively weak intensity.

The larger number of observed modes in the EEL spectra for pyridine and toluene, relative to the number for benzene, is readily attributable to the reduction in molecular symmetry. In addition, the vibrational frequencies do not shift much relative to liquid phase frequencies. Hence, we can then conclude that all three molecules exhibit similar and weak bonding to the surface. Neither the steric effect of the methyl group on toluene or the lone pair of electrons localized on the nitrogen atom seem to change the bonding of these molecules to the substrate at 180K.

The intensities of the peaks in the specular direction also provide information concerning the orientation of the molecules with respect to the surface plane. The vibrational motions which all three molecules exhibit are ν_{11} and the C-H stretching motion. The loss peak for ν_{11} is the most intense peak in the spectrum for benzene, toluene and pyridine, whereas the ν_{C-H} stretch is very much less intense for all three molecules (in the specular direction). From the intensity of the out-of-plane modes relative to the in-plane modes we conclude that these molecules, at 180K, lie flat on the Pd(111) surface with the molecular ring plane oriented parallel to the surface plane.

These molecules appear to be "physisorbed" to the Pd(111) surface at 180K. This physisorbed state is perhaps a precursor to a chemisorbed state indicating an activation barrier to chemisorption. At room temperature, benzene is chemisorbed on the Pd(111) surface as shown by Waddill et. al..[20] Furthermore, a low temperature benzene desorption

peak is observed in the thermal desorption spectrum (T_{max}=260K)[44] as well as a high temperature desorption peak. A physisorbed state for pyridine adsorption on Pd(111) at 180K would explain why the electron energy loss spectrum for pyridine adsorbed on Ag(111) (for coverages below 0.5 monolayers) is so similar. Silver interacts very weakly with pyridine. Recently, using Extended Huckel Theory, a small activation barrier for benzene chemisorption on Rh(111) was predicted.[45] At 180K the bonding of these molecules, benzene, toluene and pyridine, to the palladium surface can be understood in terms of either a Van der Waals induced dipole interaction with the surface metal atoms or perhaps a very weak electron donor-acceptor type bond, where the highest filled occupied π orbitals donate electrons into the low lying empty metal valence orbitals.

The adsorption structure of benzene, at 300K, has been postulated based on vibrational spectra by Waddill and Kesmodel.[20] There is an increase in the number of loss peaks observed in their EEL spectra of benzene and perdeutero benzene at 300K, relative to what we observe at T=180K. Also in the room temperature spectra the frequency of the loss peak associated with the C-H out-of-plane bending motion is identified at 720 cm^{-1}, 25 cm^{-1} higher in frequency then what is observed in this study at T=180K and 47 cm^{-1} higher than ν_{11} in liquid benzene. In addition, the frequency of the loss peak associated with the C-H stretching motion, at 300K, is at 2990 cm^{-1}, 60 cm^{-1} lower in frequency then that observed at T=180K and 72 cm^{-1} lower than in liquid benzene. Both the increase in the number of loss peaks and the shift in frequency of the C-H out-of-plane bend and C-H stretch, away from liquid phase values, is due to a greater interaction of the benzene molecules with

the surface at 300K. This, we interpret, is due to a chemisorbed state of benzene on this surface at 300K, and a "physisorbed" state of benzene on this surface at T=180K. The proposed adsorption geometry of chemisorbed benzene[20] is one where the ring plane is parallel to the surface plane and in an adsorption site of low symmetry, C_s.

There is however an alternative explanation for the difference in the number of loss peaks in the 180K benzene/Pd(111) EEL spectra relative to the 300K spectra, which can not be ruled out. The increase in the number of loss peaks observed in the specular direction for benzene adsorbed at 300K could merely be a manifestation of the excitation of the low frequency motions of the benzene plane relative to the surface. This would destroy the average coplanarity of the molecule relative to the surface and hence increase the number of surface dipole allowed modes.

Preliminary studies on the room temperature adsorption of toluene suggests a chemisorption state similar to that observed for benzene.[20] The most intense peak in the electron energy loss spectrum, of $C_6H_5CH_3$ adsorbed at 300K on Pd(111), is observed at 760 cm^{-1}, we assign this peak to the out-of-plane bend. The frequency of γ_{C-H} has increased by 20 cm^{-1} for toluene when adsorbed at 300K relative to adsorption at 180K. More importantly the frequency of γ_{C-H} has shifted away from the liquid phase value of 729 cm^{-1},[43] indicating chemisorption of toluene at room temperature. This temperature dependent adsorption behavior of toluene is quite similar to that of benzene on this surface as discussed above. A detailed study on the temperature dependence of these molecules adsorbed on Pd(111) would be quite interesting in the temperature range between 180-300K.

At 310K, and saturation coverage, pyridine is chemisorbed to the surface with the ring plane oriented away from the surface plane. The EEL spectrum for pyridine adsorbed at T=310K shows an increase in the intensity of the in-plane modes relative to the out-of-plane modes, at the specular angle. In particular the intensity ratio for the out-of-plane motion at 740 cm^{-1} relative to the C-H stretch at 3080 cm^{-1}, which is of course an intrinsically in-plane motion, has decreased markedly. Here an electron donor-acceptor type description can be used to explain the bonding to the surface. The pyridine molecule behaves as a Lewis base donating electron density, via the nitrogen lone pair, into the lowest lying unoccupied molecular orbitals of the metal. Our results are consistent with the conclusions made by Netzer and Mach from their studies on pyridine adsorption on Pd(111) using ultraviolet photolectron spectroscopy and electronic energy loss spectroscopy.[46]

The alpha-pyridyl species proposed as the pyridine adsorption structure on Pt(111) at 300K based on the EEL spectrum, as discussed in the proceeding section, is not formed on the Pd(111) surface. The comparison of the EEL spectrum for the pyridine-Pd system, at 310K, to the IR spectra of the organometallic osmium-complexes $Os_3(CO)_{11}(NC_5H_5)$ and $HOs_3(CO)_{10}(NC_5H_4)$ favors an intact pyridine as in the $Os_3(CO)_{11}(NC_5H_5)$ complex. The thermal desorption data is also consistent with associative pyridine adsorption at 310K on Pd(111).[47] The decomposition of pyridine on this surface was followed by monitoring hydrogen evolution (AMU=2). A low temperature (<473K) hydrogen peak was not observed. Whereas low temperature facile C-H bond cleavage occurred on the Pt(111) surface.

3. CONCLUSION

These two metals, platinum and palladium, have similar interatomic distances (~2.76Å), work functions (5.6 eV-Pd(111), 5.7eV-Pt(111))[4] and the same number of valence electrons. Questions raised are: what is the cause of these differences?, why do these molecules bond more strongly to the platinum surface?, and, why is there no apparent activation energy to chemisorption for these molecules on platinum while there is an activation barrier on palladium? We can understand the weaker adsorbate-metal bond for palladium relative to platinum by first understanding the bonding between the metal atoms. The values for the heats of atomization for palladium and platinum are 91 and 133 kcal/mole, respectively.[5] This 42 kcal/mole difference in the heats of atomization of these two metals is attributed to an increase in the bonding effectiveness of the d electrons when going from the second to third transition series.[5] The greater nuclear charge for platinum affects the s and p electrons greatly but not the d electrons. This is a consequence of the larger angular momentum of the d orbitals, the d electrons do not approach the nucleus as closely as the s and p electrons. This means the orbital-extent or orbital diffuseness is much greater for the 5d orbitals than the 4d orbitals. The s and p electrons, according to Brewer-Engel theory (see Ref. 5), determine longe-range structure, i.e. metal atom packing which is cubic close-packed for Pt and Pd. The metal d electrons determine short-range bonding. Although all the electrons, s, p and d, contribute to the bonding in the metal, it is mainly the difference in the bonding of the d electrons which accounts for the stronger platinum metal bonds.

The same metal bonding concepts can be used to describe the adsorbate-metal bond. The Brewer-Engel theory has, of course, been developed to explain properties of the bulk metal. Extensions of this theory to explain surface phenomena must be viewed as empirical and qualitative. The asymmetry which occurs at the surface will effect the orbital energies and in addition the crystal field effects for the d orbitals will be different at the interface relative to the bulk. However, the stronger bonding of these molecules (benzene, toluene and pyridine) to platinum can be attributed to the greater overlap of the d-orbitals with the adsorbate molecular orbitals. Recently, Brewer-Engle Valence-Bond theory has been successful in both describing the hydrogen chemisorption on electrode surfaces for group VIII metals and group VIII metal alloys, and in explaining the electrocatylitic hydrogen evolution for these systems.[48]

The zero or smaller energy of activation for chemisorption of these molecules on Pt(111) can also be understood in terms of the stronger bonding of benzene to the Pt(111) surface in the final state, i.e. the chemisorbed state. For similar reactants and reaction pathways, in gas and liquid phase chemistry, a correlation between E_a^*, the energy of activation, and the ΔH of the reaction can be found. As the final state is lowered in energy the activation barrier goes down in energy. An example of this is the halogenation reaction of alkanes.[49] The differences in the chemisorbed states for benzene on Pt and Pd readily explains the smaller activation barrier to chemisorption for Pt relative to Pd.

Koel et. al. has postulated that the frequency of the out-of-plane bending motion can be used as a measure of the strength of the benzene-

metal ineraction.[21] If we use the frequency of the C-H out-of-plane motion as a measure of this interaction we find that for the fcc metals studied , this correlates well with ΔH of atomization. The frequency of γ_{C-H}, for benzene adsorbed on the (111) face of different metals, is observed at 700 cm^{-1}-Ag(111)[24] < 720 cm^{-1}-Pd(111)[20] < 730 cm^{-1}-Ni(111)[19] < 776cm^{-1}-Rh(111)[21] < 830 cm^{-1}-Pt(111)[18]. The value of the $\Delta H_{atomization}$ of these metals[(5)] are found to increase in a similar manner i.e., 68 kcal/mole-Ag < 91 kcal/mole-Pd < 102.8 kcal/mole-Ni < 133 kcal/mole-Rh < 135 kcal/mole-Pt. The value of $\Delta H_{atomization}$, for transition metals, is a sensitive function of d orbital filling and periodic row, the effect of both of these factors on $\Delta H_{atomization}$ has been discussed fully by Brewer.[5]

These ideas can be extended to understanding the adsorption of other hydrocarbons on these two surfaces. Ethylene, for example, has been extensively studied on both the (111) surface face of platinum and palladium. The low temperature EEL spectrum (T≅140K) for C_2H_4 on these two surfaces, is very different. Ethylene rehybridizes on Pt(111),[13] from sp^2 to sp^3 hybridization. The two carbon atoms are covalently bonded to the platinum surface. The C-C stretching frequency is at 1050 cm^{-1} [13] on Pt(111). Whereas on Pd(111) the C-C stretching frequency for ethylene is observed at 1502 cm^{-1} .[50] Again the stronger bonding of ethylene to the Pt surface relative to the Pd surface can be readily explained, in terms of the greater effective d orbital bonding for Pt and therefore Pt-C bond formation.

We have correlated the strength of adsorbate-metal interactions, at least for benzene chemisorption, with bulk metal bonding as measured by the heat of atomization of the metal. There are however many different

factors which contribute to the bonding of adsorbates to metal surfaces. For example, geometrical factors are certainly an important consideration. The surface chemistry of a particular metal depends greatly on the surface crystallography. This is especially true for the surface chemistry of stepped and kinked surfaces as compared to atomically flat surfaces. A striking example of this is the greater extent of dehydrogenation of cyclohexene to benzene on the stepped Pt(557) and kinked Pt(654) surface as compared to the atomically flat Pt(111) surface.[51]

In summary we propose the following:

(i) There is a larger activation barrier for chemisorption of benzene, toluene and pyridine on the palladium (111) surface as compared to the platinum (111) surface. And at 180K these molecules are "physisorbed" to the palladium surface.

(ii) The differences in surface chemistry of these two congeners, Pt and Pd, are attributed to the greater effective bonding of the d electrons in platinum relative to palladium. The interaction of benzene, toluene and pyridine is clearly stronger with the platinum surface. The driving force in the surface chemistry of these two aromatics on the platinum surface is the formation of covalent metal-carbon bonds, whereas this is not the case for palladium.

The surface chemistry of hydrocarbons adsorbed on these two catalytically important metals, Pt and Pd, is demonstrably different. This study has focused on the clean metal surfaces. A comparison of the effects of adatoms on these two metals will be an important step in our understanding of industrial catalyst.

CHAPTER IV

PHOTOCHEMICAL STUDIES OF PHYSISORBED AND CHEMISORBED CIS AND TRANS 1,2-DISUBSTITUTED ETHENES ON Pt(111) AND Pd(111) SURFACES

1. INTRODUCTION

There has been little study of the photochemistry of molecules adsorbed on metal surfaces. A variety of processes have been discussed that tend to discourage such study. The major concern is connected with energy transfer from the adsorbate to the metal, which is thought to be prohibitively rapid and operating through several decay channels (for a complete discussion see reference 7). Thus, vibrational deactivation of the adsorbate can occur via excitation of the phonon modes of the metal while deactivation of excited electronic states of the adsorbate might occur either by electron-hole pair creation or by plasmon excitation.

A number of photolysis studies have focused on the photodesorption process using both ultra-violet and infrared light sources. McAllister and White's early work on UV photodesorption of carbon monoxide from Ni surfaces did not discern if the photodesorption was due to a local quantum effect, i.e. photon absorption by a CO molecule followed by subsequent desorption of that particular molecule.[52] Infrared irradiation using high power pulsed laser sources has also been employed to study the photodesorption process. Chuang's pulsed CO_2 laser studies of pyridine desorption from Ag(110) and from silver films showed that both direct and indirect substrate heating promoted the more weakly bound molecules to desorb.[53]

Other photophysical studies include measurements on the phosphorescent lifetimes of electronically excited states held in the

vicinity of a cold metal surface by an inert spacer layer, e.g. solid argon.[54-56] The d^{-3} distance dependence on the energy transfer rate from electronically excited molecules to the solid surface has been found to agree well with Chance, Stilbey, and Prock's classical predictions,[57] at least down to 7Å. Interestingly the distance dependence has been found experimentally to be the same for both semiconductor and metal surfaces,[58] although the electronic band structures of these materials are quite different. Attempts to measure lifetimes of excited states for molecules which are in direct contact with a surface have not been successful.[54-56] The present theory excludes the possibility of orbital overlap of the adsorbate and the surface (i.e. chemical bonding to the surface). However these predictions, if applicable at close approach, would indicate sub-picosecond (or less) deactivation times.[59]

In this work we test the validity of this current thought. We believe that these are the first photochemical studies, for molecules which are in the vicinity of a smooth transition metal surface and the first study to show direct photochemical change for a molecule chemisorbed to a metal surface. The first systems we chose to study were cis and trans 1,2-dichloroethene and trans 2-butene physisorbed, as multilayers (approximately 2-10 layers), on Pd(111). The photochemistry of cis and trans 1,2-dichloroethenes have been studied in the gas [60a,b] and liquid[61] phase as well as in cryogenic matrices.[62] Similar photochemical studies on the 2-butenes have also been done in the gas phase.[63] The reason for choosing these systems is twofold; first the photochemistry of the multilayer should be similar to the photochemistry which occurs in the gas and liquid phase; this is documented in the

literature and serves as a guide in these studies, second the molecules in the multilayer are in the vicinity of the metal but not directly coupled to the surface atoms and therefore the bulk metal. The possibility of energy dissipation to the surface, via chemical bonds, will then be eliminated, thus removing a potential major deactivation mechanism. In addition the chromophore being excited will be an internal transition of the molecule and therefore will be relatively well understood in terms of the excited state potential energy surfaces.

The experiments described above were successful in that photochemical change was observed with UV light as will be discussed later in more detail. The next step and the subject of the second part of this chapter, was photochemical studies of 1,2-dichloroethene both chemisorbed and physisorbed to Pt(111). Again photochemical changes were observed for a monolayer, i.e. the chemisorbed state, and are very different from the photochemistry of the multilayer (physisorbed state). The excitation chromophore for the chemisorbed state is not as well understood as that for the physisorbed state, again this will be discussed in more detail. The effect of surface coverage as well as the thermal behavior of the dichloroethenes was also probed in this study.

The surface chemistry of ethylene has been extensively studied. The electron energy loss spectrum has been reported for this simple C_2 hydrocarbon adsorbed on many metals, including Pt(111) and Pd(111) surfaces. The adsorption sturcture of ethylene on Pt(111) has been determined to be 1,2 "di-sigma" bonded to the surface at 150K,[13] i.e. both carbon atoms are covalently bonded to the surface atoms. As the temperature is raised to 300K a new surface species is formed.[12] The adsorption structure of this hydrocarbon fragment has been determined to

be an ethylidyne species (See Discussion in Chapter 2). The bonding of ethylene on Pd(111) is much weaker than on platinum and at low temperatures (140K) the ethene molecule approximately retains its sp^2 hybridization on the surface.[50]

Avery has studied the surface chemistry of alkyl substituted ethenes: pentene and cis and trans 2-butene, on Pt(111) using thermal desorption and electron energy loss spectroscopy.[64] The adsorption of these molecules have been determined to bond to the platinum surface in a similar fashion to that of ethylene at 140K. The hybridization about the carbon atoms in these alkyl-substituted ethenes is sp^3. The thermal chemistry of pentene and cis and trans 1,2-butene differs from that of ethylene on Pt(111) in that no alkylidyne formation is observed upon warming the substrate to 300K.

Described in this section will be the surface chemistry, adsorption structure and thermal chemistry, as well as the photochemistry of the adsorbed substituted ethenes. The observation of photochemical behavior is the most novel aspect of this study. Some questions which we have sought to answer include the following. How does the adsorption structure of the dichloroethenes differ from that of ethene on the surface? Will similar thermal processes be observed, e.g. will a chloroalkylidyne species form on Pt(111)? And how does the photochemistry of these molecules when adsorbed on a metal surface compare to that in the gas phase, liquid phase or in cryogenic matrices?

2. RESULTS AND DISCUSSION

A. UV ELECTRONIC EXCITATION OF CIS AND TRANS 1,2-DICHOROETHENE AND TRANS 2-BUTENE PHYSISORBED ON Pd(111)

Thermal Desorption Spectroscopy

Thermal desorption studies were done for trans 2-butene. Figure 22 shows the thermal desorption curve for trans 2-butene adsorbed on Pd(111) at 120K. The heating rate, β, in these experiments was 12K/sec. Two desorption peaks are evident in the parent ion spectrum (AMU=56). A desorption peak with a T_{max}=156K increases in intensity with increasing coverage, never reaching a saturation coverage. The higher temperature desorption peak, with a desorption rate maximum T_{max}=213K, initially increases with increasing coverage and then saturates at higher exposures. The coverage dependence of the intensities of these peaks indicate monolayer and multilayer desorption for the high and low temperature peak, respectively.

The thermal desorption curve, monitoring the parent ion, AMU=96, for trans 1,2-dichloroethene adsorbed on Pd(111) at T=120K is shown in figure 23. There is a single desorption peak in the spectrum with a desorption rate maxima at 170K. This peak continually increases with increasing coverage never saturating. Again this is indicative of multilayer desorption.

Electron Energy Loss Spectroscopy

The electron energy loss spectra for the 2-butene isomers, cis and trans, were recorded in the specular direction. Shown in figure 24 is

Figure 22. Thermal desorption spectrum of trans 2-butene adsorbed on Pd(111) at 120K, monitoring the parent ion AMU=56.

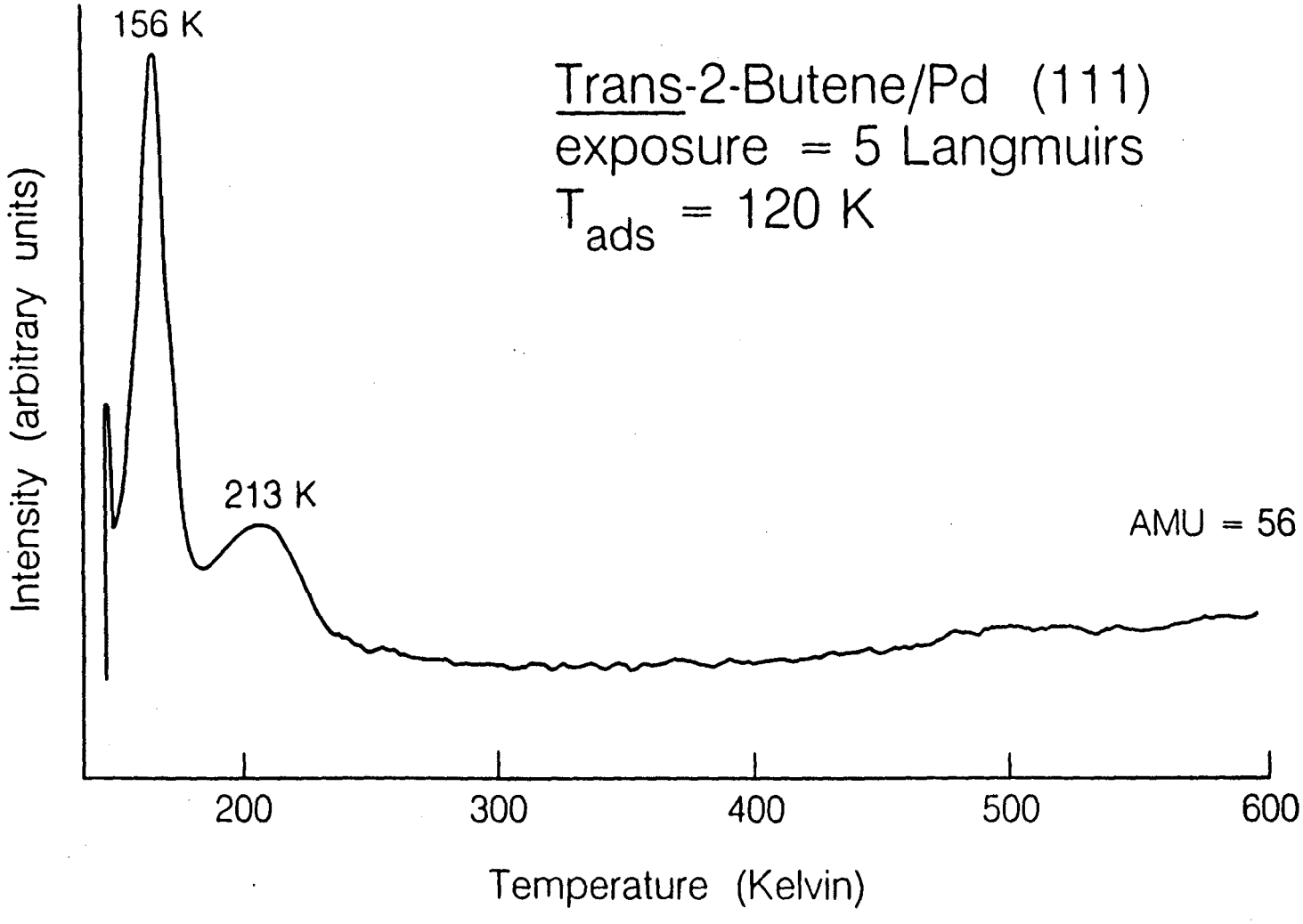
156 K
213 K
Trans-2-Butene/Pd (111)
exposure = 5 Langmuirs
T_{ads} = 120 K
AMU = 56
Intensity (arbitrary units)
200
300
400
500
600
Temperature (Kelvin)

Figure 23. Thermal desorption spectrum of trans 1,2-dichloroethene adsorbed on Pd(111) at 120K, monitoring the parent ion, AMU=96.

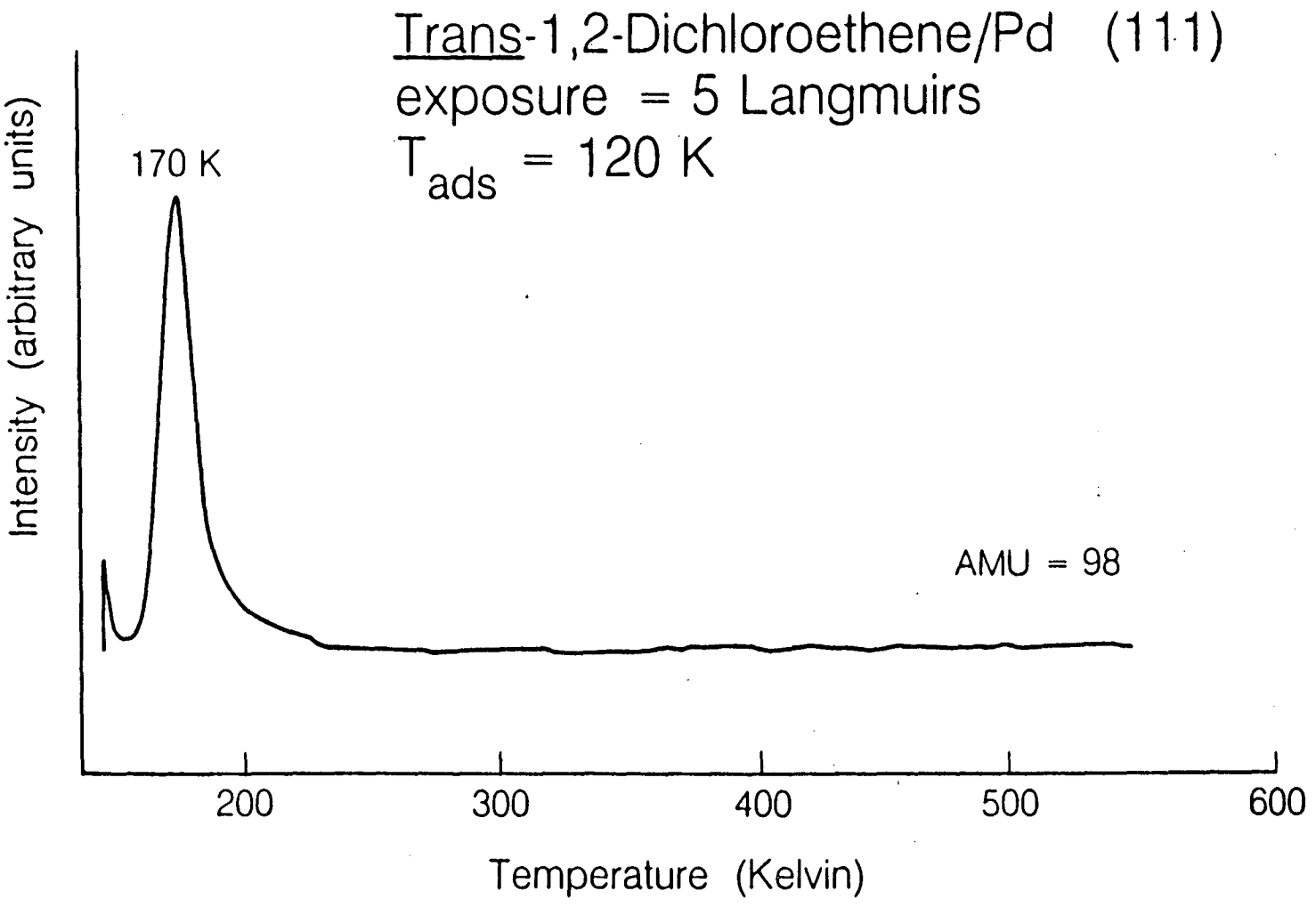
Trans-1,2-Dichloroethene/Pd (111)
exposure = 5 Langmuirs
T_{ads} = 120 K
170 K
AMU = 98
Intensity (arbitrary units)
200
300
400
500
600
Temperature (Kelvin)

the EEL spectrum recorded for a 5 langmuir exposure of trans 2-butene on a clean Pd(111) surface held at 120K. Loss peaks in the spectrum are at 1420, 2930, 3025, 990, 1650, 450 and 1780 cm^{-1}. The cis isomer was similarly studied. The EEL spectrum recorded after a 5L exposure is shown in figure 25. Loss peaks are observed at 2985, 1440, 705, 1000, 1650 and 1800 cm^{-1}. The peaks observed at approximately 1800 cm^{-1} in both the cis and the trans EEL spectra are due to CO chemisorbed to the palladium surface in a three fold hollow site.[9]

A clean Pd(111) sample was exposed to 5 x 10^{-8} torr of trans 1,2 dichloroethene for 100 sec, corresponding to a 5 langmuir dose. This was enough to produce a multilayer as determined by thermal desorption spectroscopy (vide infra). The electron energy loss spectrum recorded after this gas exposure is shown in figure 26. The most intense peak in the spectrum is observed at 900 cm^{-1}. Other loss peaks in the spectrum are observed at 770, 3100, 1290, and 1620 cm^{-1}, in order of decreasing intensity.

A similar 1 langmuir gas exposure of cis 1,2-dichloroethene on a clean Pd(111) surface was done (enough to produce multilayers). Figure 27 shows the electron energy loss spectrum recorded in the specular direction of cis 1,2-dichloroethene adsorbed on Pd(111). Loss peaks are observed at 720, 850, 585, 3100, 1190, 1290 and 1590 cm^{-1} in order of decreasing intensity.

UV Photochemistry of Cis and Trans Disubstituted Ethenes

2-Butenes

After broadband photolysis ($\lambda > 200nm$) of trans 2-butene, an electron energy loss spectrum was recorded. Figure 28 shows the spectra

Figure 24. Electron energy loss spectrum of multilayers of trans 2-butene adsorbed on Pd(111) at T=120K.

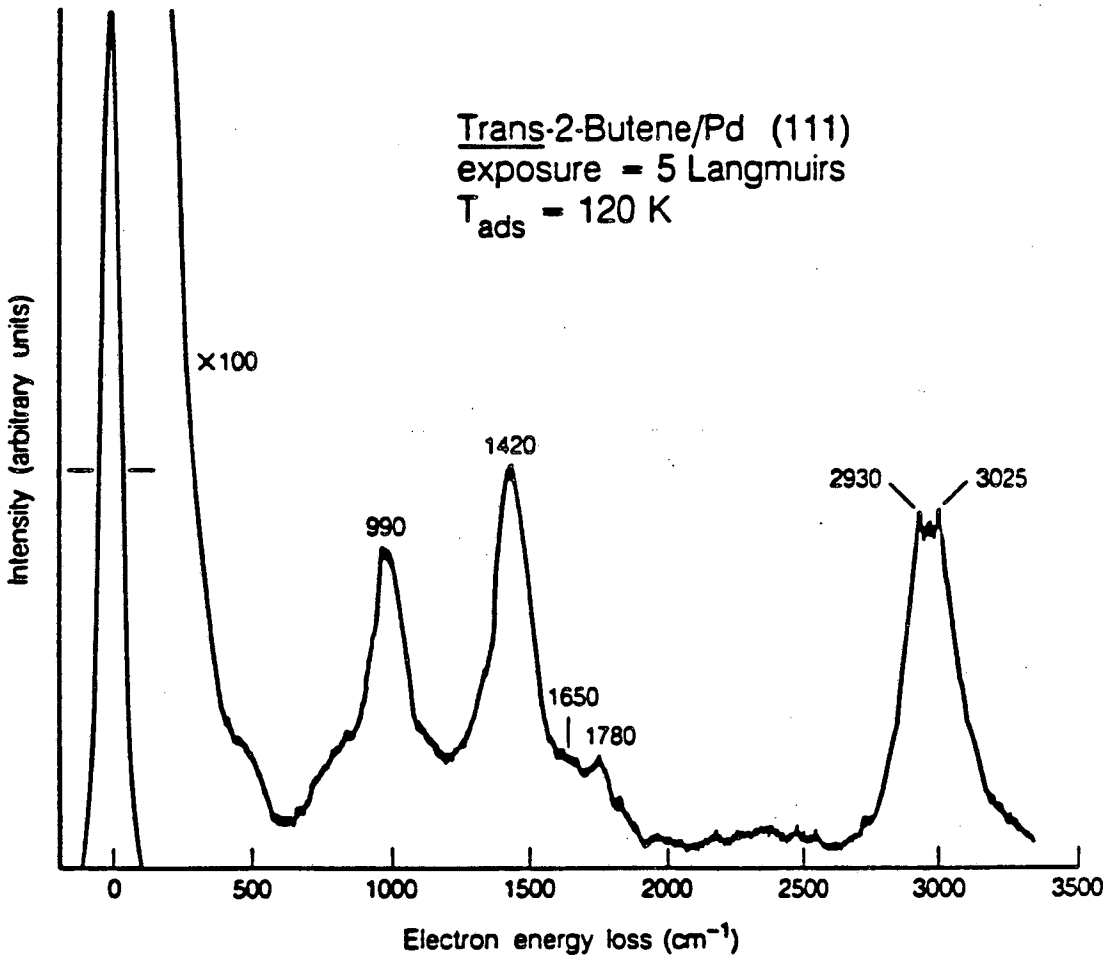
Trans-2-Butene/Pd (111)
exposure = 5 Langmuirs
T_{ads} = 120 K
×100
990
1420
1650
1780
2930
3025
Intensity (arbitrary units)
0
500
1000
1500
2000
2500
3000
3500
Electron energy loss (cm^{-1})

Figure 25. Electron energy loss spectrum of multilayers of cis 2-butene adsorbed on Pd(111) at T=120K.

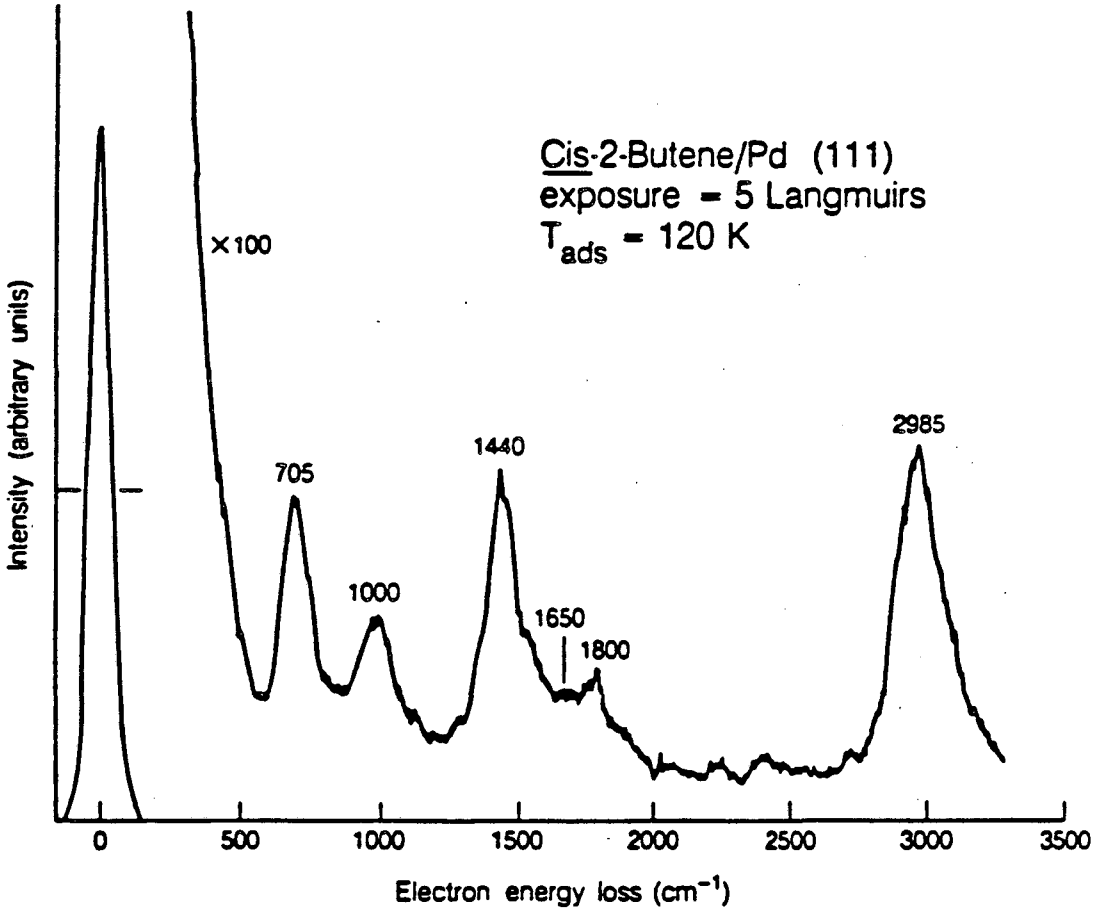
Cis-2-Butene/Pd (111)
exposure = 5 Langmuirs
T_{ads} = 120 K
×100
705
1000
1440
1650
1800
2985
Intensity (arbitrary units)
0
500
1000
1500
2000
2500
3000
3500
Electron energy loss (cm^{-1})

Figure 26. Electron energy loss spectrum of multilayers of trans 1,2-dichloroethene adsorbed on Pd(111).

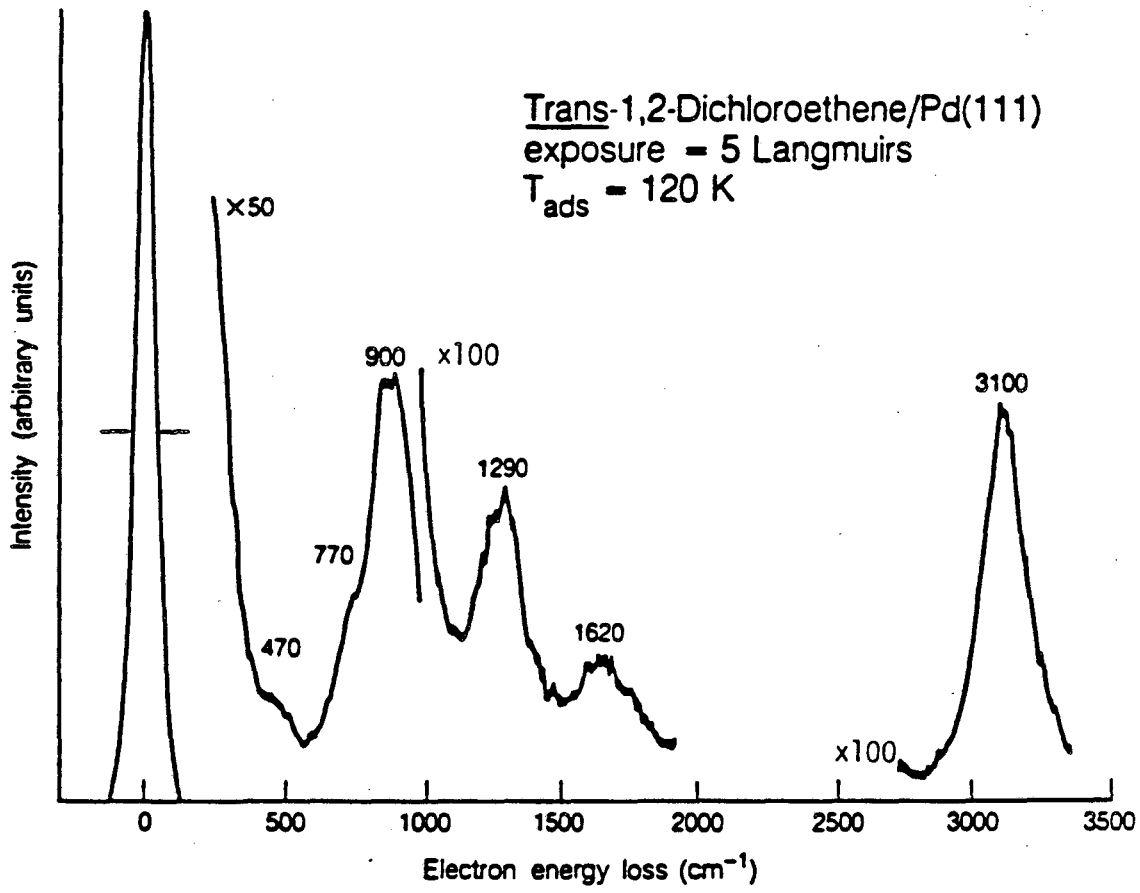
Trans-1,2-Dichloroethene/Pd(111)
exposure = 5 Langmuirs
T_{ads} = 120 K
×50
900
×100
3100
1290
770
470
1620
x100
Intensity (arbitrary units)
0
500
1000
1500
2000
2500
3000
3500
Electron energy loss (cm^{-1})

Figure 27. Electron energy loss spectrum of multilayers of cis 1,2-dichloroethene adsorbed on Pd(111).

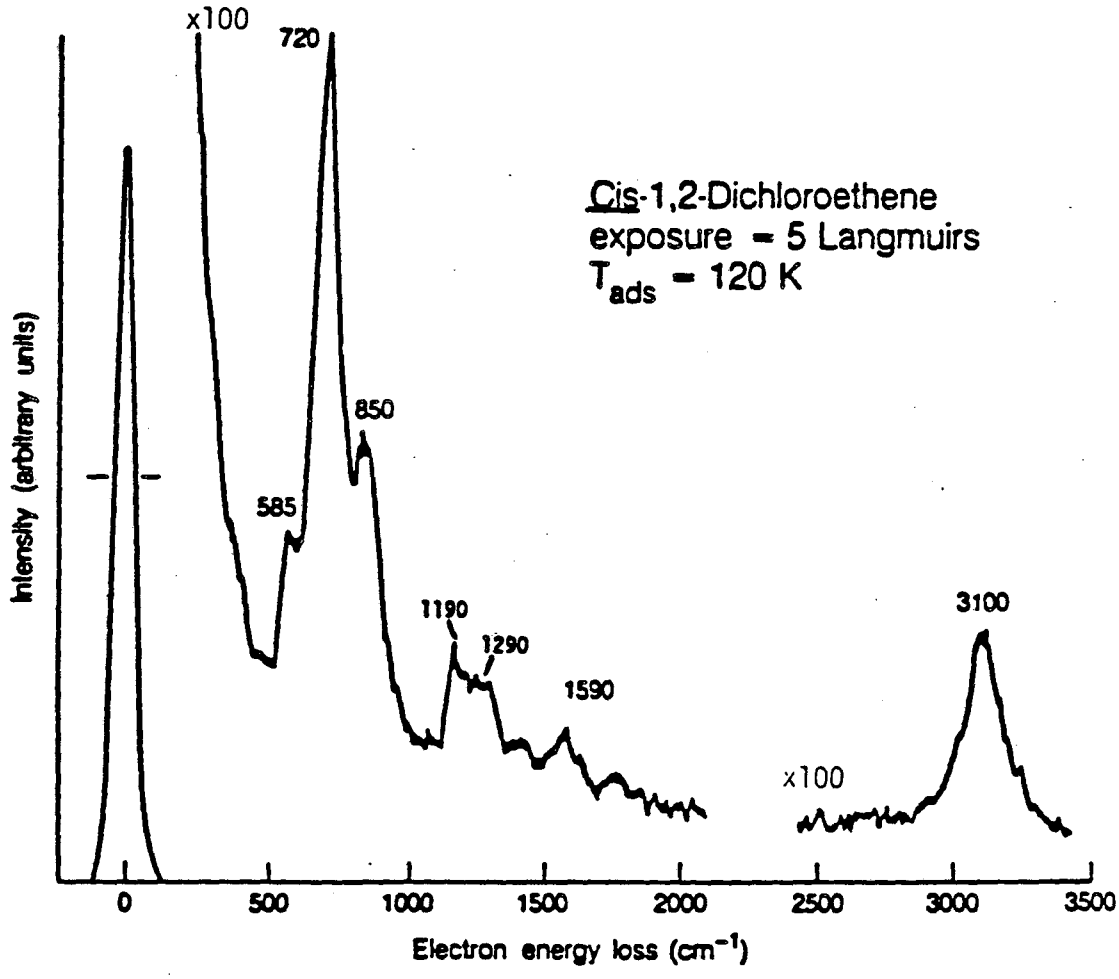
x100
720
850
585
1190
1290
1590
3100
x100
Cis-1,2-Dichloroethene
exposure = 5 Langmuirs
T_{ads} = 120 K
Intensity (arbitrary units)
0
500
1000
1500
2000
2500
3000
3500
Electron energy loss (cm^{-1})

recorded after 66 and 112 minutes of photolysis, along with the spectrum recorded before photolysis (Figure 28). There is a decrease in the peak at 990 cm^{-1} while a new peak at 710 cm^{-1} grows in. Other spectral features stay approximately the same after photolysis. In another experiment 5 langmuirs of trans 2-butene was photolyzed with a CsI filter placed in front of the Hg lamp, thus photolyzing with light of wavelengths greater than 237nm. As shown in figure 29b no significant changes were evident after 75 minutes of photolysis. Immediately after the above 75 minute photolysis the CsI filter was removed and the sample was then photolyzed an additional 21 minutes with the full output of the Hg lamp (Fig. 29c). This indeed resulted in the spectral changes that were discussed previously.

1,2-Dichloroethenes

The broadband photolysis of a 5 langmuir dose of trans 1,2-dichloroethene was followed as a function of photolysis time by electron energy loss spectroscopy. The electron energy loss spectrum, after photolysis times of 15, 25, 35 and 57 minutes, of trans 1,2-DCE is shown in figure 30. Figure 30 shows the spectral region, from 600 - 1750 cm^{-1}. Spectral changes were observed only in this part of the spectrum as the sample was photolyzed. The most intense peak in the parent spectrum at 900 cm^{-1} decreases considerably in intensity. Concurrent with the decrease in intensity for the 900 cm^{-1} is the growth of a new peak at 720 cm^{-1}.

The electron energy loss spectrum of a 5 langmuir exposure of cis 1,2-dichloroethene after broadband photolysis, for 52 minutes, is shown in figure 31. For the cis isomer the most intense loss peak in the EEL spectrum occurs at 720 cm^{-1} (See Figure 27). After photolysis this peak

Figure 28. Electron energy loss spectra following broadband UV photolysis of trans 2-butene after a) 0 minutes b) 66 minutes and c) 112 minutes.

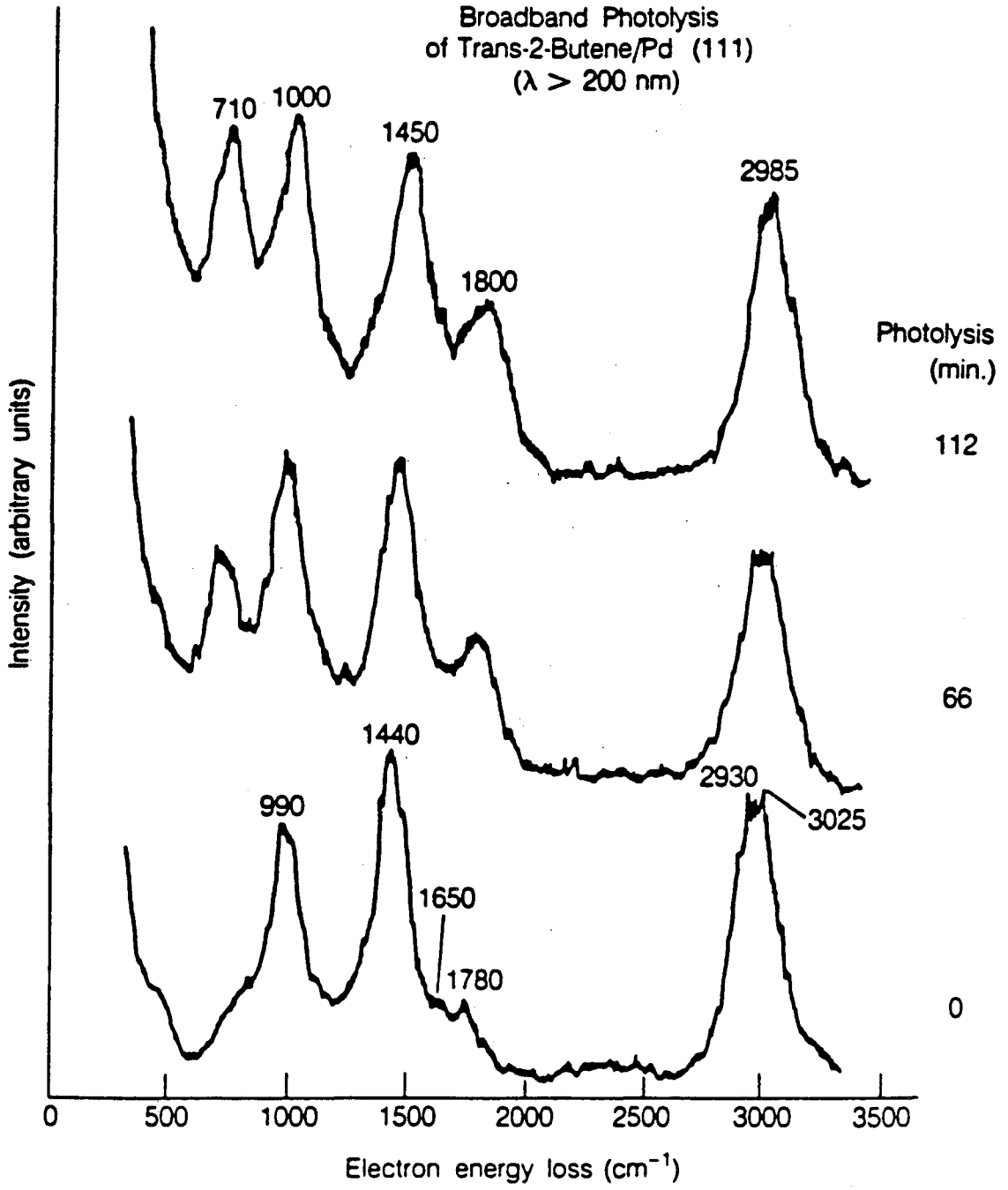

XBL 8612-9295

Figure 29. Electron energy loss spectrum after UV photolysis of trans 2-butene, a) prior to photolysis b) with a CsI filtered lamp for 75 minutes c) unfiltered Hg lamp for 21 minutes.

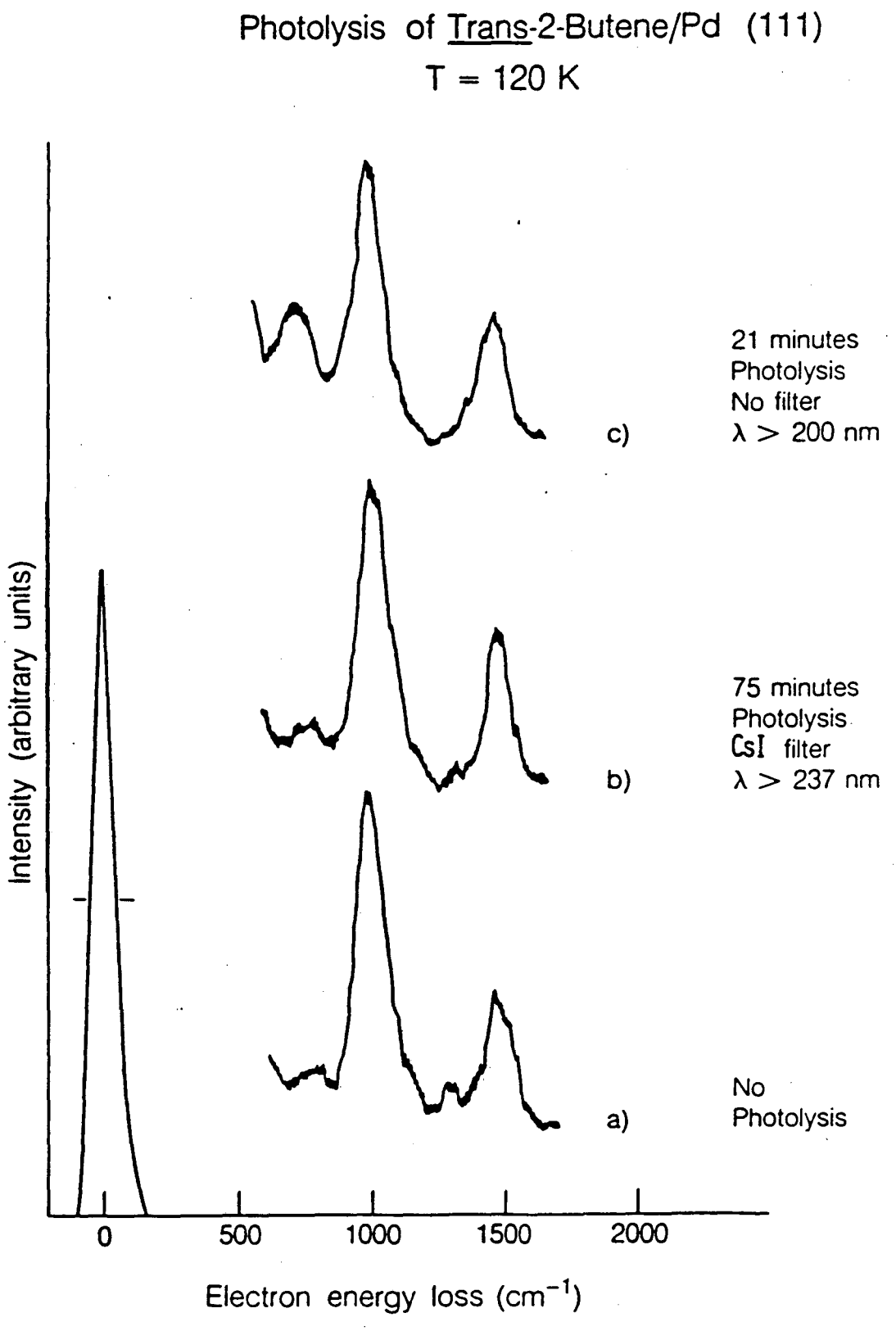
Photolysis of Trans-2-Butene/Pd (111)
T = 120 K
Intensity (arbitrary units)
c)
21 minutes
Photolysis
No filter
λ > 200 nm
b)
75 minutes
Photolysis
CsI filter
λ > 237 nm
a)
No
Photolysis
0
500
1000
1500
2000
Electron energy loss (cm⁻¹)

Figure 30. Electron energy loss spectra following broadband photolysis of trans 1,2-dichloroethene as a function of photolysis time.

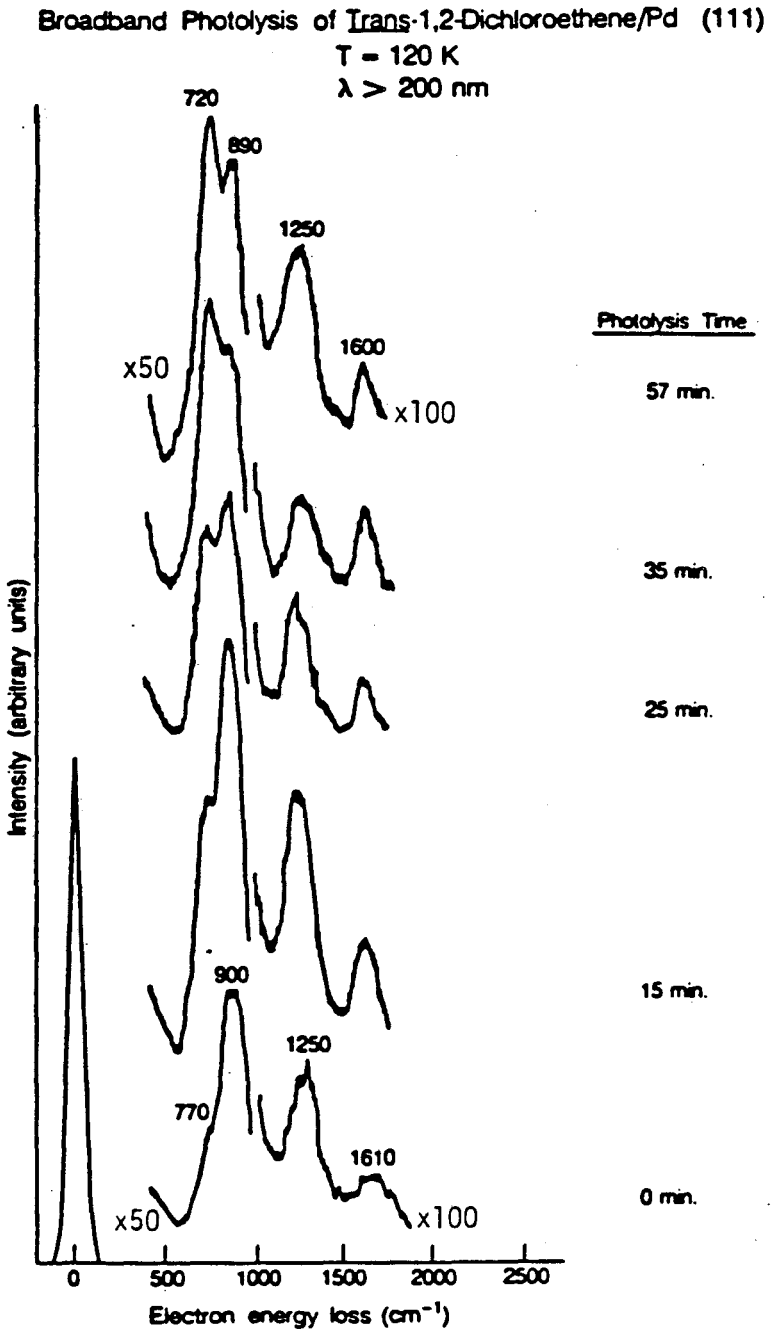
Broadband Photolysis of Trans-1,2-Dichloroethene/Pd (111)
T = 120 K
λ > 200 nm
720
890
1250
1600
x50
x100
Photolysis Time
57 min.
35 min.
25 min.
15 min.
0 min.
900
1250
770
1610
x50
x100
Intensity (arbitrary units)
0
500
1000
1500
2000
2500
Electron energy loss (cm⁻¹)

Figure 31. Electron energy loss spectrum after 52 minutes of UV photolysis (λ>200 nm) of cis 1,2-dichloroethene adsorbed on Pd(111), T=120K.

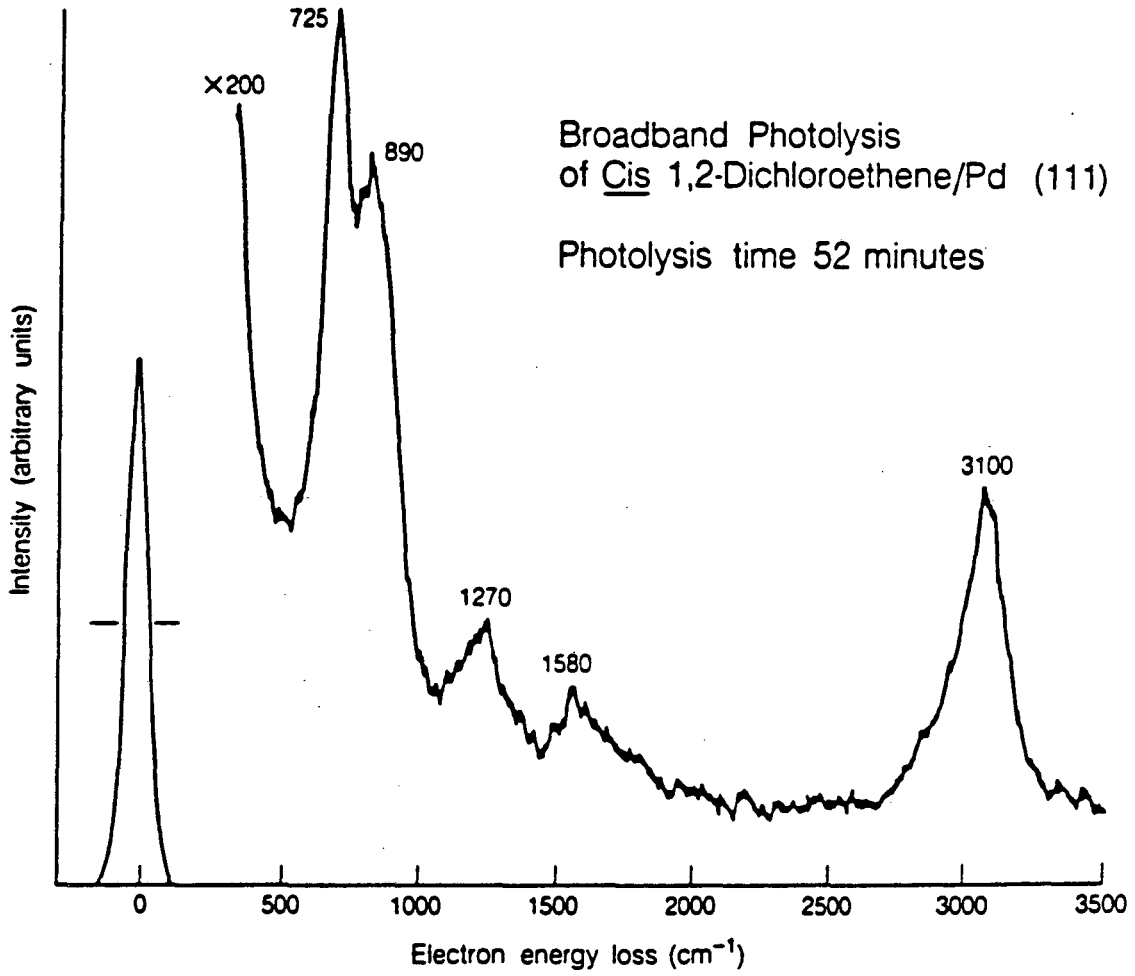
725
×200
890
Broadband Photolysis
of Cis 1,2-Dichloroethene/Pd (111)
Photolysis time 52 minutes
3100
1270
1580
Intensity (arbitrary units)
0
500
1000
1500
2000
2500
3000
3500
Electron energy loss (cm⁻¹)

decreases in intensity and a peak near 890 cm^{-1} becomes much more prominent. Also, the loss peak at 585 cm^{-1} may be lost and there seems to be change in the contour of the broad loss peak at 1250 cm^{-1}.

DISCUSSION

2-Butene

The assignment of the multilayer EEL spectra of *cis* and *trans* 2-butene is straightfoward. Table 11 and 12 lists the frequencies and assignment of the EEL spectra for the *trans* and *cis* isomer, respectively. The assignment was made by direct comparison to the infrared spectra of these molecules in the gas phase.[65] Due to the poor resolution associated with an EEL spectrum, some of the loss peaks were assigned to more than one band in the IR spectrum. In the EEL spectrum of *trans* 2-butene the C-H stretching motion is seen for the methyl and alkene hydrogens at 2930 and 3025 cm^{-1}, respectively. The asymmetry of the loss peak, in the *cis* 2-butene spectrum at 2985 cm^{-1} suggests that the peak is associated with both the C-H stretching motion of the alkene and methyl hydrogens, although these are not resolved in the spectrum. The carbon-carbon stretching motion is weak but observed at 1650 cm^{-1} in both the *cis* and *trans* 2-butene spectra. This is close to the gas phase IR value of 1672 cm^{-1} for the *cis* isomer and the Raman value of 1681 cm^{-1} for the *trans* isomer. The large difference in the frequency of the out-of-plane motion for the *cis* and *trans* isomers have always been used in a diagnostic way to distinguish these alkene stereoisomers. This frequency of the out-of-plane motion for the 2-butenes is observed at 705 cm^{-1} for the cis and 990 cm^{-1} for the *trans* in the EEL spectrum and definitively distinguishes these two isomers. The frequencies in the

TABLE 11

VIBRATIONAL FREQUENCIES AND ASSIGMENT FOR TRANS 2-BUTENE

PHYSISORBED ON Pd(111) AT T=120K

TRANS

Mode Description	Gas Phase (IR)[a]	Multilayer (EELS)
Skeletal deformation	507(R, Ag)[b]	450
C-H out-of-plane bend	964	990
CH_3 wag	973	990
CH_3 sym. deformation	1380	1420
CH_3 asym. deformation	1450	1420
C-C stretch	1065	990
C=C stretch	1681	1650
C-H (methy)	2950	2930
C-H (ethyl)	3050	3025

a. Kilpatrick, J.E. and Pitzer, K.S., J. Research Natl. Bur. Standards, Vol. 38 (1947) 191.

b. R=Raman, Ag=symmetry representation

TABLE 12

VIBRATIONAL FREQUENCIES AND ASSIGNMENT FOR CIS 2-BUTENE

PHYSISORBED ON Pd(111) at T=120K

CIS

Mode Description	Gas Phase (IR)[a]	Multilayer (EELS)
C-H out-of-plane bend	673	705
CH_3 wag	1018(A_1),[b] 1064(B_2)	1000
CH_3 sym. deformation	1380	1440
CH_3 asym. deformation	1450	1440
C-C stretch	978	1000
C=C stretch	1672	1650
C-H stretch (methyl)	2950	2985
C-H stretch (ethyl)	3050	2985

a. Kilpatrick, J.E., and Pitzer, K.S., J. Research Natl. Bur. Standards, 38 (1947) 191.

b. A_1, B_2 symmetry representation for the C_{2v} point group

EEL spectra for this motion are within 30 cm^{-1} to what is observed in the IR spectrum of these two isomers in the gas phase.

As a 5 langmuir sample of trans 2-butene is photolyzed with the full spectrum of the mercury arc lamp, isomerization to the cis form is evident (see figure 28). The 705 cm^{-1} loss peak associated with the out-of-plane bending motion of the cis form grows in as a fuction of photolysis time. As discussed above this peak distinguishes in the EEL spectrum the cis isomer from that of the trans. The extent of conversion of the trans to the cis form can be calculated by comparing the ratio of A_{705}/A_{990} in the parent spectrum of the cis form to that of the spectrum after photolysis of trans 2-butene. Where A_{705} is the area of the 705 cm^{-1} peak and similarly A_{990} is the area of the peak at 990 cm^{-1}. This ratio for the parent spectrum is 1.38. Comparing this to the value of 0.74 for the ratio of A_{705}/A_{990} after photolysis of trans 2-butene indicates that 52 ± 5 % of the trans isomer has interconverted to the cis form. This calculation assumes that the extinction coefficient for this out-of-plane motion is the same for these two isomers.[66]

An important question which naturally arises from these results is what influence, if any, does the Pd metal surface have on the photochemistry of trans 2-butene? Most of the molecules in the multilayer are not in direct contact with the Pd surface atoms and as discussed above only weakly interact with the metal surface. Therefore any interaction must be through the intervening material. The first step in determining the possible influence of the conducting metal surface on the photoprocess, is to compare the photochemistry of the 2-butenes described here to that of the photochemistry observed in the gas

phase.

The photochemistry of the 2-butenes in the presence of triplet photosensitizers, such as Hg atoms, has been studied extensively by Cundell and Palmer.[63] The major photochemical process of either the cis of the trans isomer in the presence of excited state Hg atoms (^3P) is isomerization. A smaller fraction of the electronically excited 2-butenes decompose to form radical pairs, with the methyl and 1-butene radicals accounting for most of the radicals produced. The mechanism proposed by these workers to account for all the observed photochemistry, isomerization and fragmentation is the following: excited state Hg atoms (^3P) are quenched by the 2-butene molecules which after excitation are in a high vibrational level in the triplet manifold (presumably a $(\pi-\pi^*)^3$ transition). Consequently from this hot triplet state the molecule either isomerizes of decomposes. The extent of these two competing processes is dependent on both reactant and buffer gas pressures, with the isomerization reaction always being dominant.

Within the resolution and sensitivity obtained in these experiments conversion of trans 2-butene to the cis form is the only photochemical reaction that is observed. Whether the photoreaction is occuring on a singlet or triplet excited potential energy surface is unclear. Broadband photolysis, with the full Hg arc, of the physisorbed state closely mimics that of the triplet photosensitized chemistry described above for the gas phase. Although photoreaction occurring on an excited triplet surface does seem to be a lucrative explanation at this point the non-reactivity of the trans 2-butene when irradiated with a CsI filtered Hg lamp ($\lambda > 237$nm) discounts this mechanism. Excited state Hg atoms in the photosensitized reactions have an energy content of 112

kcal/mole corresponding to 253.7nm light absorbed in the $^1S-^3P$ atomic transition. This is approximately 8 kcal/mole less energy then the 237nm light used in these experiments. Clearly there is enough energy to access the triplet state with 237nm light, provided there is enough light absorbed to cause noticeable isomerization. In any event we conclude that the photoreaction need not be occurring on a triplet surface.

The ultra-violet absorption spectrum for the 2-butenes was taken by Jones and Taylor and others.[67] The recorded spectra shows a broad absorption band with a λ_{max} centered at 175 and 180nm for the cis and trans isomers respectively. The tails of the absorption band extend out to ~200nm for both isomers. The tail of the absorption band is attributed to the $(\pi-\pi^*)^1$ electronic transition. At a first glance it is surprising that the photo-reaction is occurring with such propensity in the physisorbed ad-layer when only a very small portion of the absorption band, with a low extinction coefficient, is being accessed.

Assuming the intensity of the electric field from the lamp is the same in the presence or absence of the smooth Pd(111) surface the shift of the transition dipole to the red would account for the propensity of the cis and trans 2-butenes to photoisomerize upon irradiation with 200nm light. A red shift due to a perturbation by the surface means that the upper state is lowered in energy with respect to the ground state. The dramatic decrease in photochemistry with wavelengths of light greater then 237nm indicates the tail of the absorption band has dropped off significantly by 237nm.

Dichloroethenes

The assignment of the loss peaks in the EEL spectrum for the trans

and cis 1,2-dichloroethene multilayer spectra, on Pd(111), are given in Tables 13 and 14. Similar to the 2-butene assignment, the vibrational frequencies of the cis and trans 1,2-dichloroethene was made by direct comparison to the frequencies and assignment for these molecules in the gas and liquid phase. The agreement between the EEL multilayer spectrum and the IR frequencies[42] is good. The most intense peak in the EEL spectrum, at 720 cm^{-1} for the cis isomer and 900 cm^{-1} for the trans, correspond to the out-of-plane motion of the hydrogens. Again we see the large frequency difference of 180 cm^{-1} for this motion makes it relatively easy to distinguish between the cis and trans form. The other loss peaks do not readily distinguish between these two isomers.

Broadband irradiation of ($\lambda > 200nm$) of trans 1,2-dichloroethene as a function of photolysis time is shown in figure 30. The intensity of the loss peak at 900 cm^{-1} decreases as a new peak at 720 cm^{-1}, grows in. A steady state with the radiation field is reached after approximately 50 minutes, with no further change in the EEL spectrum seen. Figure 32 shows the growth of the 720 cm^{-1} peak as a function of photolysis time, superimposed on the graph is the concurrent decrease in intensity of the 900 cm^{-1} peak.

Similarly broadband photolysis of cis 1,2-dichloroethene shown in figure 31 for 52 minutes results in the same steady state as seen for the trans. There is a decrease in the 720 cm^{-1} peak upon photolysis with a concurrent increase in the 890 cm^{-1} peak, as can be seen from the comparison of figure 27, showing no irradiation, to figure 31 after 52 minutes of broadband irradiation.

The ultra-violet spectra of the chlorinated ethenes in the gas phase has been reported by Berry.[68] For the 1,2-dichloroethene isomers

TABLE 13

VIBRATIONAL FREQUENCIES AND ASSIGNMENT FOR TRANS 1,2-DICHLOROETHENE PHYSISORBED ON Pd(111) at T=120K

TRANS Mode Description	Gas Phase IR[a]	Multilayers (EELS)
C-Cl asymmetric stretch	828(vs)[b]	770(s)
C-H out-of-plane bend	900(s)	900(vs)
C-H in-plane bend	1200(s)	1290
C=C stretch	1587(R)	1620(w)
C-H asymmetric stretch	3090	3100(s)

a. Reference 42.

b. s=strong, m=medium, w=weak and R=Raman.

TABLE 14

VIBRATIONAL FREQUENCIES AND ASSSIGNMENT FOR CIS

1,2-DICHLOROETHENE PHYSISORBED ON Pd(111) AT T=120K

CIS

Mode Description	Gas Phase (IR)[a]	Multilayer (EELS)
CCCl Deformation	571(m)[b]	585(m)
C-H out-of-plane-bend	697(vs)	720(vs)
C-Cl symmetric stretch	714(m)[c]	720(vs)
C-Cl asymmetric strecth	857(s)	850(s)
C-H in-plane bend	1183(w)[c]	1190(m)
C-H in-plane bend	1303(m)	1290(m)
C=C stretch	1590[c]	1590(w)
C-H symmetric stretch	3072	3100(s)
C-H asymmetric stretch	3077[c]	3100(s)

a. Reference 42

b. R=Raman

c. liquid phase, ref. 42

Figure 32. Growth and decay curves for loss peaks at 720 and 900 cm^{-1} respectively, during the photolysis of trans 1,2-dichloroethene.

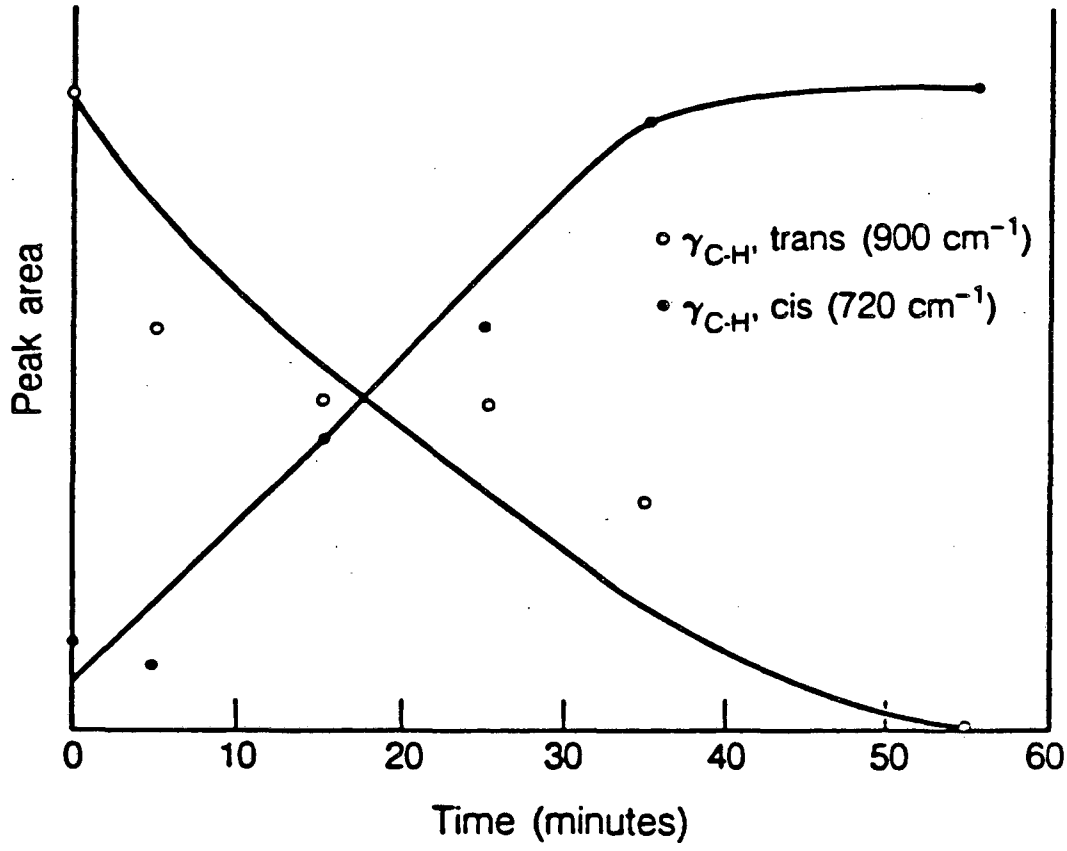
Peak area
Time (minutes)
0
10
20
30
40
50
60
γ_{C-H}, trans (900 cm^{-1})
γ_{C-H}, cis (720 cm^{-1})

the absorption band peak maxima occurs at 190 and 195nm for the cis and trans forms respectively. The tail of the absorption band extends out to ~230nm for both isomers. The main contribution to the oscillator strength of this absorption band is the $(\pi-\pi^*)^1$ transition. Weaker transitions which are thought to be hidden under the more intense $(\pi-\pi^*)$ are the $(n\pi^*)^1$ and the $(n-\sigma^*)^1$. These, of course, correspond to a nonbonding electron localized on the chlorine atom so they are expected to be at longer wavelength than the $\pi-\pi^*$ transition. Hence they may become more significant in photolysis when exciting the long wavelength tail of the absorption band. The extent that these transitions must be considered in the photochemistry of these molecules remain unclear.

The UV photochemistry of the dichloroethenes has been shown to be quite complex. A gas-phase study of all three isomers of dichloroethene by Ausubel and Wijnen[60] showed that many photoproducts were produced upon irradiation. A detailed study by Cartland and Pimentel[62] on the direct photolysis and photosensitized reactions of the dichloroethenes deposited in krypton matrices showed that the photoreactivity was strongly dependent on the initial excited state potential energy surface. In contrast to the complex gas phase photolysis, only two photoprocesses were observed in the direct broadband photolysis of the dichloroethenes in a Kr matrix, isomerization and HCl elimination. the simpler photochemistry of the dichloroethenes in the rare gas matrix has been attributed to the suppression of secondary reactions and cage effect inhibition of free radical formation.

The complexity of the photoreactivity of cis and trans 1,2-dichloroethene in the gas phase would appear at first to make the analysis of UV irradiation of physisorbed 1,2-dichloroethenes more

difficult then the 2-butene. However, with the sensitivity and resolution obtained in these experiments the and only dominant photoreaction channel for both cis and trans 1,2-dichloroethene appears to be isomerization. Isomerization was the major photoprocess in the direct irradiation of cis and trans 1,2-dichloroethene in the gas phase[60] and cryogenic matrices.[62] As was observed in a matrix environment, the simplicity of the photochemistry of multilayers of dichloroethene could be due to the suppression of secondary reactions and radical formation in this ad-layer.

In summary, photochemistry of di-substituted alkenes physisorbed on Pd(111), at T=120K, was demonstrated. For trans 2-butene and cis and trans 1,2 dichloroethene photoisomerization was the only photoprocess observed. Within the sensitivity and resolution of these experiments no other photoproducts were detected. Excitation of an electron from a π bonding orbital to a π antibonding orbital, $(\pi-\pi^*)^1$, would explain the observed photochemistry of the 2-butenes as well as the 1,2-dichloroethenes physisorbed on Pd(111).

2. RESULTS AND DISCUSSION

B. PHOTO- AND THERMO- CHEMISTRY OF CIS and TRANS 1,2-DICHLOROETHENE ADSORBED ON Pt(111)

Electron Energy Loss Spectroscopy As A Function of Surface Coverage

Figure 33 shows the electron energy loss spectrum (at the specular angle) for cis 1,2-dichloroethene(DCE) adsorbed on Pt(111) at 110K, as a function of surface coverage. For monolayer and sub-monolayer coverages, (Fig. 33a and b), loss peaks are observed at 650, 2985, 1010, 1250 and 445 cm^{-1} (in order of approximate decreasing intensity). The loss peaks observed at 470 and 2080 cm^{-1} are attributed to the Pt-C and C≡O stretching frequencies for co-adsorbed carbon monoxide, from background gases in the UHV chamber. The frequencies of these loss peaks at 470 and 2080 cm^{-1} agree with the values obtained by Baro and Ibach of 480 and 2105 cm^{-1} for CO adsorbed on a top-site on Pt(111) at 92K.[69] As the coverage is increased, the most intense loss peak in the spectrum begins to broaden considerably and the loss peak maximum shifts to higher frequency from 650 to 690 cm^{-1} (Fig. 33c). Additional loss peaks are observed at 1610 and 3080 cm^{-1}. As the coverage is further increased the 690 peak shifts to 720 cm^{-1} and 3080 to 3090 cm^{-1}, giving essentially the spectrum of the liquid (Figure 33d). The loss peaks for chemisorbed cis 1,2-DCE are hidden under the more intense loss peaks for the multilayer, although the C-H stretch of the monolayer is still evident at 2995 cm^{-1}.

The trans isomer was similarly studied, and the electron energy loss spectrum for this molecule chemisorbed on Pt(111) as a function of

Figure 33. Electron energy loss spectrum (recorded in the specular direction) of cis 1,2-dichloroethene adsorbed on Pt(111) as a function of increasing exposure, a. 0.1 L b. 0.35 L c. 0.65 L and d. 0.80 L (where L=Langmuirs).

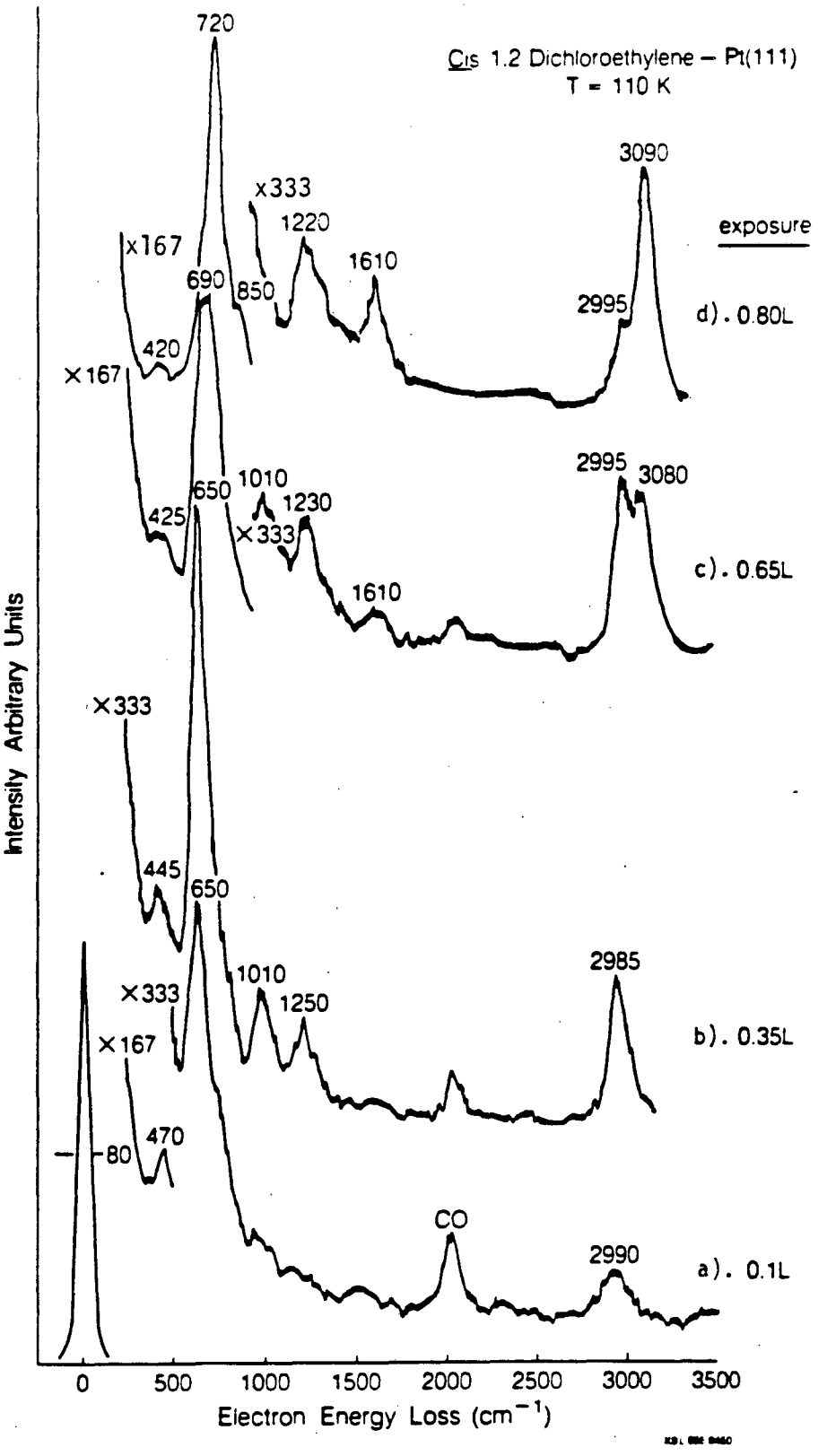
Cis 1.2 Dichloroethylene – Pt(111)
T = 110 K
exposure
d). 0.80L
c). 0.65L
b). 0.35L
a). 0.1L
720
3090
x333
1220
x167
690
850
1610
2995
420
x167
650
1010
2995
3080
425
1230
x333
1610
x333
445
650
2985
1010
x333
1250
x167
470
80
CO
2990
Intensity Arbitrary Units
0
500
1000
1500
2000
2500
3000
3500
Electron Energy Loss (cm⁻¹)

Figure 34. Electron energy loss spectrum (recorded in the specular direction) of trans 1,2-dichloroethene adsorbed on Pt(111) as a function of increasing exposure, a. 0.15L b. 0.45 L and c. 0.70 L (where L=Langmuirs).

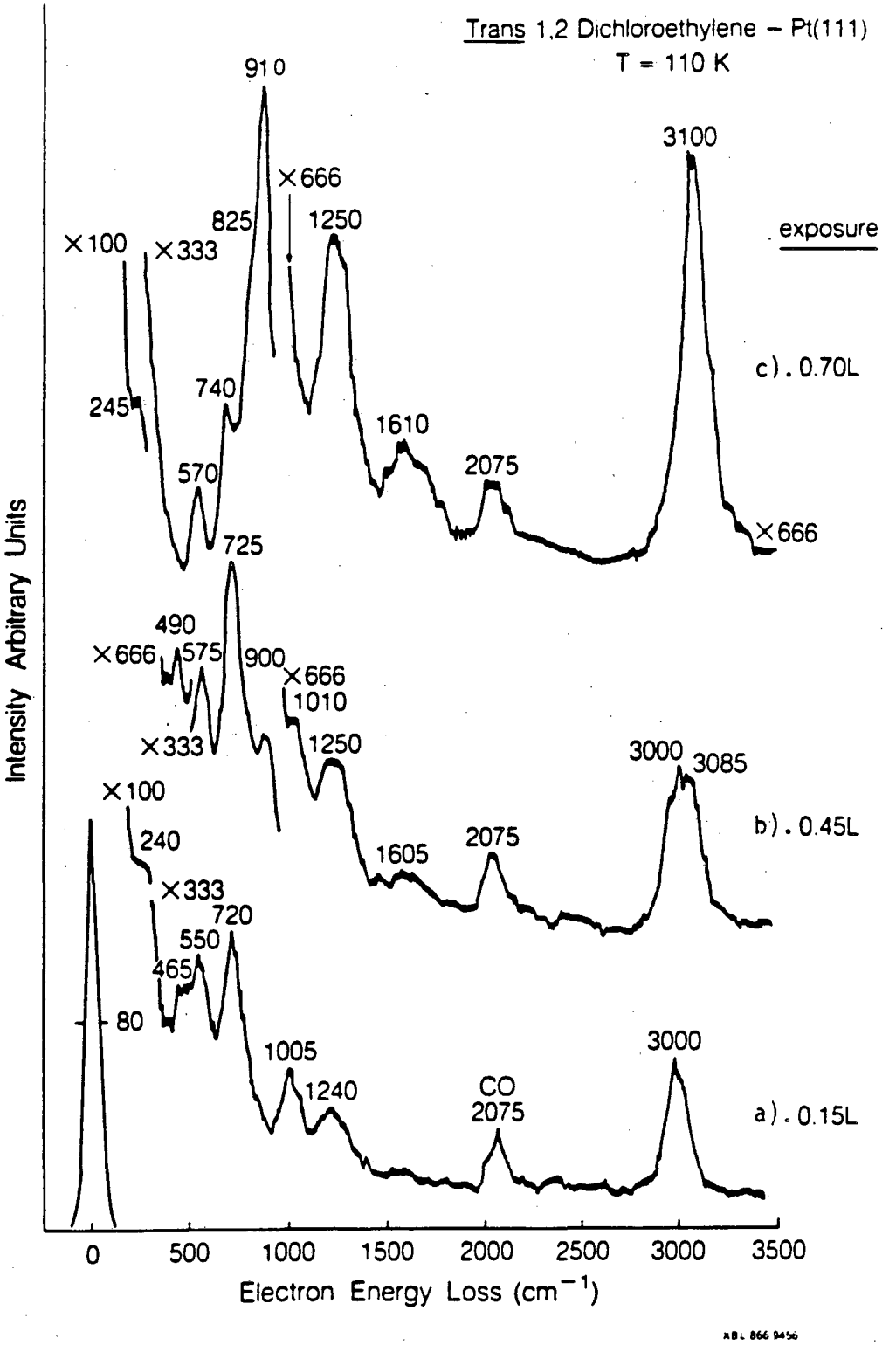
Trans 1,2 Dichloroethylene – Pt(111)
T = 110 K
exposure
c). 0.70L
b). 0.45L
a). 0.15L
Intensity Arbitrary Units
Electron Energy Loss (cm⁻¹)
0
500
1000
1500
2000
2500
3000
3500
910
825
1250
3100
×666
×100
×333
740
245
570
725
1610
2075
490
575
900
1010
3000
3085
240
720
550
465
80
1005
1240
CO
2075
1605

coverage is shown in Figure 34. For monolayer or sub-monolayer coverages loss peaks are observed at 720, 3000, 550, 1005 and 1240 and 240 cm^{-1} (in order of decreasing intensity). The loss peaks at 465 and 2075 cm^{-1} are attributed to co-adsorbed carbon monoxide. As the coverage is increased an intense loss peak at 910 cm^{-1} with a shoulder at 825 cm^{-1} becomes the most prominent spectral feature. A new loss peak is also observed at 1610 cm^{-1}. As with the cis isomer the frequency of the C-H stretch has shifted up by approximately 100 cm^{-1}, to 3100 cm^{-1}, in the multilayer spectrum.

Table 15 lists the frequencies and assignments of the loss peaks for the multilayer spectrum of cis and trans 1,2-dichloroethene. The assigments for the multilayer spectra are made readily by direct comparison to the infrared spectra of these molecules in the gas and liquid phase,[42] as was discussed in the previous section for multilayer adsorption on Pd(111). Loss peaks observed for the monolayer spectra are also listed in Table 15. The spectral features for monolayer coverages of the cis and trans isomers are qualitatively similar, though not identical, and each differs markedly from appropriate liquid phase spectrum. From the frequencies of the loss peaks in the monolayer spectra the molecular structures of the adsorbed dichloroethenes can be deduced as will be discussed.

Thermal Chemistry

Figure 35 shows the EEL spectrum of cis 1,2-dichloroethene as a function of temperature. In each case the sample was warmed to the desired temperature and held there for two minutes, then cooled back down to 110K before an EEL scan was taken. Multilayers were initially adsorbed onto the surface held at 110K, as the temperature is raised to

TABLE 15

TABULATED FREQUENCIES FOR CIS AND TRANS 1,2 DICHLOROETHYLENE ADSORBED ON Pt(111) AT 110K

CIS

Mode Description	Gas Phase (IR)[a]	Multilayer (EELS)	Monolayer
CCCl Deformation	571(m)		445
C-H out-of-plane-bend	697(vs)	720	650
C-Cl symmetric stretch	714(m)	720	1010
C-Cl asymmetric strecth	857(s)	850	1250
C-H in-plane bend	1183(w)	1220	2985
C-H in-plane bend	1303(m)		
C=C stretch	1590	1610	
C-H symmetric stretch	3072	3090	
C-H asymmetric stretch	3077	3090	

TRANS

Mode Description	Gas Phase IR	Multilayers (EELS)	Monolayer
			240
C-Cl asymetric stretch	828(vs)	825(sh)	550
C-H out-of-pland bend	900(s)	910	720
C-H in-plane bend	1200(s)	1250	1005
C=C stretch	1587(R)	1610	1240
C-H asymetric stretch	3090	3100	3000

a. s=strong, m=medium, w=weak and R=Raman.

Figure 35. Electron energy loss spectrum of cis 1,2-dichloroethene as a function of temperature, a. 158K b. 205K and c. 270K.

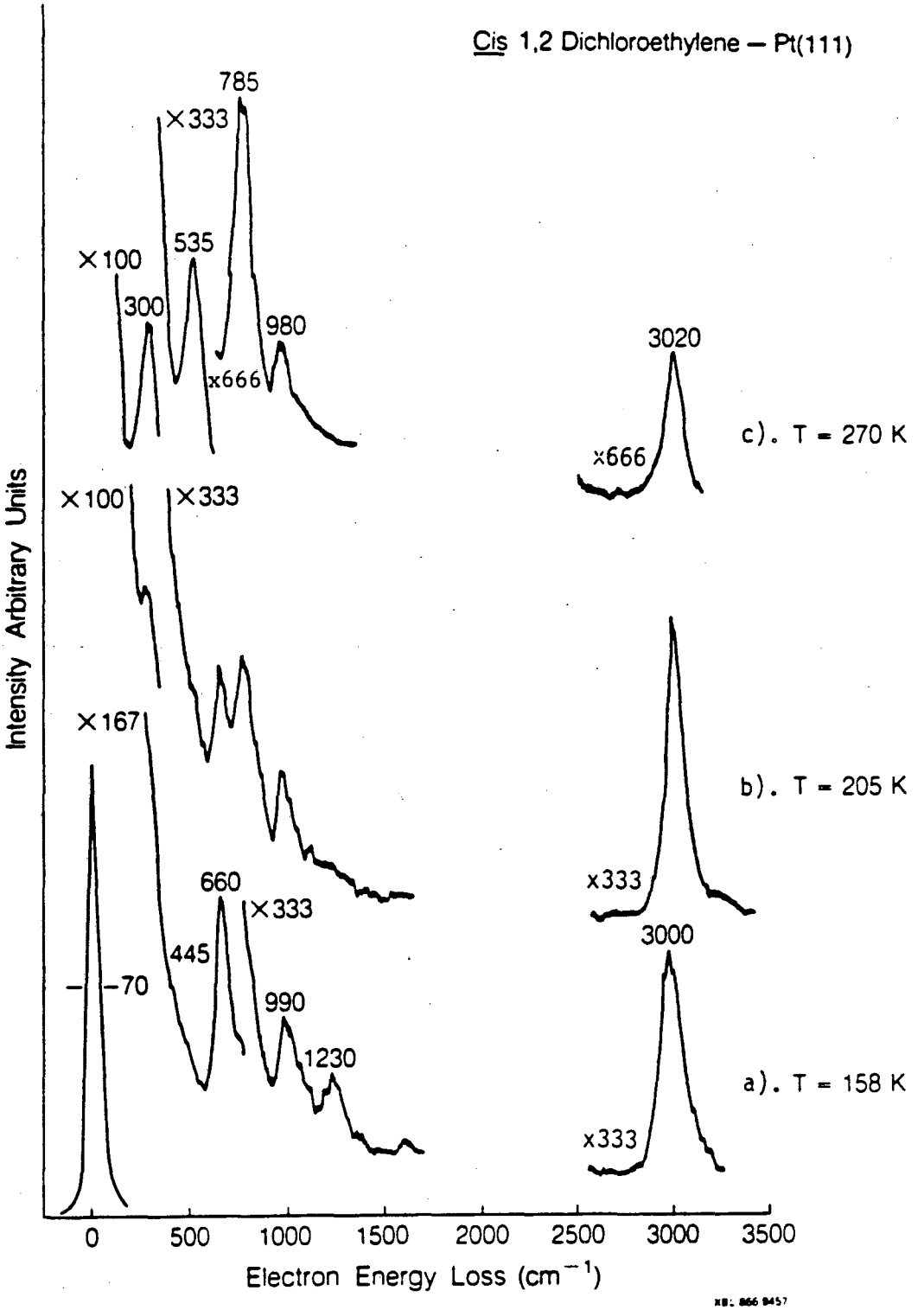
Cis 1,2 Dichloroethylene — Pt(111)
Intensity Arbitrary Units
Electron Energy Loss (cm⁻¹)
0
500
1000
1500
2000
2500
3000
3500
785
×333
×100
535
300
980
x666
3020
x666
c). T = 270 K
×100
×333
×167
b). T = 205 K
x333
660
×333
445
3000
−70
990
1230
a). T = 158 K
x333

158K peaks associated with the multilayer disappear and only loss peaks due to the chemisorbed species are seen. After warming to 205K (Fig. 35b) there is a decrease in intensity of the 660 cm^{-1} loss peak while a loss peak at 785 cm^{-1} begins to appear. In addition, the 1230 cm^{-1} peak and the 445 cm^{-1} peak decrease in intensity as new spectral features appear at 300, 535 and 980 cm^{-1}. The frequency of the C-H stretch also shifts to higher frequency, by approximately 20 cm^{-1}. The thermal behavior of the trans 1,2-dichloroethene is quite similar to that of the cis isomer. The EEL spectrum for trans 1,2-dichloroethene initially adsorbed at 110K and warmed to 270K, is shown in figure 36. Loss peaks are observed at 280, 520, 770, 1000 and 3010 cm^{-1}.

Thermal desorption spectrum for trans 1,2-DCE adsorbed on Pt(111) at 110K is shown in figures 37 and 38. Figure 37 shows the trace of the parent ion, AMU=96. The initial dichloroethene exposure was 5×10^{-9} torr-100 sec and the heating rate during the desorption experiment was 15K/sec. There are two molecular desorption peaks in the thermal desorption spectrum. The temperature of the desorption rate maxima of these two peaks occur at 158K and 247K for the high and low temperature peak respectively.

The gaseous products from the decomposition of the 1,2-dichloroethenes adsorbed on Pt(111) was also monitored by thermal desorption spectroscopy. When the mass spectrometer was set at an AMU=2, 35 and 36 desorption peaks were observed (see Figure 38). These three masses correspond to hydrogen, atomic chlorine and hydrogen chloride evolution. The desorption rate maxima were observed at T_{max}=463K for both atomic chlorine and hydrogen chloride. The coincidence in T_{max} for AMU=35 and 36 indicates that the AMU=35 signal

Figure 36. Electron energy loss spectrum of trans 1,2-dichloroethene after adsorption at 110K and warming to 270K. The temperature of the sample was 110K when the EEL spectrum was recorded.

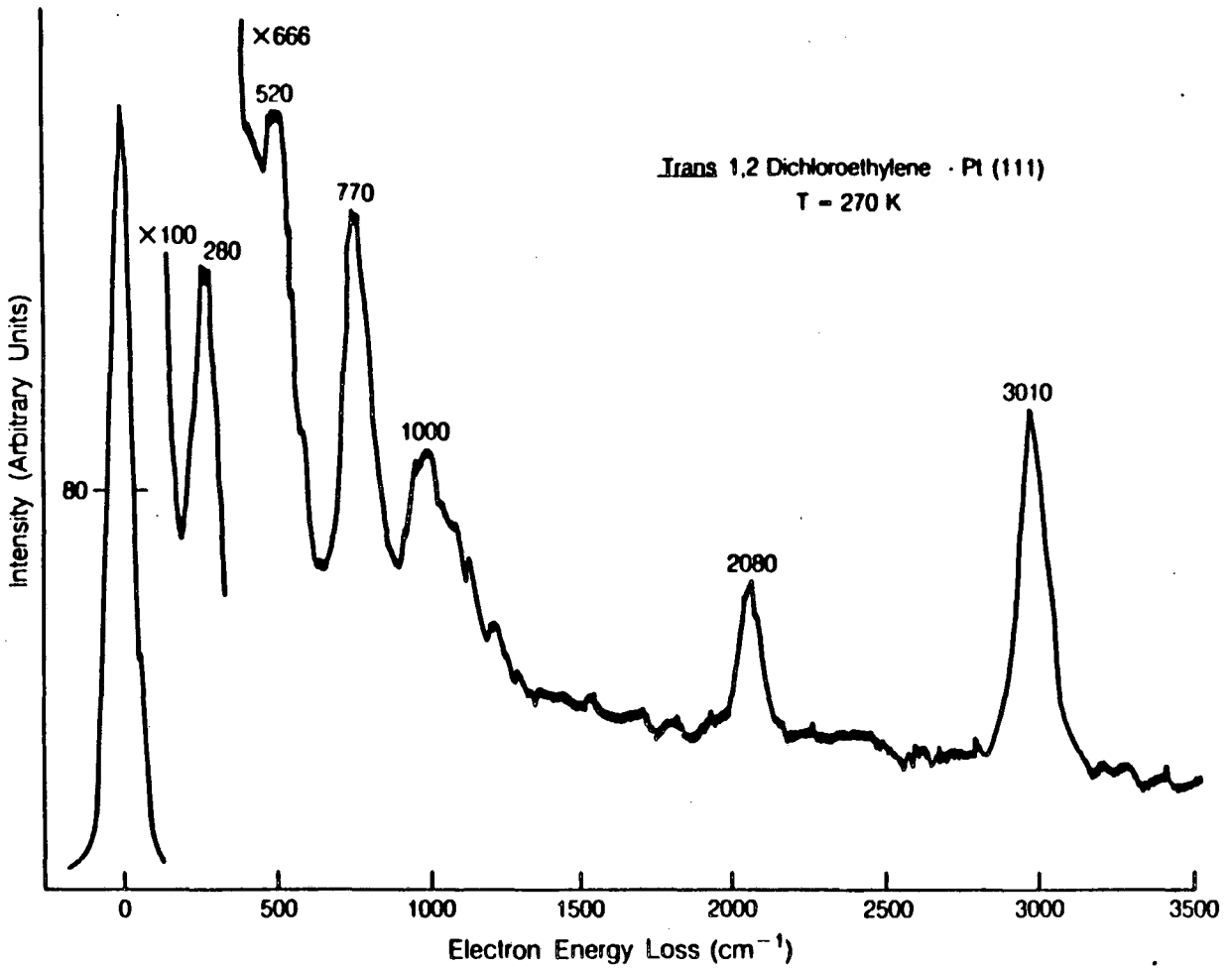
×666
520
770
×100
280
1000
3010
80
2080
Trans 1,2 Dichloroethylene · Pt (111)
T = 270 K
Intensity (Arbitrary Units)
0
500
1000
1500
2000
2500
3000
3500
Electron Energy Loss (cm⁻¹)

Figure 37. Thermal desorption curves for cis 1,2-dichloroethene monitoring the parent ion, AMU=96.

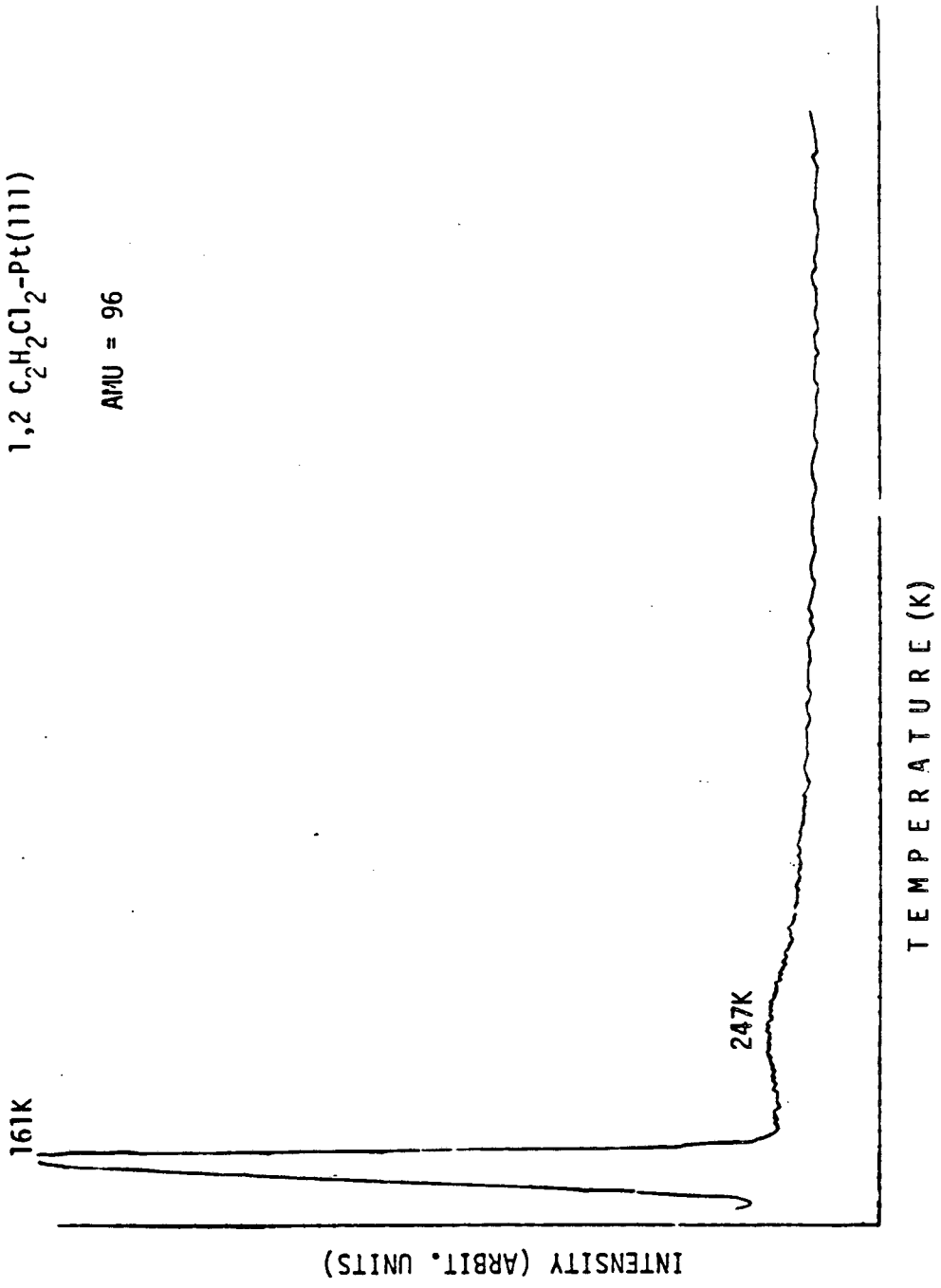
1,2 $C_2H_2Cl_2$-Pt(111)
AMU = 96
161K
247K
TEMPERATURE (K)
INTENSITY (ARBIT. UNITS)

Figure 38. Thermal desorption curves monitoring the decomposition products of cis 1,2-dichloroethene, H_2 and HCl.

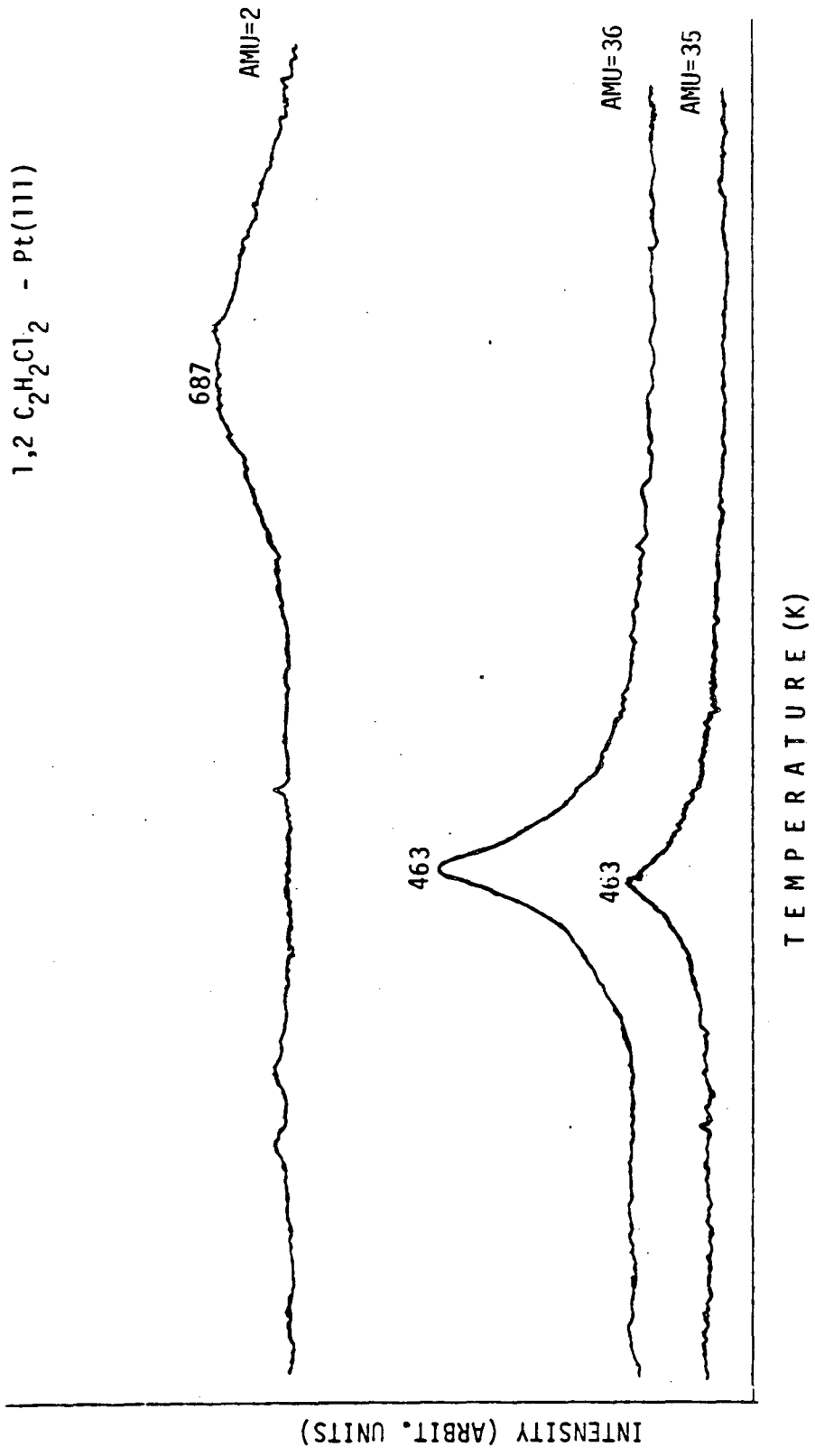
1,2 $C_2H_2Cl_2$ - Pt(111)
AMU=2
687
AMU=36
463
AMU=35
463
TEMPERATURE (K)
INTENSITY (ARBIT. UNITS)

arises from the fragmentation of HCl in the mass spectrometer. The hydrogen desorption rate maximum occurs at a significantly higher temperature than that for HCl with a T_{max}=687K. When the mass spectrometer was set at AMU=70, corresponding to Cl_2, no desorption peak was seen when the temperature of the sample was warmed from 110-1000K. Auger analysis after the thermal desorption experiment showed a carbon signal at 272eV, as well as the expected platinum peaks, but no signal due to Cl at 137eV was observed.

Photochemistry

Broadband photolysis (λ>200nm) of multilayer coverages of trans 1,2-dichloroethene results in the spectrum shown in figure 39. The intensity of the loss peak at 910 cm^{-1} decreases during the photolysis, whereas the intensities of the other loss peaks remain approximately the same. In addition, an intense new peak at 725 cm^{-1} begins to grow in upon photolysis as well as a peak at 220 cm^{-1}. As would be expected these results are similar to that observed for multilayers on Pd(111) as discussed in the previous section.

A monolayer of cis 1,2-dichloroethene was initially adsorbed on the surface prior to photolysis, figure 40a shows a typical monolayer spectrum. The monolayer coverage was prepared in one of two ways, either multilayers were initially adsorbed on the surface and warmed to T=158K, i.e. past the first desorption peak as described above, or an initial exposure of 0.35L was dosed, as shown in figure 33 this exposure is before the onset of multilayer formation. After 90 minutes of broadband ultra-violet irradiation (λ>200nm) of a monolayer of cis 1,2-dichloroethene, changes are evident in the electron energy loss spectrum. After irradiation with the full Hg lamp, λ>200 nm, new loss

Figure 39. Electron energy loss spectra following the broadband UV photolysis of multilayers of trans 1,2-dichloroethene adsorbed on Pt(111) as a function of time.

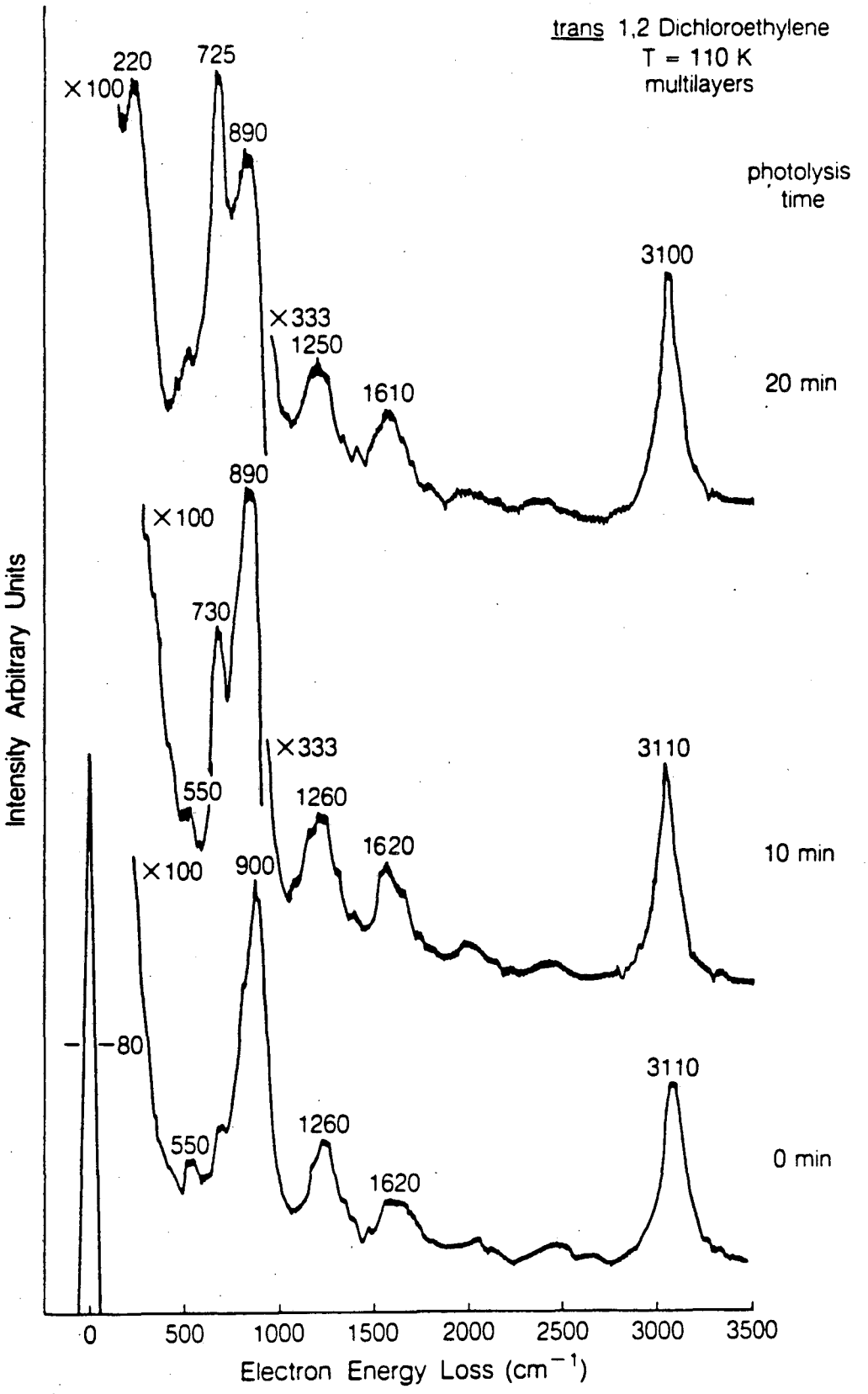
trans 1,2 Dichloroethylene
T = 110 K
multilayers
photolysis time
220
725
×100
890
3100
×333
1250
1610
20 min
890
×100
730
550
×333
3110
1260
1620
10 min
×100
900
−80
3110
550
1260
1620
0 min
Intensity Arbitrary Units
0
500
1000
1500
2000
2500
3000
3500
Electron Energy Loss (cm⁻¹)

Figure 40. Electron energy loss spectra of one monolayer of cis 1,2-dichloroethene adsorbed on Pt(111) a) before photolysis b) after 90 minutes of photolysis with an unfiltered Hg lamp (λ>200 nm).

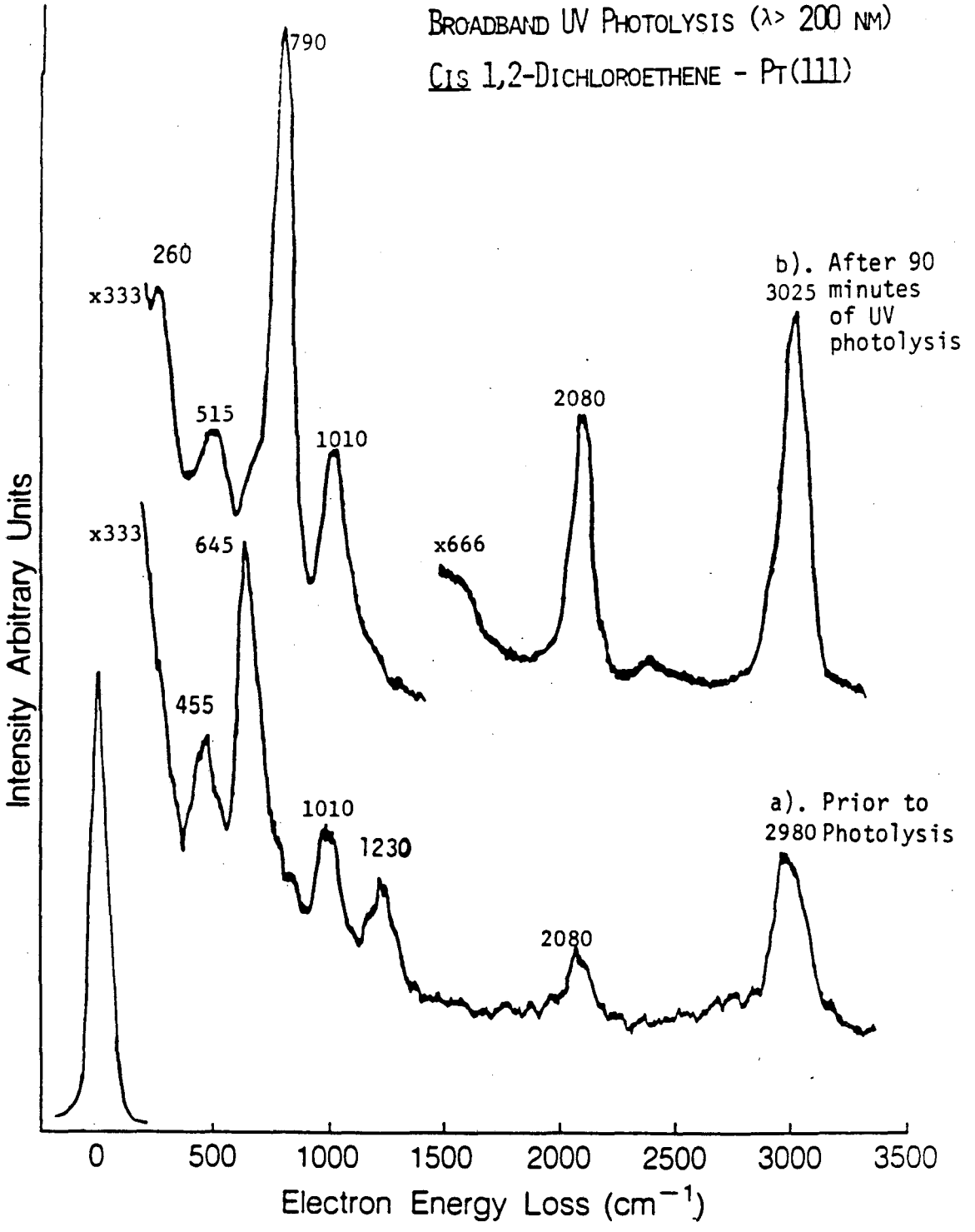
Broadband UV Photolysis (λ> 200 nm)
Cis 1,2-Dichloroethene - Pt(111)
790
260
x333
515
1010
2080
3025
b). After 90 minutes of UV photolysis
x666
x333
645
455
1010
1230
2080
2980
a). Prior to Photolysis
Intensity Arbitrary Units
0
500
1000
1500
2000
2500
3000
3500
Electron Energy Loss (cm⁻¹)

peaks are observed at 790, 3025, 1010 515 and 260 cm^{-1}, in the electron energy loss spectrum, as shown in figure 40b. In a similar fashion the trans isomer was studied. Figure 41 shows the spectra obtained after irradiation (λ>200nm) of the trans form. Loss peaks are observed at 780, 1010, 3020, 510 and 265 cm^{-1}. In addition to the spectral changes discussed above, there is also an increase in the amount of CO on the surface after photolysis as measured by the intensity of the loss peak at 2080 cm^{-1}. This is attributed to CO from the background gases in the chamber adsorbing on the surface in available vacant sites and is not attributed to any photochemistry.

The EEL spectrum after broadband ultra-violet irradiation of a different sample of a monolayer coverage of trans 1,2-dichloroethene with a CsI filter placed in front of the lamp is shown in figure 42. The CsI filter, as discussed before, cuts out the shorter UV wavelengths from 200-237 nm. The electron energy loss spectrum after photolysis is shown in figure 42. Loss peaks are seen at 300, 520, 785, 990 and 3020 cm^{-1}.

DISCUSSION

Structure Analysis of Adsorbed 1,2-DCE on Pt(111) at 110K

The multilayer spectra for both the adsorbed dichloroethenes map readily onto the respective gas phase spectra,[7] differing on the average by 18 cm^{-1} for cis 1,2-DCE and 20 cm^{-1} for the trans isomer. The largest discrepancies are found, for both molecules, in the C-H in-plane bend of +37 and +50 cm^{-1} for the cis and trans isomer, respectively. The overall agreement indicates that the multilayer adsorbed molecules retain their alkene like character and that the gas phase spectral

Figure 41. Electron energy loss spectrum after 102 minutes of broadband photolysis (λ>200nm) of trans 1,2-dichloroethene chemisorbed on Pt(111).

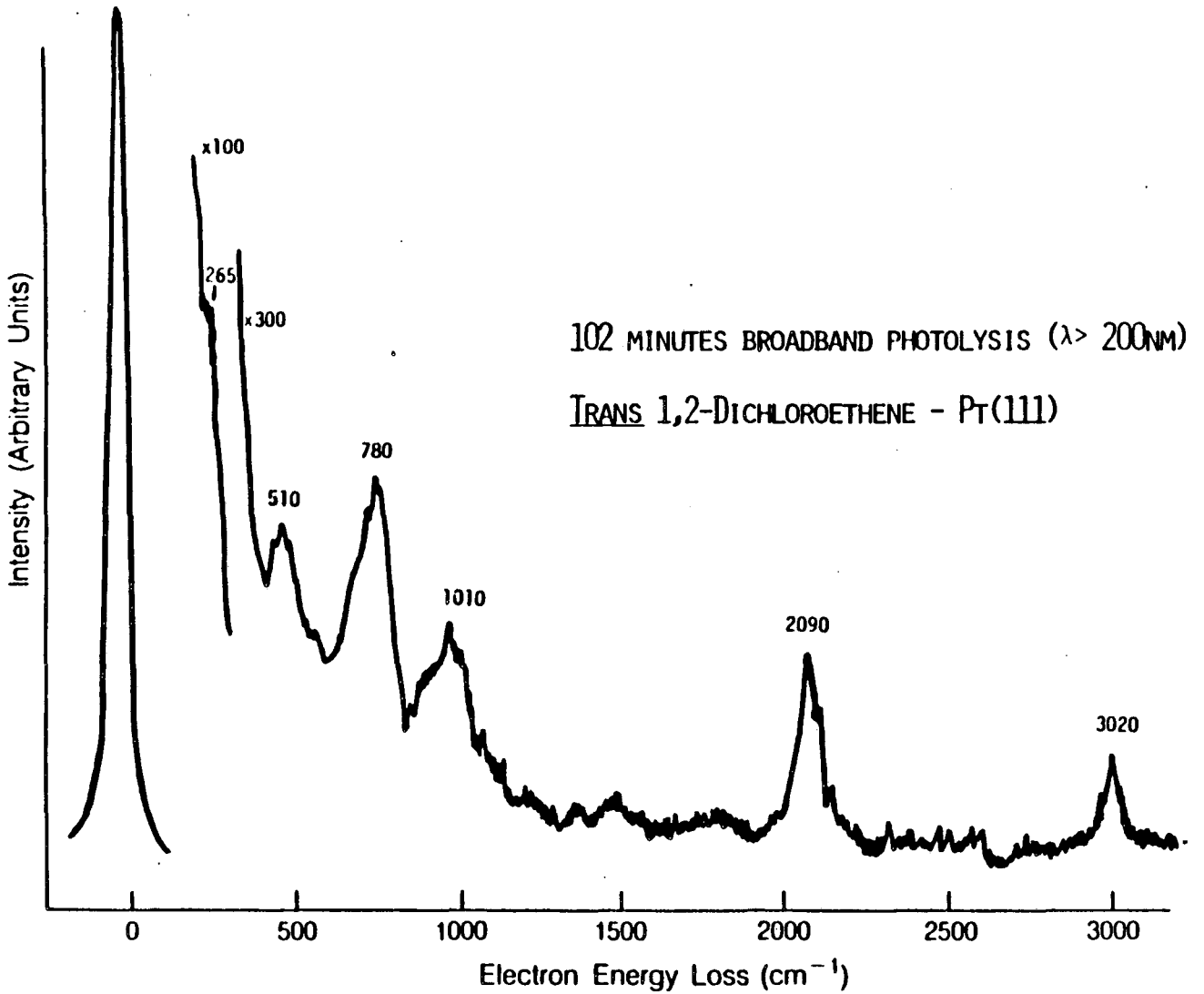

102 MINUTES BROADBAND PHOTOLYSIS ($\lambda > 200$NM)

TRANS 1,2-DICHLOROETHENE - PT(111)

Figure 42. Electron energy loss spectrum after 90 minutes of CsI filtered Hg lamp photolysis ($\lambda > 237$nm) of <u>trans</u> 1,2-dichloroethene chemisorbed on Pt(111).

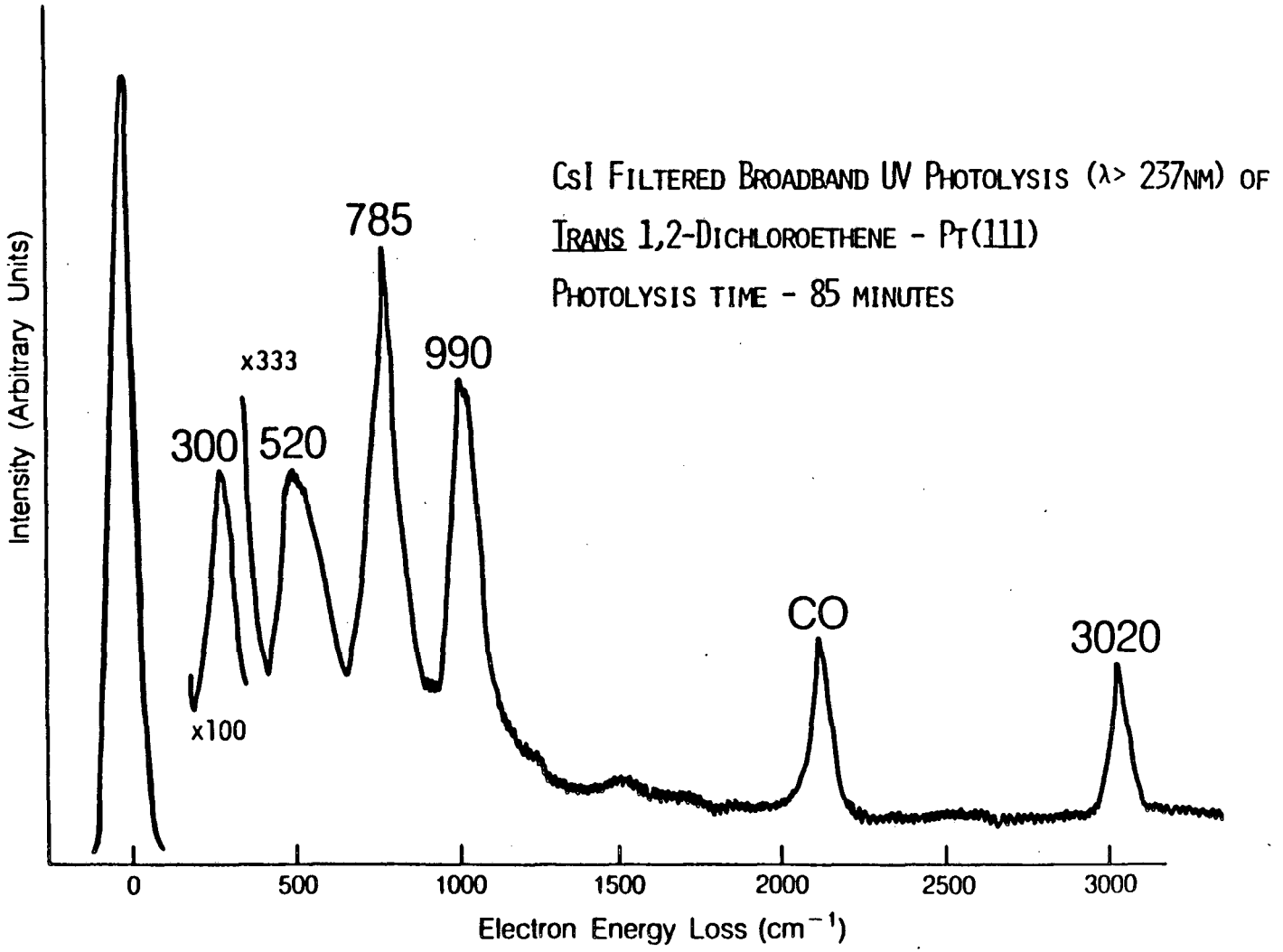
CsI Filtered Broadband UV Photolysis (λ> 237nm) of
Trans 1,2-Dichloroethene - Pt(111)
Photolysis time - 85 minutes
Intensity (Arbitrary Units)
x333
x100
300
520
785
990
CO
3020
0
500
1000
1500
2000
2500
3000
Electron Energy Loss (cm⁻¹)

assignments are applicable, as would be expected for this weakly bound layer.

An assignment for the monolayer spectra for cis and trans 1,2-dichloroethene is given in Table 16. The C-H stretching frequency is immediately revealing. For less than one monolayer coverage, this mode falls 100 cm^{-1} below its value in the multilayer spectrum and in the range defined by the C-H stretching frequencies of the chloro alkanes (gauche 1,2-dichloroethane, 2957-3005).[70] These comparisons indicate that the alkene sp^2 bonding of the carbon atoms have been replaced, in the monolayer adsorbed molecule, by an alkane sp^3 bonding. The most intense loss peak in the cis monolayer spectrum at 650 cm^{-1}, is reasonably close in frequency to the intense out-of-plane C-H mode of the parent molecule, 697 cm^{-1} (IR value), but not for trans spectrum, in which the most intense monolayer peak at 720 cm^{-1} differs by 190 cm^{-1} from the 910 cm^{-1} out-of-plane C-H mode of gaseous trans 1,2-DCE. There is, however, an alternative assignment, as C-Cl stretching frequencies, for these two loss peaks. Whereas the parent DCE molecules display C-Cl stretches at higher frequencies (cis DCE, 857, 714 cm^{-1}; trans DCE 828 cm^{-1}),[42] the 1,2 dichloroethanes have C-Cl stretches near the observed loss peaks (gauche 1,2-dichloroethene, 669, 692.5 cm^{-1}; trans 1,2-dichloroethane, 728.3 cm^{-1}).[70] Thus, the intense loss peaks at 650 cm^{-1} (cis-DCE) and 720 cm^{-1} (trans-DCE) furnish confirmative evidence that the monolayer DCE adsorbates have alkane-like molecular structures. In addition the C-C stretching motion is identified at 1010 cm^{-1} which is close to the IR value of 1027 cm^{-1} for the C-C stretching motion of 1,2 dichloroethane in the gauche form. In addition the frequency of the loss peak for the C-C stretch of ethylene adsorbed on Pt(111) at 140K[13]

is 1050 cm^{-1}. Chlorine substituents in general tend to lower the frequency of the C-C stretching motion at least for molecules in the gas and liquid phase, which is consistent with our observations. The remaining loss peaks do not discriminate alkene and alkane structures, but they have satisfactory assignments consistent with the alkane choice, as indicated in Table 16.

Finally, it is to be noted that despite the obvious similarity between the two monolayer DCE loss spectra, the differences are sufficient to guarantee that isomerization to a single adsorbed structure has not occured. This is consistent with a two-center addition to the metal surface so that, as the cis DCE adjusts to an alkane staggered conformation, it finds itself in a gauche conformation whereas the trans DCE can relax into the more stable trans conformation.

The alkane-like hybridization implies that the structural features of dichloroethane are to expected in the chemisorbed molecule, including a 1.54Å C-C bond length, approximate tetrahedral bond angles and close to a staggered configuration. The expected Pt-C bond length can be inferred from the compounds $(Pt(CH_3)_3Cl)_3$ and $(Pt(P(C_6H_6)_3)_2(C_2(C_6H_5)_2)$ which have well known structures with Pt-C bond lengths of 2.09 Å[71] and 2.01, 2.06 Å[72], respectively. We can then estimate the Pt-C bond length in the surface case as an average of these values, that being 2.05Å. Coupling these bond lengths with the expected bond angles, $\alpha = 109° 28'$; the Pt-C-C bond angle and $\theta = 60°$, θ being the dihedral angle around the C-Cl bond lead to an expected Pt-Pt separation of 3.49 Å, 26% longer than the 2.76 Å interatomic distance of the Pt surface atoms on the (111) face. However only small changes in the Pt-C-C bond angle α and

TABLE 16

VIBRATIONAL ASSIGNMENT OF CIS AND TRANS 1,2 DICHLOROETHENE CHEMISORBED ON Pt(111) at 110K

Mode Description	Cis	Trans
Pt-Carbon sym. stretch		240
Pt-Carbon asym. stretch	445	550
C-Cl stretch	650	720
C-C stretch	1010	1005
C-H bend	1250	1240
C-H stretch	2985	3000

the dihedral angle θ are needed to provide a structure consistent with the 2.76Å surface atom distances. One such combination is $\bar{\alpha}$ = 100, θ = 50. Such small angular displacements raise the energy only by a few kcal/mole,[70] so they indicate a comfortable fit for an ethane-like molecule in a staggered conformation on the (111) surface of platinum.

We propose that these surface molecules should be named as substituted ethanes. Thus, the chemisorbed product from cis 1,2-DCE can be called gauche 1,2-diplatinum(111), gauche 1,2-dichloroethane while that from trans 1,2-DCE will be gauche 1,2-diplatinum(111), trans, 1,2-dichloroethane. Both of these structures are depicted in figure 43.

Thermal Chemistry

The spectral changes on warming between 158 and 270K leave no doubt that chemical changes have occured. Furthermore, within our spectral resolution, the cis and trans DCE's give identical high temperature product spectra. Most important, this spectrum is essentially the same as that reported by Ibach and Lehwald[13] for acetylene adsorbed on Pt(111) (see Table 17). These observations indicate that warming has caused dehalogenation of the adsorbed DCE's.

We correlate the loss of chlorine from the adsorbed DCE's with the appearance of the loss peak near 290 cm^{-1} (300 cm^{-1}, cis; 280 cm^{-1} trans) a candidate for the Pt-Cl stretching motion. This proposal is supported by comparison to the Pt-Cl stretching frequencies in this same spectral region displayed by the Pt-mononuclear complexes such as trans $Pt(NC_5H_5)_4Cl_2$ (sym. 343 cm^{-1}, asym., 329 cm^{-1}) and for cis $Pt((NC_5H_5)Cl_2$ (asym. 252 cm^{-1}).[73] This peak is also assigned to the Pt-C symmetric stretch of chemisorbed acetylene. The EEL spectrum of acetylene on Pt(111) recorded in this laboratory under identical spectrometer

TABLE 17

VIBRATIONAL ASSIGNMENT OF DEHALOGENATED HYDROCARBON FRAGMENT

Mode Description	Cis Pt(111)	Trans Pt(111)	Acetylene Pt(111)[a]
	270K	270K	140K
Pt-C sym. Stretch	300	280	310
Pt-C asym. Stretch	535	520	570
C-H out-of-planebend	785	770	770
C-H in-plane bend	980	1000	985
C-C stretch	n.o.[b]	n.o.	1310
C-H stretch	3020	3010	3010

a. Frequencies from Reference 13.

b. This is a very weak loss peak in the acetylene-Pt(111) EEL spectrum.

Figure 43. Adsorption structure of cis and trans 1,2-dichloroethene on Pt(111) at 110K.

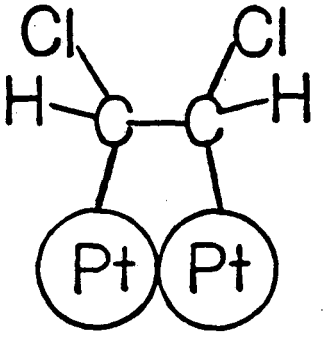

CIS

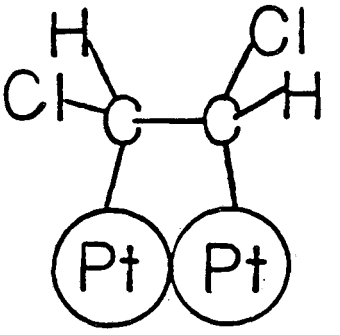

TRANS

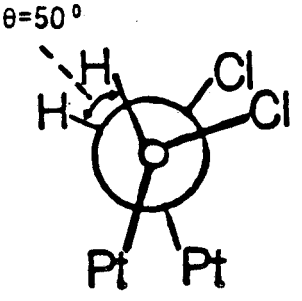

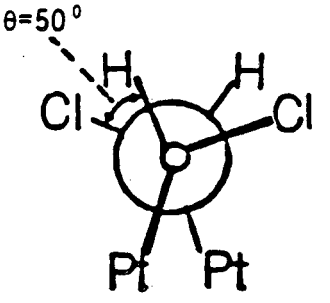

conditions (beam energy and specular angle), as was used in the dichloroethene experiments above, shows the Pt-C stretch near 300 cm^{-1} to be weak. Thus the major contribution to the intensity of this peak is attributed to the Pt-Cl stretch.

The most prominent loss peak is found near 780 cm^{-1} (cis, 785 cm^{-1}, trans, 770 cm^{-1}) and it can be compared to the out-of-plane hydrogen motions of various prototype cis-disubstituted ethenes: cis 1,2-dichloroethene, 697 cm^{-1},[42] cis 1,2-dibromoethene, 670 cm^{-1},[74] cis 2-butene, 673 cm^{-1},[65] and cis 1,2-dideuteroethene, 847 cm^{-1}.[75] In every case, this absorption is the most intense in the prototype spectrum. We conclude that the 785/770 cm^{-1} feature can be assigned to the out-of-plane hydrogen motion of a planar cis di-substituted ethene structure involving two Pt-C bonds.

The relatively low frequency of 1310 cm^{-1}, which shifts to 1250 cm^{-1} for C_2D_2, for the C=C stretching motion is indicative of a π interaction with a third surface atom.[13] The frequencies of the loss peaks in the EEL spectrum for acetylene adsorbed on Pt(111) are in good agreement with the IR absorption for the organometallic compound, $Os_3(CO)_{10}(C_2H_2)$.[76] The entire molecular configuration of chemisorbed acetylene can be described as a cis substituted ethene which is π bonded to the platinum surface. This structure can be denoted as [cis 1,2-diplatinum(111) ethene] Pt(111).

The proposed dehalogenation reaction pathway of the dichloroethenes is strengthened by the intensity behaviors of the key loss peaks. Peak areas were measured by normalizing peak intensities to the elastic peak, subtracting out the background, and integrating the resulting area under each peak. Figure 44 shows the decrease of the parent C-Cl stretching

loss peak at 660 cm^{-1} as the temperature rises. As this peak is lost, the 300 and 785 cm^{-1} product features grow together and essentially at the same rate. The data are consistent with the simultaneous production of these two features as a result of the decomposition of the parent adosrbed molecules. A summary of the dehalogenation reaction of the 1,2-dichloroethene is shown in figure 45.

The C-Cl bond energy is approximately 81 kcal/mole[77] and is readily cleaved below room temperature on the platinum (111) surface. The thermal decomposition of the di-chloroethenes is vastly different from the thermal decomposition of ethene to ethylidyne at T=300K on Pt(111). The decomposition pathway of these halogenated ethenes is also distinct from that of the alkyl substituted ethenes as studied by Avery. The thermodynamic driving force in the decomposition of cis and trans 1,2-dichloroethene is the formation of strong Pt-Cl bonds after dehalogenation of the parent molecule. The Pt-Cl bond energy has been estimated by Erley,[78] to be 47.5 kcal/mole based on thermal desorption data and an assumption of 1×10^{13} for the frequency factor.

Using bond additivity arguements, the thermal desorption data presented here, as well as literature data and known gas phase bond energies of the parent molecule, some unknown bond dissociation energies can be estimated. First the Pt-C bond energy can be deduced by considering the initial adsorption step. The heat of adsorption can be expressed as:

$$\Delta H_{ads}(DCE) = D_e(C=C) - D_e(C-C) - 2D_e(Pt-C) \qquad (11)$$

The heat of adsorption can be calculated from the thermal desorption

Figure 44. Growth and decay curves for loss peaks at 790 and 660 cm^{-1} respectively, during the thermal dehalogenation of chemisorbed cis 1,2-dichloroethene.

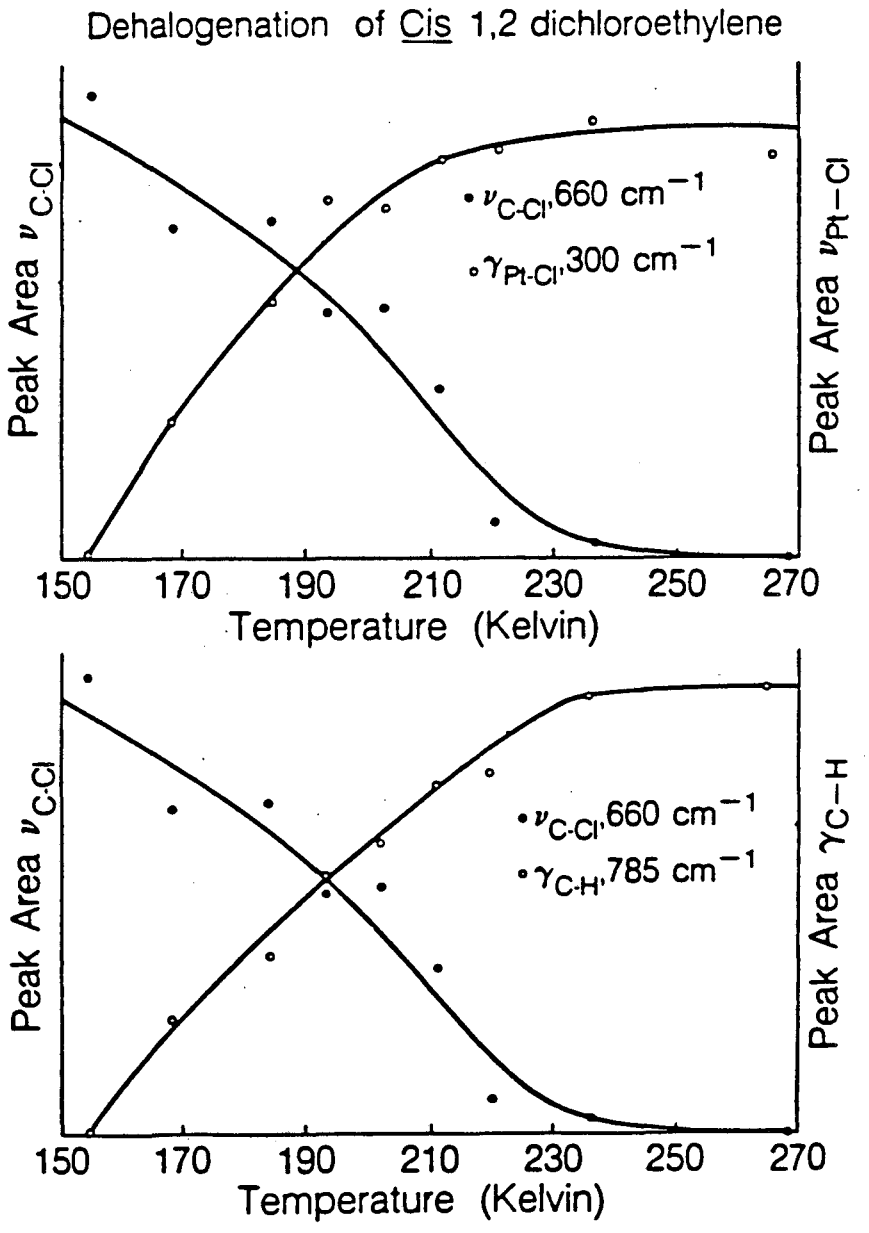
Dehalogenation of Cis 1,2 dichloroethylene
Peak Area $\nu_{C\text{-}Cl}$
Peak Area ν_{Pt-Cl}
• $\nu_{C\text{-}Cl}$, 660 cm^{-1}
∘ $\gamma_{Pt\text{-}Cl}$, 300 cm^{-1}
150 170 190 210 230 250 270
Temperature (Kelvin)
Peak Area $\nu_{C\text{-}Cl}$
Peak Area γ_{C-H}
• $\nu_{C\text{-}Cl}$, 660 cm^{-1}
∘ $\gamma_{C\text{-}H}$, 785 cm^{-1}
150 170 190 210 230 250 270
Temperature (Kelvin)

Fiugre 45. Summary of the thermal reactions, desorption and dehalogenation, for the dichloroethenes when adsorbed on Pt(111).

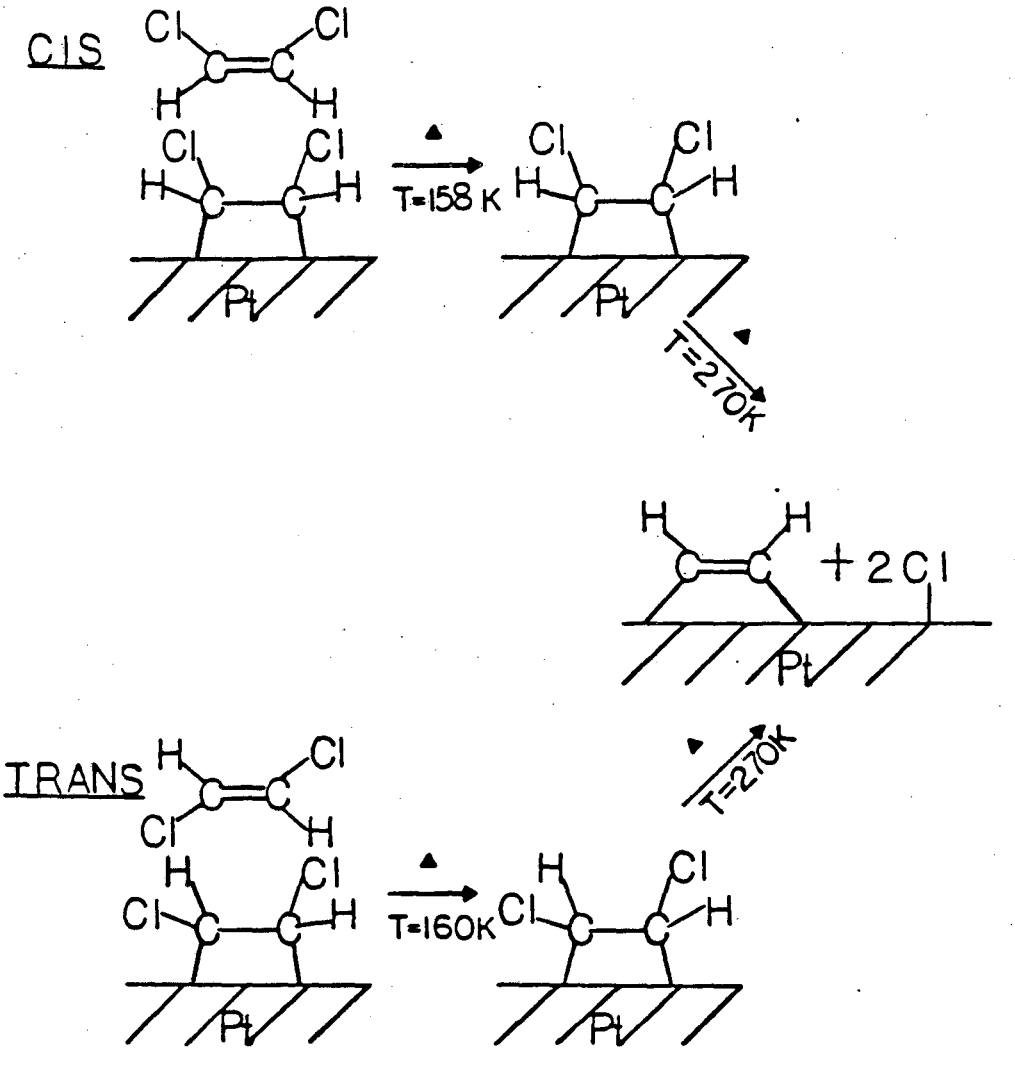
CIS
Cl
Cl
H
H
Cl
Cl
H
H
Pt
T=158 K
Cl
Cl
H
H
Pt
T=270K
H
H
+2Cl
Pt
TRANS
H
Cl
Cl
H
H
Cl
Cl
H
Pt
T=160K
Cl
H
Cl
H
Pt
T=270K

data. The value of T_{max} is 247K (see Figure 37), with a heating rate β, of 15K/sec. Assuming first order kinetics and a pre-exponential factor of 1×10^{13}, ΔH_{ads} is calculated to be 14.3 kcal/mole. Taking the values of 145.8 and 82.6 kcal/mole for the bond energies of a carbon-carbon double and single bond, respectively, the Pt-C bond energy is calculated to be 39 ± 6 kcal/mole. This is in excellent agreement with the value of 39 ± 5 kcal/mole for the Pt-C bond dissociation energy in the organometallic compound $(C_6H_5)(CH_3)_2)Pt\text{-}CH_3$.[79]

Photochemistry

Multilayer Photolysis

Broadband photolysis of multilayers of trans-1,2-dichloroethenes results in a decrease of the most intense peak in the spectrum at 910 cm^{-1}, as peaks at 725 and 220 cm^{-1} begin to grow in. Both the 910 and 725 cm^{-1} peaks are assigned to the C-H out-of-plane motion of the 1,2-DCE's for the trans and cis isomers respectively. The intensities of the other loss peaks remain approximately the same. We conclude that the broadband photolysis of multilayers of trans 1,2 dichloroethene results in the isomerization of the molecule to the cis form. This is similar to the photochemistry of the 1,2 dichloroethylene's in the liquid state,[60,61] and in cryogenic matrices[62] and as multilayers over Pd(111) as described in section 2A of this chapter.

There is a possible alternative interpretation of the results for the photolysis of the multilayer. In light of the fact that one of the most intense peaks in the monolayer spectrum of chemisorbed trans-DCE is at 720 cm^{-1}, an alternative explanation could be that photolysis of the multilayer results in photon-induced desorption of this physisorbed

state, whereby the spectral features of the monolayer are no longer masked by the spectral features attributed to the multilayer in the EEL spectrum. This explanation is rejected because there is no evidence for a peak at 3000 cm^{-1} in figure 39c, as required by the monolayer spectrum of trans-1,2 DCE in figure 34a. The second factor which causes us to believe that the photodesorption process is not an important process is that when the multilayer was photolyzed for times longer than 20 minutes, the spectrum did not change from that shown in fig. 39c. This implies a steady state has been reached with both reactants and products in equilibrium. If indeed desorption of the multilayer was occuring, all of the multilayer should desorb upon photolysis in a sufficiently long time. If however photo-isomerization was occuring a steady state would be reached when cis→trans and trans→cis isomerization rates become equal. These reasons lead us to conclude that the photodesorption is not an important factor here. And finally UV photolysis of multilayers adsorbed over Pt(111) is identical to that of multilayers adsorbed over Pd(111). The peak observed at 220 cm^{-1} is most probably due to photochemistry which is occuring in the monolayer.

The similarities in the photolysis of the multilayer of trans-1,2-DCE, i.e. photoisomerization, to the photochemistry of this molecule in the liquid phase[60] and in cryogenic matrices[62] aids in our understanding of the electronic excited state, as discussed before. The $\pi \rightarrow \pi^*$ transition is the predominant transition, i.e. has the largest extinction coefficient in the ultraviolet region for ethylene and substituted ethylenes. The singlet state $(\pi \rightarrow \pi^*)^1$ for cis-1,2-DCE lies 124 kcal above the ground state, whereas the triplet state $(\pi \rightarrow \pi^*)^3$ lies 70 kcal above the ground state.[62] Excitation with light of 200nm

corresponds to 140 kcal/mole in energy, making both the singlet and triplet states energetically accessible. Selective excitation to either the singlet or the triplet state can result in photoisomerization.[62] In the gas and liquid phase the exitation to the singlet state is spin allowed whereas excitation to the triplet state is not. Presumably the photochemistry of the multilayer proceeds via a singlet state assuming there is no breakdown in the spin selection rules for a molecule which is in close vicinity to a metal surface.

Monolayer Photolysis

Broadband photolysis of monolayer coverages, of chemisorbed trans-1,2 DCE results, within our spectral resolution, in the formation of one hydrocarbon product, C_2H_2 chemisorbed on the surface. Product formation of chemisorbed acetylene appears to be independent of photolysis wavelengths, in the UV region studied see figures 41 and 42. When a monolayer coverage of trans-1,2-DCE is photolyzed with light either of wavelengths greater than 237nm or 200nm, i.e. broadband photolysis with or without the use of a CsI filter, loss peaks in the EEL spectrum can be assigned to chemisorbed acetylene.

Photolysis using a CsI filter ($\lambda > 237$nm) results in adsorbed chlorine atoms as well as is evident by an intense loss peak at 300 cm^{-1} in the EEL spectrum (Fig. 42), whereas photolysis with the full Hg Arc ($\lambda > 200$nm) shows a weaker loss peak in the EEL spectrum at 265 cm^{-1}. The weaker feature observed at 265 cm^{-1} is assigned to a Pt-C stretch due to adsorbed acetylene. Admittedly the loss peaks at low frequencies are the most difficult peaks in the spectra from which to get reproducible data, because of the steep background from the tail of the

elastic peak. Photolysis experiments for λ>200nm were done several times to verify that the tail of the elastic peak did not in fact obscure the low frequency peak.

The photochemical reactions, of chemisorbed 1,2 DCE is summarized below:

(a=adsorbed, g=gaseous state)

$$(14) \qquad C_2H_2Cl_2(a) \xrightarrow{\lambda > 200nm} C_2H_2(a) + 2Cl(g)$$

$$(15) \qquad C_2H_2Cl_2(a) \xrightarrow{\lambda > 237nm} C_2H_2(a) + 2Cl(a)$$

To discern if we were indeed seeing changes in the primary photolysis reaction of adsorbed DCE with photolysis wavelength and not a secondary photolysis effect, i.e. initially Cl atoms adsorbing on the surface and then photodesorbing upon photolysis with 200nm light, the following experiment was done. Cis or Trans 1,2-DCE was adsorbed on Pt(111) at 110K, the sample was warmed to 270K, this thermally produces chemisorbed C_2H_2 and 2Cl (vide infra), the sample was then photolyzed with an unfiltered broadband Hg lamp for 90 minutes, after which there were no detectable changes. The intensity of the loss peak at 300 cm^{-1}, ν_{Pt-Cl}, remained the same after photolysis with 200nm light, as did all other peaks, thus showing a true wavelength dependence on the primary photochemical reaction as expressed in reactions 14 and 15 above.

The nature of the excited state for chemisorbed species is not very well understood. A great deal of theoretical work has been done on understanding excited states of adsorbates.[81] Experimentally there has been little success in observing intramolecular electronic transitions for adsorbates. Robota et.al.[82] using optical spectroscopy were not able to measure electronic transitions of several aromatics (benzene, pyridine, pyrazine and napthalene) chemisorbed on Ni(111) at 300K. However an enhancement of a Ni interband transition was observed at approximately 290 nm when these molecules were chemisorbed to the nickel surface. There has been some success measuring intramolecular transitions of chemisorbed molecules with electron energy loss spectroscopy.[83] The $\pi \rightarrow \pi^*$ transitions for a monolayer of pyridine adsorbed on Ag(111)[84] and chemisorbed on Ni(100)[85] has been measured with EELS. Charge transfer bands were also observed in the spectra and are thought to play an important role in the photochemical and photophysical processes in the surface dynamics of metal-adsorbate systems.[86]

The excitation chromophore for chemisorbed 1,2 DCE can be either molecular in nature or of a charge transfer type due to the surface-adsorbate complex. If the chromophore is indeed molecular in nature we can turn to molecular prototypes as a first guide in determining the photochemical mechanism for adsorbed 1,2-DCE. We have shown that for cis and trans 1,2 dichloroethene adsorbed on Pt(111) the C-C bond order has been reduced to one. It follows from the proceeding discussion on the adsorption structure of the chemisorbed dichloroethenes that the electronic transitions and absorption spectra of 1,2 dichloroethane would be our first choice as a prototype

molecule. The first absorption band (the band at longest wavelength) for alkyl halides has been attributed to an $n-\sigma^*$ transition, where a nonbonding electron localized on the chlorine atom in the ground state is excited to a sigma antibonding orbital.[87] The second absorption band for the alkyl halides results in elimination of the hydrogen halide, HX.[87]

The room temperature UV electronic absorption spectrum of 1,2 dichloroethane, dissolved in n-octane, in the region from 200-260 nm is shown in figure 46. The photolysis of gaseous 1,2 dichloroethane was studied by Yates and Hughes.[88] Chlorine atom detachment was the primary photoreaction, leaving C_2H_4Cl as the hydrocarbon fragment. Acetylene was also observed but in very small quantities. If we assume that we can directly compare the excited electronic states and photoreactivity of 1,2 dichloroethane to that of chemisorbed 1,2 DCE then a mechanism for the photochemistry of chemisorbed 1,2 DCE can be postulated. Although the wavelength of the peak maxima and the extent of the tail of the absorption band will be different for chemisorbed DCE as compared to 1,2 dichloroethane in the gas phase or in solution.

We list below four plausible reaction mechanisms for the photolysis of chemisorbed 1,2 DCE:

16a. $C_2H_2Cl_2$ (a) $\xrightarrow{h\nu}$ $[C_2H_2Cl^{\bullet} + Cl] \xrightarrow{h\nu} C_2H_2$ (a) + 2Cl

b. $\xrightarrow{h\nu}$ $[C_2H_2Cl^{\bullet} + Cl] \xrightarrow{h\nu} C_2H_2$ (a) + 2Cl

c. $\xrightarrow{h\nu}$ C_2H_2 (a) + 2Cl

d. $\xrightarrow{h\nu}$ C_2H_2 (a) + Cl_2

In reaction 16a photolysis of the reactant results in the chlorine atom detachment forming the radical C_2H_2Cl which in a subsequent step detaches a second chlorine atom, with a final product of acetylene and two chlorine atoms. Reaction 16b is similar to 16a in that the radical C_2H_2Cl is formed but now a second photon is needed for the second Cl atom to detach. In reaction 16c photodetachment of two chlorine atoms is caused by one photon in a single step. Finally in reaction 16d molecular Cl_2 elimination occurs upon photolysis.

The mechanism by which the photo-induced reaction proceeds can be any one of the four listed above. One possible explanation for the differences in the photochemistry at $\lambda > 237$nm and $\lambda > 200$nm can be attributed to the total energy content of the photoproducts. If we assume that after chlorine atom detachment (or molecular elimination) a considerable amount of the excess energy is left in the chlorine product (either atomic or molecular chlorine) there would be a greater amount of energy, and perhaps enough energy to desorb from the surface, when the initial photolysis of the parent molecule is excited with 200nm light as compared to 237nm. Photolysis with 200 nm light corresponds to an energy of 140 kcal whereas 237nm light corresponds to 120 kcal. Thus the Cl atom born from the photolysis reaction at 200nm would perhaps have enough energy to desorb from the surface, whereas this is not the case with photolysis of wavelengths greater than 237nm.

Although the wavelength dependence and the photochemical mechanism can be explained by considering the excitation chromophore to be an

Figure 46. UV electronic absorption spectrum of 1,2 dichloroethane dissolved in n-octane at room temperature.

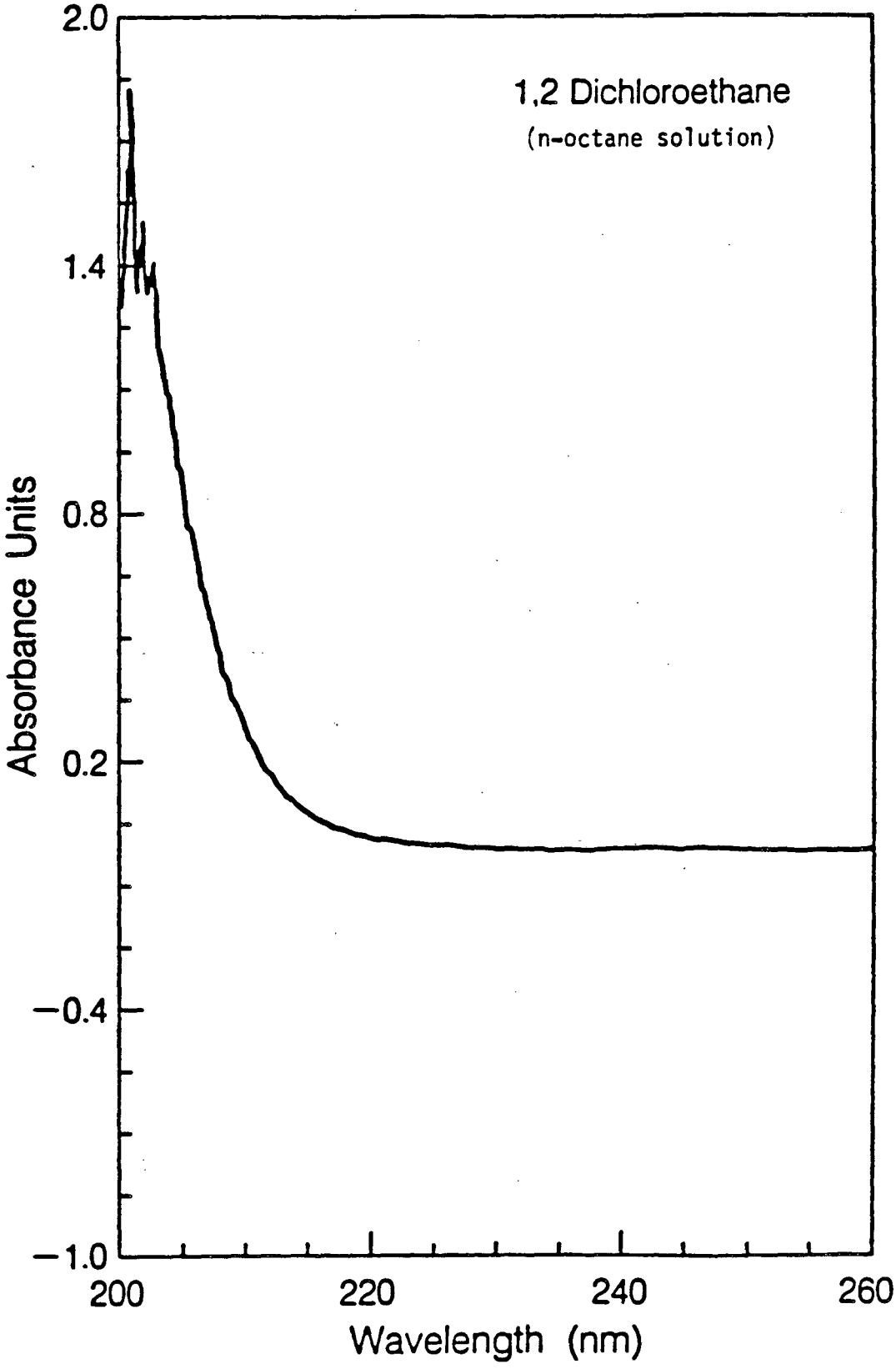
1,2 Dichloroethane
(n-octane solution)
2.0
1.4
0.8
0.2
−0.4
−1.0
Absorbance Units
200
220
240
260
Wavelength (nm)

internal transition of the adsorbate the possibility of a more collective excitation of the metal (e.g. surface plasmon, interband transition) or a charge transfer excitation cannot be excluded. If the electronic transition is more of a charge transfer type between the adsorbate and the electronic states of the metal, other compounds include inorganic and organometallic multi-nuclear, or even, mono-nuclear complexes. There is a wealth of published information on the electronic absorption spectra of transition metal complexes. Both the forbidden d→d transitions as well as the intense allowed metal-ligand charge transfer transitions have been studied. There is much less information concerning the changes in the intermolecular transitions of the ligand when coordinated to a metal center; the electronic transitions of the ligands tend to be weaker then charge transfer bands and usually occur at shorter wavelengths.

There has been a thorough study by Jorgensen[89] on the shifts of the $\pi \rightarrow \pi^*$ transition of pyridine when complexed to a transition metal atom. The (π-π^*) transition of pyridine, at 260nm for the uncomplexed molecule, in general tended toward longer wavelengths by about 20 nm in these transition metal complexes. Of the three metals studied Rh, Ir, and Pt, only Ir complexes had an absorption band, around 300nm, which can be associated with a charge transfer transition.

Unfortunately, as of now, the electronic absorption spectrum of an appropriate inorganic prototype molecule for these studies is not available. However the band structure of the solid is quite different then the local molecular orbital for organometallic compounds and would perhaps be a poor analogy. The nature of the electronic excited states for chemisorbed molecules is only speculative as of now. As the

examples of photochemical behavior of chemisorbed species increases so will out knowledge of the potential energy surfaces of excited states of adsorbates.

3. CONCLUSIONS

This chapter has been devoted to photochemical studies of adsorbates, an area of research which has been relatively unexplored. Photochemical reactivity has been demonstrated in these studies to occur for molecules in the vicinity of a metal surface, in both the physisorbed and chemisorbed ad-layers. Direct chemical bonding of the adsorbate to the surface does not prohibit unimolecular photochemistry, as was demonstrated for the dichloroethenes adsorbed on Pt(111). For potentially photochemical reactive systems, such as the dichloroethenes, we have shown that chemical reactivity is competitive with radiative and non-radiative deactivation mechanisms.

The metal surface has an interesting effect on the photochemistry. First consider the photoproducts observed for these molecules physisorbed on Pd(111). For both trans 2-butene and the dichloroethenes, isomerization was the only detectable photoreaction in the UV photolysis of the multilayer. The photochemistry of these molecules in the gas and liquid phase are much more complex, particularly for the dichloroethenes. Many photoproducts are detected upon broadband irradiation. Irradiation of cis 1,2-dichloroethene in the gas phase results in the following products: HCl, Cl_2, Cl , C_2HCl. C_2H_2. C_2H_2Cl , t-1,2-$C_2H_2Cl_2$ and 1,1-$C_2H_2Cl_2$. There is a possibility that there is some selectivity seen in the photochemistry of these molecules in the physisorbed layer. However, alternatively small quantities of other products could be forming without being detected with the sensitivity and resolution obtainable with EELS.

The differences in the photochemistry of the chemisorbed and

physisorbed layers is striking. As was shown for multilayer quantities of cis and trans 1,2-dichloroethene above a Pd surface, identical photochemistry of these molecules, i.e. isomerization, is observed above a platinum surface. The photochemistry of monolayer quantities of 1,2-dichloroethene adsorbed on Pt(111) is markedly different from that observed for the multilayer. This is attributed to different excitation chromophores for the chemisorbed and physisorbed layers. As discussed previously the alkene structure is retained in the physisorbed layer, whereas in the monolayer, covalent bonding to the surface results in an alkane structure (vide infra). The electronic transition upon UV excitation of the multilayer is a ($\pi \rightarrow \pi^*$) transition and for the monolayer there is no π bonding chromophore in the alkane adsorbate structure. Hence we postulate the transition to be an ($n \rightarrow \sigma^*$) transition. Thus we find the surface photochemistry of the monolayer is not at all in conflict with the photochemistry of the parent molecule provided we recognize that in the monolayer we are not photolyzing an olefin (for which elimination is expected) we are photolyzing a halogenated alkane (for which C-Cl bond rupture is expected).

In the introduction of this chapter, the discussion centered around lifetime phosporescence measurements made which tended to discourage the possibility of photochemistry occuring on or near a metal surface. In addition, it can be inferred that, due to high non-radiative decay rates, if photochemistry occurred the quantum yields would be low. To the contrary, these studies have shown a high propensity for photochemistry of these molecules when adsorbed to a metal surface. The photon flux from the Hg lamp is not particularly high, and the photolysis times discussed in these experiments are relatively short.

It can be concluded then that the quantum yields are high for these systems.

In summary, the metal surface has an appreciable effect on the photoreactivity of these molecules; this includes product formation, excitation chromophore, quantum yields and perhaps the relative energies of the electronic excited states compared to that of the ground state.

Chapter V

REFERENCES

1. Somorjai, G.A., Chemistry in Two Dimensions: Surfaces, Cornell University Press (1981).
2. Ibach, H., and Mills, D.L., Electron Energy Loss Spectroscopy and Surface Vibrations, Academic Press (1982).
3. CRC Handbook of Chemistry and Physics, 61st edition, Ed. Robert C. Weast, CRC Press Inc. (1980) F219.
4. Demuth, J.E., Chem. Phys. Lett., 45 (1977) 12.
5. Brewer, L., Science, 161 (1968) 115.
6. Pimentel, G.C., Chairman, Oppurtunities in Chemistry, A report by the National Research Council's Committee to Survey Oppurtunities in the Chemical Sciences, National Academy Press, Washington, D.C. (1985).
7. Chuang, T.J., Surface Science Reports, 3 (1983) 1.
8. Redhead, P.A., Vacuum, 12 (1962) 203.
9. Hoffman, F.M., Surface Science Reports, 3 (1983) 1.
10. Dubois, L, Ph.D. Dissertation, University of California, Berkeley (1980).
11. Katz, J.E., Davies, P.W., Crowell, J.E. and Somorjai, G.A., Rev. Sci. Instrum., 53 (1982) 785.
12. Kesmodel, L.L., Dubois, L.H. and Somorjai, G.A., J. Chem. Phys. 70 (1979) 2180.
13. Ibach, H. and Lehwald, S., Journal of Vacuum Science and Technology, 15(2) (1978) 407.

14. Skinner, P., Howard, M.W., Oxton, I.A., Kettle, S.F.A., Powell, D.B. and Sheppard, N., J. Chem. Soc. Faraday Trans. II, 77 (1981) 1203.

15. Wexler, R.M., Ph.D. Dissertation, University of California, Berkeley (1983).

16. Yin, C.-C. and Demming, A.J., J. Chem. Soc. Dalton, (1975) 2091.

17. Johnson, B.F.G., Lewis, J. and Pippard, D.A., J. Chem. Soc. Dalton, (1981) 407.

18. Lehwald, S., Ibach, H. and Demuth, J.E., Surface Science, 78 (1978) 577.

19. Bertolini, J.C., Dalmai-Imelik, G. and Rousseau, J., Surface Science, 67 (1977) 478.

20. Wadill, G.D., and Kesmodel, L.L., Physical Review B, 31(8) (1985) 4940.

21. Koel, B.E., Crowell, J.C., Mate, C.M. and Somorjai, G.A., J. Phys. Chem. 88 (1984) 1988.

22. Klarup, D.G., Ph.D. Dissertation, University of California, Berkeley (1986).

23. Shannahan, K.L. and Muetterties, E.L., J. Phys. Chem., 88 (1984) 1996.

24. a). Demuth, J.E., Sanda, P.N., Warlaumont, J.M., Tsang, J.C., Christman, K., "HREELS and SERS Studies of Pyridine and Benzene on Ag(111)", Vibrations at Surfaces, Ed. R. Caudana, J.-M. Giles and A.A. Lucas, Plenum Press, N.Y. (1982) 391.

b). Demuth, J.E., Christman, K., and Sandra, P.N.,

Chem. Phys. Letters , 76 (1980) 201.

25. DiNardo, J.N., Avouris, P., and Demuth, J.E., J. Chem. Phys., 81 (1984) 2169.

26. Wexler, R.M., Tsai, M.-C., Friend, C.M., and Muetterties, E.L., J. Am. Chem. Soc., 104 (1982) 2034.

27. Wexler, R.M., Ph.D. Thesis, University of California, Berkeley (1983).

28. Howard, M.W., Kettle, S.F., Oxton, I.A., Powell, D.B., and Sheppard, N., J. Chem. Soc. Faraday Trans. II, 77 (1981) 397.

29. Skinner, P., Howard, M.W., Oxton, I.A., Kettle, S.F., Powell, D.B., and Sheppard, N., J. Chem. Soc. Faraday Trans. II, 77 (1981) 1203.

30. Shapley, J.R., George, G.M., Churchill, M.R., and Hollander, F.J., Inorganic Chemistry, 21 (1982) 3295.

31. Kettle, S.F.A. and Strangellin, P.L., Inorganic Chem., 18 (1979) 2749.

32. Wiberg, K.B., Walters, V.A., Wong, K.N., and Colson, S.D., J. Phys. Chem., 88 (1984) 6067.

33. Abon, M., Bertolini, J.C., Billy, F., Massardier, J. and Tardy, B., Surface Science, 162 (1985) 395.

34. Davis, S.M., Gordon, B.E., Press, M. and Somorjai, G.A., J. Vac. Sci. Technol., 19 (1981) 231.

35. Johnson, A.L., Muetterties, E.L., Stohr, J., and Sette, F., J. Phys. Chem., 89 (1985) 4071.

36. Morrison, R.T. and Boyd, R.N., "Organic Chemistry", 3rd edition Allyn and Bacon Inc., Boston (1973) 579.

37. Muetterties, E.L., Chemical Society Reviews, 11 (1982) 283.

38. Christmann, K., Ertl, G. and Pignet, T., Surface Science, 54 (1976) 365.

39. Gentle, T.M., Grassian, V.H., Klarup, D.G., and Muetterties, E.L., J. Amer. Chem. Soc., 105 (1983) 6766.

40. Gentle, T.M. and Muetterties, E.L., J. Phys. Chem., 87 (1983) 6766.

41. Bertolini, J.-C., Massardier, J. and Dalmai-Imelik, G., J. Chem. Soc. Faraday Trans. 74 (1978) 1720.

42. Shimanouchi, T., Tables of Molecular Vibrational Frequencies Consolidated, 1 NSRDS-NBS 39, Consolidated 2, J. Phys. Ref. Data, 6 (1977) 993.

43. Wilmhurst, J.K. and Bernstein, H.F., Canadian Journal of Chemistry 81 (1985) 911.

44. Rucker, T.G., Logan, M.A., Gentle, T.M., Muetterties, E.L. and Somorjai, G.A., J. Phys. Chem., 90 (1986) 2703.

45. Garfunkel, E.L., Minot, C., Gavezzotti, A. and Simonetta, M., Surface Science, 167 (1986) 177.

46. Netzer, F.P. and Mack, J.U., J. Chem. Phys., 79 (1983) 1017.

47. Gentle, T.M., Ph.D. Dissertation, University of California, Berkeley (1984).

48. Jaksic, M.M., Plenary lecture presented at the Scandinavian Symposium on Catalysis, Lund, Sweden, September (1985).

49. Morrison, R.T., and Boyd, R.N., "Organic Chemistry", 3rd edition Allyn and Bacon Inc, Boston (1973) Chapter 3.

50. Gates, J.A., and Kesmodel, L.L., Surface Science, 124 (1983) 78.

51. Davies, S.M. and Somorjai, G.A., J. Catal., 60 (1980) 78.

52. McAllister, J.W., and White, J.M., Journal of Chemical Physics, 58 (1973) 1496.

53. Chuang, T.J., Journal of Electron Spectroscopy and Related Phenomena, 158 (1985) 125.

54. Campion, A., Gallo, A.R., Harris, C.B., Robota, H.J. and Whitmore, P.M., Chemical Physics Letters, 73 (1980) 447.

55. Whitmore, P.M., Robota, H.J., and Harris, C.B., J. Chem. Phys., 76 (1982) 1560.

56. Brus, L.E. and Rossetti, R., J. Chem. Phys., 76 (1982) 1146.

57. Chance, R.R., Prock, A. and Silbery, R., in Advances in Chemical Physics, edited by I. Prigogene and S.A. Rice, Wiley, New York (1978) 1.

58. Whitmore, P.M., Alivisatos, A.P. and Harris, C.B., Phys. Rev. Letters, 50 (1983) 1092.

59. Waldeck, D.H., Alivasatos, A.P. and Harris, C.B., Surface Science, 158 (1985) 103.

60. a). Wijnen, M.H.J., J. Am. Chem. Soc., 83 (1961) 4109; Ausuberl, R., and Wijnen, M.H.J., International Journal of Chemical Kinetics, 7 (1975) 739; Ausuberl, R. and Wijnen, M.H.J., Journal of Photochemistry, 4 (1975) 248.

b). Mahncke, H.E. and Noyce Jr., W.A., J. Am. Chem. Soc., 60 (1936) 982.

61. Grabowski, Z.R. and Bylina, A., Trans. Faraday Soc. 60 (1964) 1131.

62. Cartland, H.E. and Pimentel, G.C., Journal of Physical

Chemistry, 90 (1986) 5485.

63. Cundall, R.B. and Palmer, T.F., Trans. Faraday Soc., 56 (1960) 1211.

64. a). Avery, N.R. and Sheppard, N., Proc. Roy. Soc. London A, 405 (1986) 1.

b). Avery, N.R. and Sheppard, N., Proc. Roy. Soc. London A, 405 (1986) 27.

65. Kilpatrick, J.E. and Pitzer, K.S., J. Research Natl. Bur. Standards, 38 (1947) 191.

66. Singmaster, K.A., private communication. FTIR Matrix isolation studies of cis and trans 2-butene show that for an equal number of mmoles deposited the absorbance units for the out-of-plane C-H bend are within ∓10% for these two isomers.

67. a).Jones, L.C. and Taylor, L.W., Anal. Chem., 27 (1955) 228.

b).Gary, J.T. and Pickett, L.W., J. Chem. Phys., 22 (1954).

68. Berry, M.J., J. Chem. Phys., 61 (1974) 3114.

69. Baro, A.M., and Ibach, H., J. Chem. Phys, 71 (1979) 4812.

70. Mizushima, S.-I., Structure of Molecules and Internal Rotation, Academic Press Inc (1954).

71. Rundle, R.E. and Sturdivant, J.H., J. Am. Chem. Soc., 69 (1947) 1561.

72. Glanville, J.O., Stewart, J.M. and Grim, S.O., J. Organometallic Chem. (1967) 9.

73. Durig, J.R., Mitchell, B.R., Sink, D.W. and Willis Jr., J.N., Spectrochimica Acta., 23A (1967) 1121.

74. Dowling, J.M., Puranik, P.G.and Meister, A.G., J. Chem. Phys. 26 (1957) 233.

75. Frei, H. and Pimentel, G.C., J. Chem. Phys., 78 (1983) 3698.

76. Anson, C.E., Keiller, B.T., Oxton, I.A., Powell, D.B., and Sheppard, N., J. Chem. Soc. Chem. Commun. (1983) 470.

77. Cottrell, T.L., The Strength of the Chemical Bond, Buttersworth Scientific Publication, London (1958)

78. Erley, W., Surface Science, 94 (1980) 281.

79. Egger, K.W., J. Organometallic Chemistry, 24 (1970) 501.

81. Persson, B.N.J. and Avouris, Ph., J. Chem. Phys., 79 (1983) 5156.

82. Robota, H.J., Whitmore, P.M. and Harris, C.B., J. Chem. Phys., 76 (1982) 1692.

83. Avouris, Ph., DiNardo, N.J. and Demuth J.E., J. Chem. Phys., 80 (1984) 491.

84. Avouris, Ph. and Demuth, J.E., J. Chem. Phys., 75 (1981) 4783.

85. DiNardo, N.J., Avouris, Ph. and Demuth, J.E., J. Chem. Phys., 81 (1984) 2169.

86. Avouris, Ph. and Demuth, J.E., Surface Science, 158 (1985) 21.

87. Calvert and Pitts, Photochemistry, John Wiley and Sons, Inc. (1966) 522.

88. Yates, W.F. and Hughes, L.J., J. Phys. Chem., 64 (1960) 672.

89. Jorgensen, C.K., Absorption Spectra and Chemical Bonding in Complexes, Pergamon Press Ltd. (1962) 192.

ACKNOWLEDGEMENTS

No woman is an island, to rephrase a famous quote. There have been so many people whom have been a part of my life during these many years as a graduate student and now is the time to thank them all.

First I would like to thank my research director George C. Pimentel for all the help and guidance he has given me during the past three years. From the first day I joined the group George made me feel welcome, I really appreciated that. Being a member of the Pimentel research group has been a rewarding experience I'll never forget.

At the start of my graduate career I was very fortunate to be able to work with the late Earl L. Muetterties. Earl's enthusiasm for chemistry was truly remarkable. It was under Earl's influence that I became interested in surface science and transition metal chemistry. All the members of the Muetterties research group were instrumental in the early days of my graduate years, in particular Tom Gentle who helped me get the EELS system working.

The support staff at MMRD was essential in making these experiments work. In particular Weyland Wong was extremely helpful in the design and the redesign of the cooling system. Working with Weyland was always fun and I dedicate to him one bottle of my perfume to remember me by.

For non-technical support I would like to thank my friends Renee Brouillette (the politician), Patti Casey (the pseudo graduate student), Linda Cima (the accountant/housewife), Kelly Owen (the traditional feminist) and Karen Singmaster (the amazing scientist). These five women have made my life here in Berkeley an interesting experience.

The love and support from my parents and brother these past five years has helped me get through the rough times when nothing seemed to be working.

Finally, and most importantly, I would like to thank Mark Young for all his love, encouragement and patience.

This work was supported by the National Science Foundation Grant CHE-83-07159 and by the Director, Office of Energy Research, Office of Basic Energy Sciences, Chemical Sciences Division of the U.S. Department of Energy under Contract DE-AC0376SF00098.

LAWRENCE BERKELEY LABORATORY
TECHNICAL INFORMATION DEPARTMENT
UNIVERSITY OF CALIFORNIA
BERKELEY, CALIFORNIA 94720